Theses and Dissertations

1-1-2013

Fault Aware Soft Restart of an Islanded Microgrid Using an Inverter Coupled Energy Storage System

Asif Anwar
University of South Carolina

Follow this and additional works at: http://scholarcommons.sc.edu/etd

Fault Aware Soft Restart of an Islanded Microgrid Using an Inverter Coupled Energy Storage System

by

Asif Anwar

Bachelor of Science
University of Dhaka, 2003

Master of Science
University of Dhaka, 2005

_____

Submitted in Partial Fulfillment of the Requirements

For the Degree of Doctor of Philosophy in

Electrical Engineering

College of Engineering and Computing

University of South Carolina

2013

Accepted by:

Roger A. Dougal, Major Professor

Charles Brice, Committee Member

Herbert L. Ginn, Committee Member

Jamil Khan, Committee Member

DEDICATION

To

Abbu & Ammu

ACKNOWLEDGEMENTS

My most sincere appreciation to my advisor, Dr. Roger A. Dougal for his precise guidance and support during the course of my PhD studies at the Power and Energy Systems group in University of South Carolina. His valuable advice and encouragements in both academic and in personal matters has helped me to become the person I am today. With his constant encouragements for developing good leadership and collaborative skills, has made me a better professional.

Thanks to my PhD committee members: Dr. Charles W. Brice, Dr. Herbert L. Ginn and Dr. Jamil A. Khan for their timely advice and valuable feedback. I would also like to thank Dr. Yucheng Zhang and Dr. Hasan Ali who were always ready to guide me during the difficult times.

None of this work would have been possible without the enthusiastic support of the faculties and staffs of the Electrical Engineering department. I was always encouraged by the support of my colleagues Philip, Kathleen, Tianlei, Dan, Huaxi, Pietro, Antonino and Blanca, who were always ready to share their ideas and discuss in every opportunity. Being able to pursue my research in this group made me a good team person.

Thanks to Dr. Asif Khan who first offered me a PhD position in his lab for which I was able to come to come to USA to pursue my PhD studies.

I would also like to acknowledge the support of my sponsor: the Office of Naval Research (ONR) and the collaborative effort of the Electric Ship Research and Development Consortium (ESRDC) under grant no. N00014-08-1-0080.

None of this work would have been possible without enduring the hardships that my family suffered and the sacrifices that my dear (late) father and my mother made for me during my PhD studies. My heartfelt thanks to my family for the ceaseless support they provided, to make me capable of overcoming the challenges faced during my PhD studies.

ABSTRACT

This research developed a method for autonomous operation of an inverter-coupled energy storage system for safe islanding– re-energization – and reconnection of the facility-island or microgrid to the utility / distribution circuit in a seamless manner in the event of a fault. This enables the energy storage system to function as an autonomous source within the utility power distribution system without the need to re-engineer the existing protection coordination in the distribution system. Fault detection based on voltage measurements from the inverter terminals are used to detect a fault and isolate the energy storage-powered facility with negligible power feed into the fault. The voltage-frequency modulation capability of the inverter is used to effect a controlled power restoration to the islanded facility which limits the motor starting inrush or the load pickup current to a predefined value. A subsequent reconnection to the main source / utility takes place when the islanded network is phase- and voltage-matched with the utility grid or the main source generator. The method is termed as "Fault-Aware-Soft-Restart" and is shown to be completed within a time period which can be as low as 0.5 s and is able to limit the inrush current to 150% of the nominal value. The controlled energization and synchronous reconnection of the energy storage-powered island, inherently avoids breaker reclosing transients and consequent false trips which degrades equipment reliability and lifetime. Voltage dips experienced by nearby customers and delayed-voltage-recovery effect caused by motor starting inrush resulting from generally

practiced restoration procedures in industrial plants are also avoided.

Decreasing cost of microsources such as microturbines, photovoltaics, and fuel cells combined with the growing demand for electrically powered commodities, against the limited capacity of centralized power generation has caused increased number of installations of distributed energy resources. Large scale (utility) battery energy storages up to 50 MW capable of providing - area power quality regulation to service reliability (UPS), are already installed and are reported in recent literatures. To prevent relay desensitization due to current infeed, and asynchronous reclosing, operational restrictions are imposed which offset the benefits of these energy storage systems. This work shows that by embedding appropriate controls into the energy storage inverter, both the major problems of unwanted fault-feeding and service restoration of "dead" circuits can be avoided. This innovation is the key toward enabling a plug-and-play environment in which many micro sources can operate harmoniously with one another with a minimum of expensive, custom site engineering.

Effectiveness of this method is proved for an industrial power network which suffers large financial losses caused by power interruptions. The method ensures personnel safety, and has the potential to avoid costs due to process downtime, motor startup and additional charges due to power quality problems during across-the-line starts. The test scenarios also include a shipboard MVAC power system in which the method is shown to provide a safe, fast and robust service restoration to a load zone. The method is shown to be very effective for such autonomous offshore power system, where improving system reliability and survivability with limited resources is much more challenging.

The dissertation also shows a method to model the electrical characteristics of a

distributed generation power system during the different stages of service restoration using the soft-restart method. Assortment of load types in a facility, their startup current behavior during different stages of restoration and their diversity factors are taken into account for the model. Design parameters such as: energy requirement, location and inverter-size, as well as the power quality indices for the distributed generation system can be estimated from the model to devise the appropriate operating algorithm for the energy storage system module.

TABLE OF CONTENTS

LIST OF ABBREVIATIONS

CLPU .... Cold Load Pick-Up

CB .... Circuit Breaker

DG... Distributed Generation

DR... Distributed Resource

DER... Distributed Energy Resource

ES.. Energy Storage

ESS... Energy Storage System

FACTS .... Flexible AC Transmission System

HVAC .... Heating, Ventilation and Air-Conditioning

MVDC... Medium Voltage Direct Current

MVAC... Medium Voltage Alternating Current

PLL .... Phase Locked Loop

RMS .... Root Mean Square

SRF-PLL.. Synchronous Reference Frame Phase Locked Loop

CHAPTER 1

1. INTRODUCTION

1.1. CONTRIBUTIONS OF THIS RESEARCH

- Developed the methodologies for an inverter-interfaced distributed energy resource installed in a distributed generation system so that it can operate as a *self-controlled* entity in the system and yet appear harmless to the existing protection in the area electric power system.

- Developed the method for effecting an automatic and controlled power restoration following a fault, to the facility loads which may be an industrial plant, residential load-center or an MVAC load-zone in an electric ship, followed by a fast and seamless transfer of the loads to the main power source or utility.

- Demonstrated the effectiveness and benefits of a "fault-aware-soft-restart" method for an industrial plant of the size of a few megawatts, or an offshore autonomous microgrid by improving reliability of equipment and continuous service.

- Shows the method to model the electrical characteristics of a distributed generation power system comprising of a variety of connected loads/facilities during the different stages of power restoration.

1.2. MOTIVATION

1.2.1. PROBLEM STATEMENT

Emergence of smaller generating systems, including internal combustion engines, microturbines, photovoltaics, and fuel cells, has brought evolutionary changes in the regulatory and operational climate of traditional electric utilities. The electricity industry is at a tipping point where the accelerating pace of change is creating opportunities for disruption. This is caused by two decades of energy policy and industry structural changes combined with accelerating social and technological evolution. The result is significant changes in the economics, operation, structure and regulation of the electric industry. Today, industry leaders and emerging business are developing strategies and new business models to succeed in this transformation. In this regard, ensuring system protection as well as flexibility in terms of power maneuvering has remained a challenge. Centralized power transmission capacities are fast approaching their maximum limits, while customer side power demand along with the energy cost is on the rise. In this context, distributed energy resources–small power generators typically located at sites where their generated electric and thermal energy is used–are a promising option to meet growing customer needs for economic and reliable electric power. In addition to generators, the distributed energy resources portfolio also includes energy storage and load control for which DGs are essentially embedded into the traditional generation-transmission-distribution system. However, this fast changing load-source architecture now has to be backed-up by either, an upgrade of the line equipment and protection circuitry or, enforcing regulatory and operational restrictions on these microsources. These restrictions limit the capability of DGs and offset their benefits as auxiliary and modifiable resources.

Figure 1.1 shows a DG inserted into the end of a feeder line, and Figure 1.2 shows the

instantaneous voltage and current characteristics in the event of a fault on the feeder.
Referring to Figure 1.2, the major impacts of a DG on the protection and the power
quality of the bulk system in the event of a fault can be distinguished into 3 different
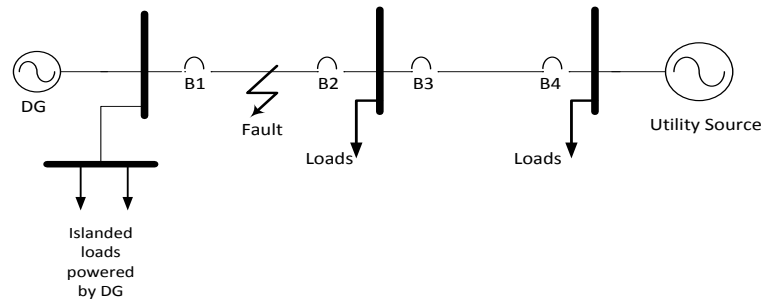time-events. These are summarized in Figure 1.2

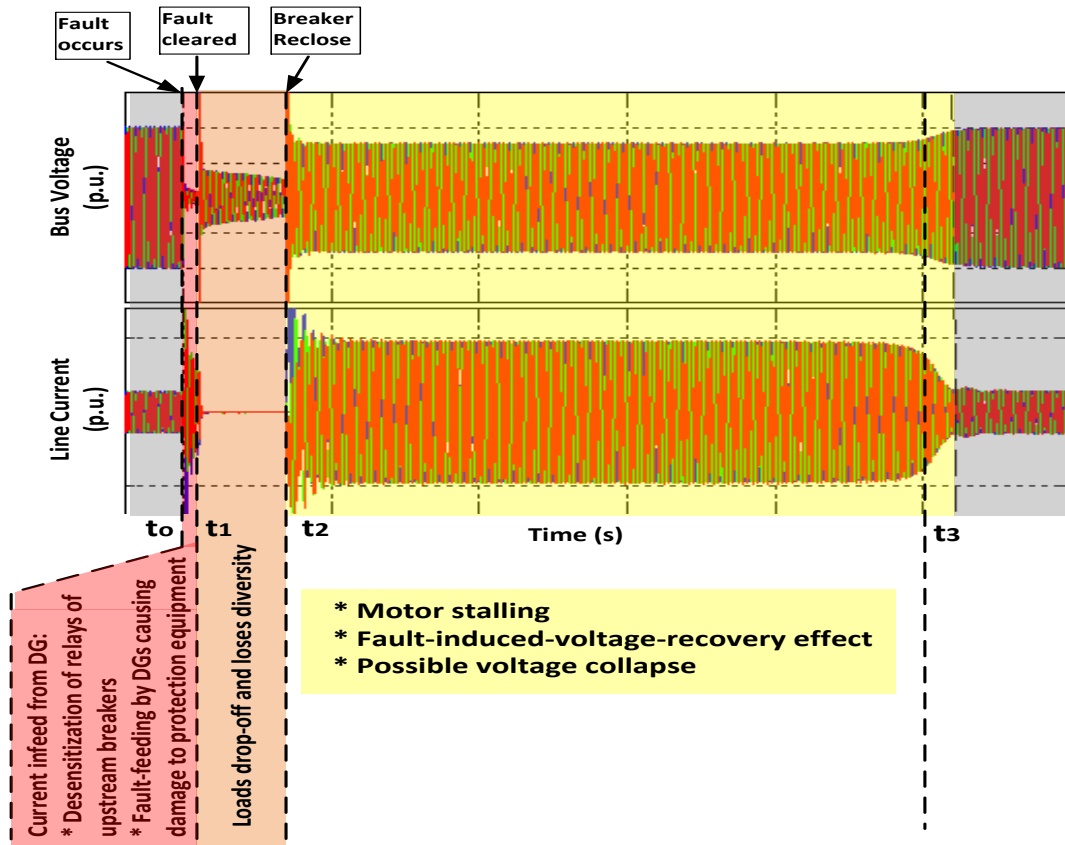Figure 1.1: Distributed Generation inserted into the traditional radial distribution feeder.

Figure 1.2:: Sequence of events and associated problems that occur due to insertion of
DG in the feeder in the event of a fault.

Table 1.1: Impact of DG(s) on the power system during the different sequence of a fault event .

Time Period	Typical Time Frame	Voltage and Current Characteristic	Effects on Protection/Line and System Loads
$t_0 - t_1$	3-5 cycles (0.05 – 0.08 s) This is the time needed for AC circuit breakers to operate.	Voltage Sags to a very low value due to high fault current flowing into the fault.	− DGs react to the voltage sag by feeding power into the circuit. − Desensitizes upstream feeder relays causing a non-operation of the breaker. − Feeds the fault with additional current, prolonging the arcing time and may damage the protection equipment.
$t_1 - t_2$	0.3 – few seconds This is the typical duty of medium voltage circuit breakers.	There may be some residual voltage in the line due to motors and capacitors that decays with time depending on inertia of the system.	− Loads drop-off quickly as the circuit is de-energized. − Industrial processes are interrupted causing financial losses. − Depending on the duration of the outage, loss of load diversity in residential networks causes difficulty in service restoration.
$t_2 - t_3$	Few seconds -- few minutes. This is the Load pick up time after a successful reclosing.	Voltage dips occur during this period due to load-pick-up currents which may be 5-6 times the nominal current.	− High starting inrush currents for motors require the upstream line-equipment and transformers to be 5-6 kVA per motor hp. − Over-stresses the thermal and electrical limits of line-equipment and protection circuitry. − Causes fault-induced-delayed-voltage-recovery effect and may cause a voltage collapse.

This research provides a method and the control algorithm for an inverter-coupled energy storage system to mitigate the three most significant protection problems in a distributed generation system, which is:

1. Reduced reach of protection relays (or desensitization of relays) due to connection of DG sources, which may cause protection devices to fail.

2. Fault-feeding by the inverter-coupled energy resources which has failed to trip themselves offline in the event of a fault.

3. Difficulty (or failure) of service restoration to highly loaded distribution circuits following an interruption which were originally powered by distributed resources.

The three most important problems mentioned above are described briefly in the

4

following sections.

1.2.2. PROBLEM DESCRIPTION

1.2.2.1. REDUCED REACH OF PROTECTION RELAYS

To illustrate the impact of DG on its feeder's overcurrent relay performance, the prototype feeder in Figure 1.3 is used. The feeder's load is assumed to be equally distributed along the feeder. The feeder is protected with an over-current relay, R, and is supplied from the substation.
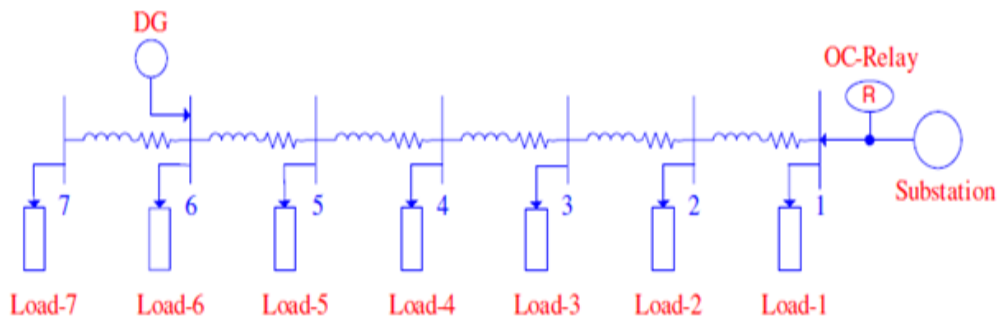

Figure 1.3: A seven-node (radial) distribution circuit.

Since relays are set to protect a certain distance of the feeder, the presence of a DG will reduce the reach of the OC relay, thus leaving medium impedance faults at the end of the feeder undetected. The phenomenon is explained using Figure 1.4 and Figure 1.5 for a total feeder load of 6 MVA, with a 600 kW DG operating at 0.9 pf connected at bus 6.

Before connecting the DG to the feeder, a fault at bus 7 with $R_f = 10.4\ \Omega$ will create a current at the relay = 710 amps, and the relay will trip. After connecting the DG, the same fault will create a fault current at the relay of 650 amps, thus the relay will not trip. Figure 3 represents the maximum fault resistance at each bus that will create fault current that can still be detected by the relay at each bus with the DG connected at bus 6. The reduction in reach is increased with the amount of power injected by the DG. For a

5

specific R_f as the DG power increase the relay reach decrease, until the whole feeder becomes unprotected against that specific fault resistance [1]-[3].
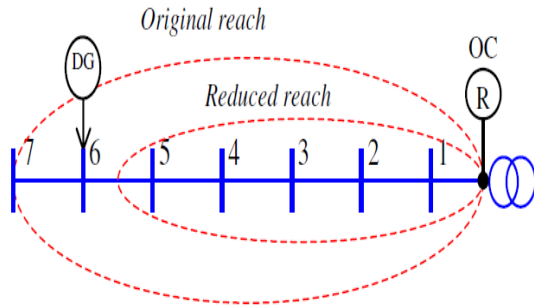

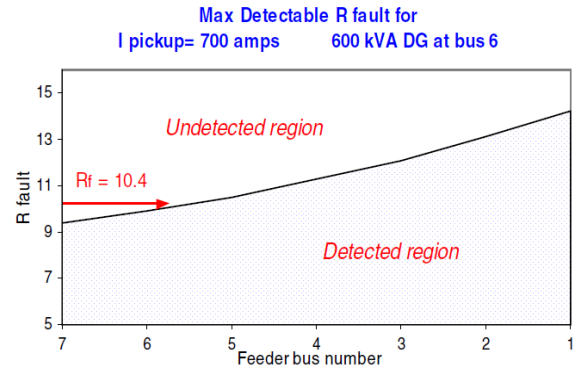Figure 1.4: Reduced reach for relay R, due to DG infeed.

Figure 1.5: Example case showing "desensitizing" effect on relay R.

[1]-[11] have analyzed the impact of DGs on voltage profiles and protection coordination of distribution feeders. Their analysis shows limitations on the maximum capacity of DGs to maintain existing protection coordination. [1],[3],[7] and [9] provides procedure to calculate allowable DG size to maintain existing protection coordination as well as reap economic benefits in lieu of available DG technologies.

This research provides a guideline by which the protection settings at the distribution feeder will remain unaffected with the installation of an inverter coupled DG, and without imposing size and regulatory restrictions on the DG connection.

1.2.2.2.   FAULT-FEEDING BY THE DG(S) IN THE EVENT OF "FAILURE TO TRIP"

One of the major impacts of an inverter-coupled energy storage system on a feeder will be during the fault conditions, as they will contribute to the fault current. Aside from its impact on the protection relay settings of the feeder, the inverter coupled energy storage mischievously contributes to the fault current and may cause a destructive failure of protection equipment.

Ideally, all DGs would disconnect before the first reclosing attempt of (fault-clearing) CBs so that the utility fault clearing equipment can proceed normally.
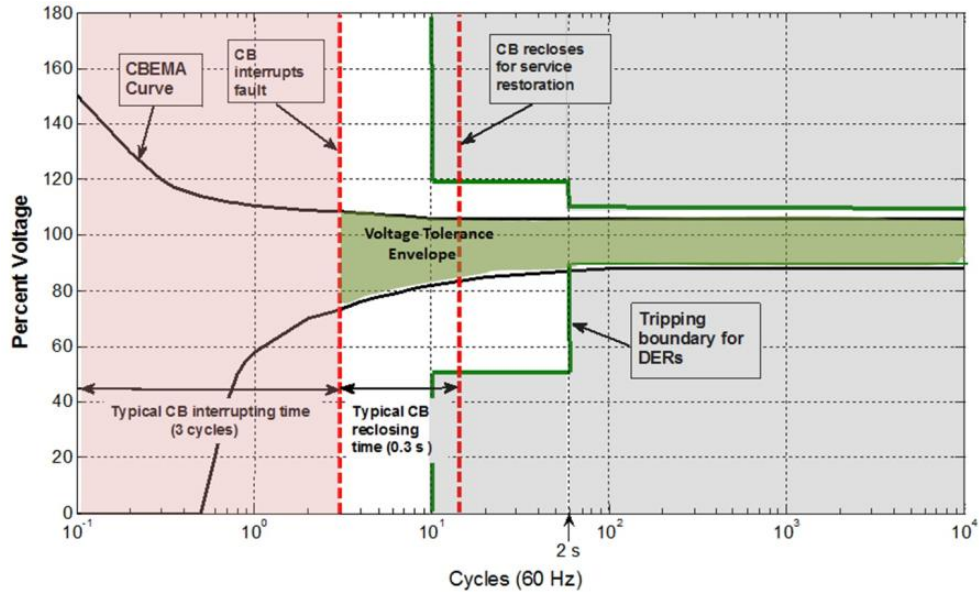
Figure 1.6: CBEMA curve and tripping boundary for DERs according to Std: 1547-2008 and Std. 446-1995 [12], [13], and a typical CB operating duty [14]-[16].

Figure 1.6 illustrates the operational restrictions imposed on DGs to prevent desensitization of relays due to current infeed, and prevent asynchronous reclosure on to an islanded network. The important points to note from Figure 1.6 are:

- DGs operating in "co-generation" mode must be successfully disconnected before the first reclosing attempt of line CBs occur (shown by the red dashed lines).

- Even a fast clearing fault (self-clearing, or cleared by CB in 3 cycles) cannot prevent voltage sensitive loads to drop-out according to the CBEMA curve [12].

- If the voltage tolerance boundary of equipment *is* modified to sustain operation during short interruptions, an automatic reclosing of CBs will occur after about

0.3 s. Since the ESS is tripped off to avoid asynchronous reclosure with the live bus, motor starting inrush and associated voltage depression cannot be avoided.

In general, the operation and control of an inverter-coupled DG are essentially based upon the thevenin equivalent circuit seen from its terminals.

$$Y_{th} = f(V_{th}I_{inv}) \tag{1.1}$$

$$P_{inv\_ref} = f(Y_{th}) = f(V_{th}, I_{inv}) \tag{1.2}$$

Where, Y_{th} is the thevenin equivalent admittance seen from inverter terminals,

V_{th} and I_{inv} are the inverter terminal voltage and output current respectively and

P_{inv_ref} : the inverter output power reference calculated from V_{th} and I_{inv}.
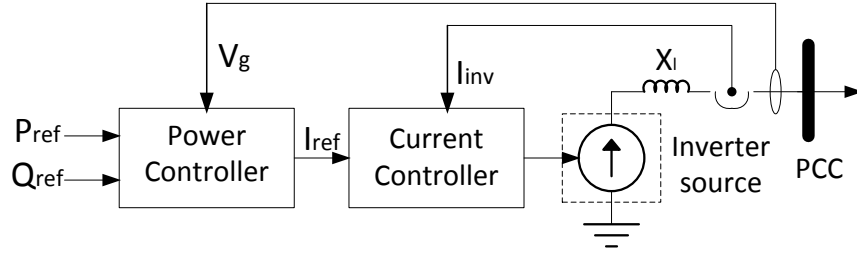
Figure 1.7: General inverter control scheme.

Generally, inverter controls consist of a fast current control loop nested under a comparatively slower outer voltage control loop that generates the current references for the inner control loop as shown in Figure 1.7. The response of the inverter to a disturbance on the system during the subtransient period is as follows:

1. A new current reference is generated by the outer power control loop which is a function of the measured system voltage (V_g), and the commanded reference power (P_{ref}, Q_{ref}).

$$I_{ref} = f(V_g, P_{ref}, Q_{ref}) \qquad (1.3)$$

2. The inner current control loop immediately starts responding to the generated reference and is only limited by the controller saturation limits.

In (1.3), although P_{ref} and Q_{ref} can be kept constant, when the inverter's power output command is externally controlled, I_{ref} depends on the voltage measurement. As a result any voltage fluctuation is countered by an increased power output by the DG to compensate for the voltage. This behavior often has negative consequences in the cases of inverter coupled energy sources. Inverters having no inertia in their output, responds immediately to changes in the ac power system by injecting power into the system. If a fault-induced voltage sag seen by the inverter at its terminals is not low enough, or the output current is not high enough, it may fail to trip offline and continue to feed the fault. The consequences are:

In addition to the problem of desensitizing or inducing the effect of "reduced reach" of the protection relays (as described in the previous section), an increase in fault current due to the DG infeed causes the fault arc to continue to burn causing more damage to conductors and insulators. Even for restorable insulation, reliability and lifetime of equipment are greatly reduced resulting in the fact that the chances of future failures will be greater.

If the DG fails to trip offline before the breaker attempts its first reclose, the asynchronous reclosing causes unnecessary short-circuit forces through transformers, line equipment and customer equipment [16].

In this research take advantage of these highly reliable interconnection protection

relays and communication links to operate the islanding breaker enabling the operation sequence: fault-detection – islanding and restoration – synchronous reclosing to transfer the load zone back to the utility.

1.2.2.3. DIFFICULTY (OR FAILURE) OF SERVICE RESTORATION IN A DISTRIBUTION CIRCUIT FOLLOWING AN INTERRUPTION.

One of the biggest challenges in a deregulated power system where the DGs are configured to work as dispatchable units, is during service restoration following a fault. This happens due to the loss of load diversity following the interruption, and the absence of the DG sources which had to be disconnected prior to initiating the restoration. The severity of the problem depends upon duration of outage, connected loads, local weather, habits of user and thermal characteristics of the loads. Figure 1.8 shows the load current behavior following a power outage in a utility grid on the southeastern United States. The load before the interruption was 144 A, and when the transformer was re-energized a peak current of 960 amperes was recorded which was 6.7 times the pre-outage current. The ratio of the two current levels at 1 s and 10 s is approximately 2:1. Also the load diversity started to take effect in approximately 1000 seconds [21].

The above phenomenon is popularly known as "Cold Load Pick Up" in the utility and may often cascade into a bigger problem if not recovered quickly. The high load pick-up currents mainly produced by motor starting inrush of HVAC units in residential communities or line-connected motors in industries causes:

1. The fault induced voltage recovery (FIDVR) effect, and consequently
2. Load-shedding to prevent a possible voltage collapse.
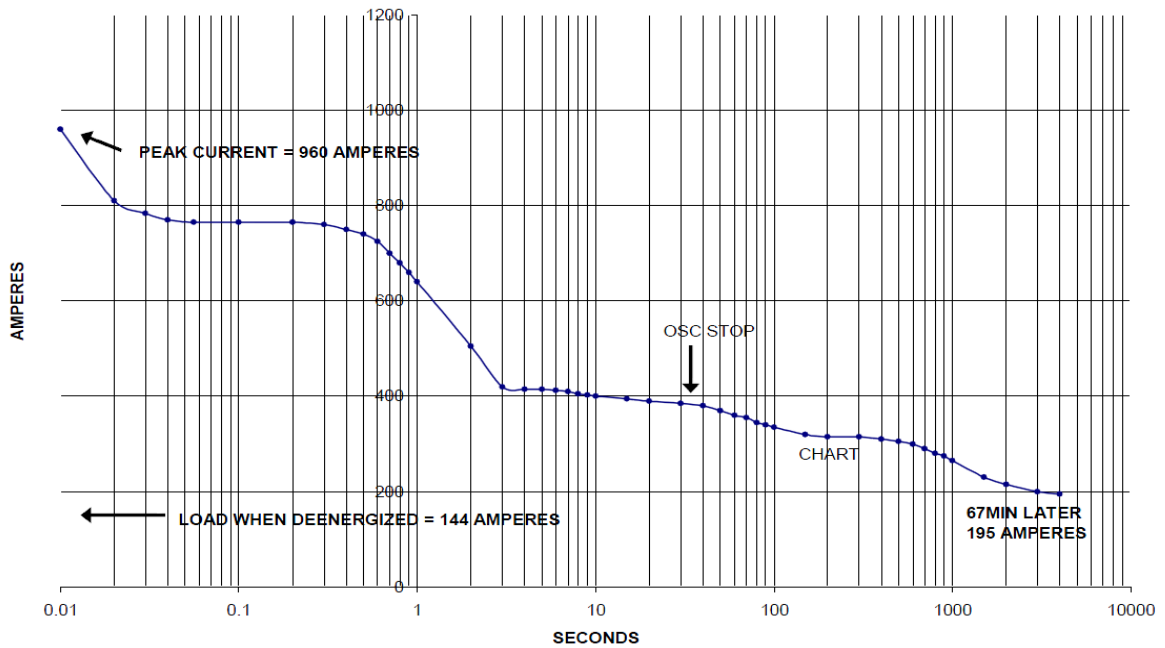
Figure 1.8: Current through transformer following re-energization [21].

Figure 1.9 illustrates the FIDVR effect due to restarting of loads in a residential community in California consisting of a large percentage of air-conditioning (A/C) loads. During restart, compressor motors in the A/C units draws 5-6 times its steady-state current, but are unable to restart against the full head of pressure resulting in further depression of system voltage until tripped by the thermal overload relay.

Air-conditioning (A/C) loads can be as much as 50% of the summer load in some areas [22]. Equation (1.4) can be used to calculate the minimum voltage required to successfully restart HVAC units [23].

$$V_{min\_start} = \sqrt{\frac{T_L}{T_{start}}} \times 100 \text{ \%}$$

(1.4)

Above equation is formulated from the relation:

11
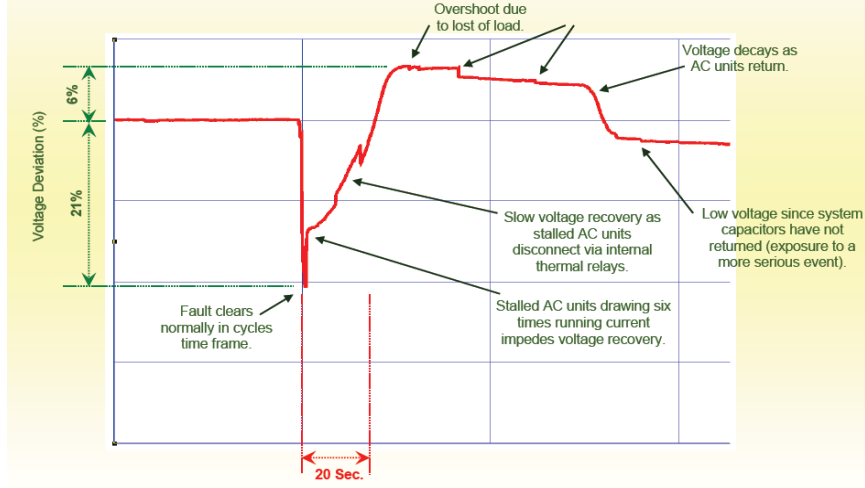
Figure 1.9: AC Stall Voltage Signature during FIDVR (reproduced from [24]).

$$T_e \propto V^2 \tag{1.5}$$

If most of the motors in a system are of the standard design-B type, the minimum voltage required to restart from stalled condition is V_{min_start}= 82 %. This value assumes the conditions: $T_L = 100$ %: fully loaded compressor motor in the post-fault condition and, $T_{start} = 150$ %: required starting torque for design-B motors.

Also the minimum tolerable voltage required to prevent a running motor from decelerating to a stalled condition can be calculated as:

$$V_{min} = \sqrt{\frac{T_L}{T_{pull-out}}} \times 100\ \% = 70\ \% \tag{1.6}$$

Where: $T_L = 100$ %: assuming a fully loaded compressor motor, and $T_{pull-out} = 200$ %: pull-out torque for design-B motors.

Although, undervoltage relays for motor contactors are conventionally set between 75-80% to prevent motor stalling problem, a sustained voltage dip below 0.9 p.u at the area

electric power system (Area EPS) may cause powering down or drop-off of consumer equipment on the Area EPS bus. The voltage recovery that takes several seconds may eventually lead to a cascaded voltage collapse and even a blackout [24]-[26].

CHAPTER 2

2. CURRENT STATE-OF-THE-ART TO MITIGATE PROTECTION PROBLEMS IN DISTRIBUTED GENERATION

2.1. STATE-OF-THE-ART TECHNOLOGIES TO PREVENT FAULT-FEEDING AND ASYNCHRONOUS RECLOSURE

A fast fault detection technique for inverter-coupled DGs which can be applied to any system is hard to realize as fault and load characteristics vary widely. Usually an inverter-coupled DG is equipped with a protection scheme that turns itself off when the current reaches its maximum limit. This limit is generally twice the rated inverter current. A low-voltage turn off can also be implemented, but its response is slower than the current-based protection. The biggest problem of a current (or voltage) based turn-off is for high-impedance or distant faults which may not trigger the inverter trip-off. [2],[3] shows a method to extend the conventional fault analysis methods, so that an inverter-coupled DG contribution can be estimated. The method also defines the condition based on the line parameters of the bulk system for which the inverter will be able to trip off successfully.

Present practices to prevent the inverter-coupled DG to feed a fault is based upon a fast disconnection from the bulk power system based upon the voltage measurement at its terminals. The requirements are defined in the standard 1547.2 and is given in Table 2.1. [13].

Table 2.1: Interconnection System Response to Abnormal Voltages [13]:

Voltage range (% of the base voltage)	Clearing time (s)
V<50	0.16
50≤V<88	2.00
110<V<120	1.00
V≥120	0.16

One of the consequences of a failure to trip-off the DG is the danger of reclosing on to an out-of-phase network powered by the DG. The reclosers in the feeder have been designed to operate on a timer-based duty, assuming a "dead-bus" condition in the network to which it is reclosing on to. This supposedly de-energized load-zone is now energized by the DG, if it had failed to disconnect before the first reclosing attempt of the breaker.

Island-detection techniques described in literatures [29]-[31] provides a method for fast detection and prevention of DGs from operating independently. Typically, since islanded operation of DGs were not allowed due to lack of technical and regulatory standards until recently, so there has been a substantial amount of technological developments in the successful detection of islanded systems [29]-[32]. Unless there is mutual agreement between utility and the DG owner, islanded operation is not allowed because of safety hazards; and DGs being a weak source, unable to provide acceptable power quality to customers. The detection methods for anti-islanding mainly utilizes frequency relays (81U/O) to detect the slip frequency (f_{slip}), acceleration (df_{slip}/dt), and vector shift relays (popularly known as phasor measurement and control units, PMCUs) to enable a wide-area or remote detection capability. PMCUs provide synchronized measurement of voltage and current phasors using wireless communication link or GPS to a synchrophasor vector processor (SVP) that executes the logic for detecting islanded

condition and disconnect the system. These PMCU based units rely upon the time-stamping provided by GPS and are popularly used at the transmission level. Both wide-area and local area measurements are utilized to detect islanding and monitoring [31].
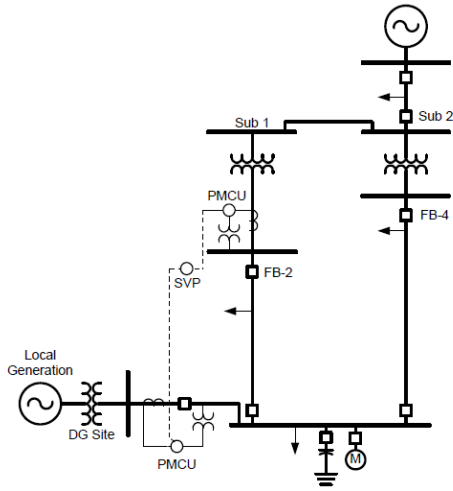
Figure 2.1: Wide-area based anti-islanding protection of a power system *(Reproduced from [30])*
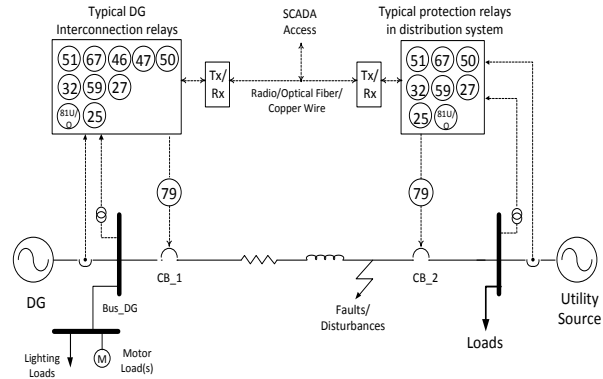
Figure 2.2: Typical protection relays in a distributed generation power system [29],[31] - [32].

Figure 2.1 shows a typical islanding protection based on wide-area measurement. Time-synchronized measurement of voltage and current phasors are obtained from PMCU1 and 2 using some form of communication link and transmitted to SVP which executes logic for detecting the island sends out switching signals for CB relays [29] - [31]. Table 2.2 shows the function of the different types of relays used in protection equipment including sequence detection and under/over voltage/frequency based island detection.

Table 2.2: Explanation of relay numbers [29].

Relay Number	Application / Function
21	distance
25	synchronizing
27	undervoltage
27N	neutral undervoltage
32	directional power
40	loss of excitation
46	neg. seq. current
47	neg. seq. voltage
50	instantaneous overcurrent
50N	neutral instantaneous overcurrent
51N	neutral time overcurrent
51V	voltage-restrained overcurrent
59	overvoltage
59I	instantaneous overvoltage
59N	neutral overvoltage
60FL	voltage transformer fuse failure
67	directional overcurrent
79	reclosing
81U/O	frequency (under and over)
81R	rate of change of frequency
87	differential
LOM	loss of mains

At the distribution level, monitoring and remote reconfiguration are easily provided through communication links such as radio, optical fiber or telephone wires. Commercially available relays uses the latest advances in network-based communication technologies, including Ethernet, IEC 61850 and traditional supervisory control and data acquisition (SCADA) protocols [31]. Such intertie protection relays and communications are shown in Figure 2.2. Voltage signals are supplied from each bus and communicated through the links to allow remote monitoring and reconfiguration of protection equipment.

Some of the disadvantages of the anti-islanding methods described in literatures [29]-

[31] are:

1. The local-area measurement based detection which relies upon the slip frequency (f_{slip}), acceleration (df_{slip}/dt), may take up to 0.3 ~ 0.5 s. This may exceeds the breaker reclosing time of 0.3 s.

2. The element response for a wide-area measurement based detection, is also slow which is about ~1 s, and exceeds the time interval for the first reclosing attempt of the breaker [31].

3. Also the methods are highly dependent upon the communication technology which is undesirable.

For industrial power networks, or process line circuitry, where a substantial line voltage may be sustained due to high inertia motors, the following practices exists to avoid reclosing on to a bus with motor residual voltages:

1. Use a timer to delay restoration, so that motor internal voltages can decay to a safe level (known from actual tests).

2. Use a voltage sensor to delay restoration until the internal voltage generated by the motor(s) has dropped below some threshold (typically 25% of rated voltage).

3. Use a high-speed under-frequency relay (81U) for motors with low inertia or heavy loading to detect the outage and trip the motor before supply voltage is restored [19].

The problems in this case is that, all of the above practices use delayed restoration resulting in increased power failure cost due to extended process downtime. Also the costs and complications for service restoration is high as the motor have to be re-energized from an idle condition.

2.2. PRACTICES AND REGULATIONS FOR SERVICE RESTORATION

Under voltage load shedding (UVLS) is the most prevalent practice to avoid a widespread voltage collapse following a fault especially when the bulk of the system load consists of "stall-prone" HVAC motors. UVLS scheme is designed based upon the P-V curve shown in Figure 2.3 also known as "nose-curve" by system planning engineers. The settings and design of UVLS is carried out cooperatively by relay engineers and system planners. Pre-selected groups of loads are shed when local voltage drops to a designated level most often 89-94% with several second delay [25].
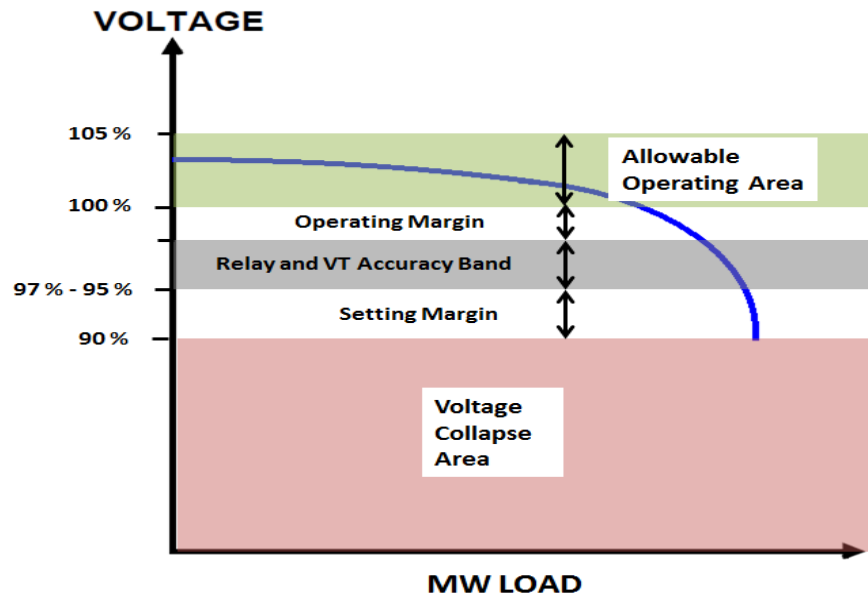
Figure 2.3: "Nose-curve" for a particular system adopted by system planning engineers to prevent a possible voltage collapse [25].

In a distributed generation scenario, a remedy is to use the DG sources to establish sufficient load diversity before reconnecting to the utility source. Recent literatures [33] - [42] have shown the effectiveness of using distributed resources as a supplemental source to establish the required load diversity through a "bottom-up" approach. In this approach the system is first divided into subsystem islands, each with black-start capability. Then,

each subsystem is stabilized, and eventually interconnected [34].

In this research we have shown a safe and robust method to seamlessly energize and reconnect an inverter interfaced distributed generation island into the grid following a fault.

CHAPTER 3

3. BACKGROUND ON GRID-TIED ENERGY STORAGE SYSTEMS

Interest in electrical energy storage systems tied into the terrestrial or off-shore autonomous grids are increasing as the opportunities for their application become more compelling in an industry with a back-drop of ageing assets, increasing distributed generation and a desire to transform networks into Smart Grids [37]. This chapter discusses benefits, application range and limitations of grid-tied energy storage systems (ESSs). The chapter also compares the functionalities offered by a commercially available ESS, with that of the proposed ESS with fault-aware-soft-restart capability.

3.1. APPLICATIONS AND BENEFITS OF GRID-TIED ENERGY STORAGE SYSTEM

Application of energy storage to distribution network, benefits customers, supply companies, and generation operator (conventional and DG) in several ways. Previous studies and a series of reports from Sandia National Laboratories assesses the cost–benefit of trans- mission and distribution upgrade deferral in addition to improving power quality [37]-[45]. Drawn from a survey of the above literature, the areas where energy storage systems can be applied can be summarized as:

- Electric (grid-supplied) energy time shift

- Transmission capacity deferral

- Voltage support and area power quality regulation

- Transmission congestion relief

- Substation on-site power for switching, communication and control equipment

- Time-of-use and demand charge management (peak shifting)

- Service reliability (UPS or back-up power)

- Renewables energy time shift, capacity firming and demand charge management

- Wind/Solar integration into grid [38].

Large scale battery energy storage in the range of 10~20 MW, already installed are reported in [39],[40], [43] and are primarily installed to provide: spinning reserve (15-20 mins) and system stabilization [39]. An example of the use of ESSs at the distribution level to mitigate voltage dips is the PREPA 20 MW Battery Project [46]. Also an example, signifying the importance of back-up power using energy storage for an industry is reported in [39] where it has been concluded that, a BESS in an aluminum industry in San Diego, can effectively prevent "freeze-up" of the produced aluminum cells during power outages.

Some heavy industries such as Pulp and Paper (80-300 MW) commonly generate a fraction (20%) of their own energy onsite. Apart from the use of these generators to operate in islanded mode to power part of the plant, they also have the capability to provide a "black-start" for service restoration [35]. Such black-start units (BSU) can also be a part of the distribution level power system and are typically about 10% of the full capacity resulting in a low fault current capacity.

The focus area in this research are comparatively smaller sized energy storage systems in the range of a few hundred kW to a few MW appropriate for load support and

autonomous operation of a facility or a circuit island. This type of modular and scalable storage systems are now commercially available targeted for applications ranging from peak load support to PQ control [44].

3.2. OPERATIONAL RESTRICTIONS ON GRID-TIED ENERGY STORAGE SYSTEMS

Potential of Energy Storage Systems reported in studies [37] -[46], are not fully utilized due to the grid regulations described in [13]. These regulations have enabled reclosers to have "single-shot" type designs to operate in a live-bus/dead-line condition during service restorations [47]. The major problems caused by ESS infeed are discussed in Chapter-1.

The restrictions imposed on the ESSs, limit its capability and offset their benefits as auxiliary and modifiable resources. However, with recent advancements in power electronic interfaces, large scale ESSs are allowed to operate in islanded mode with a mutual agreement between ESS owner and utility [45]. This has also provoked the interconnection standard Std. 1547.2-2008 to be revised to accommodate islanded operation of DGs within the newly developed grid regulations. Recently published IEEE Standard 1547.4 provides a guideline to facilitate intentional islanding for a distributed generation system [48]. But still the full potential of these systems are not utilized to provide the functionalities for:

1. Fault detection based on local measurements, to prevent fault-feeding.

2. Limit starting inrush current during restoring power to the islanded load zone to improve system reliability and service continuity.

Taking advantage of the fast dynamics of the inverter, the above functionalities can be easily provided to mitigate the major protection and power quality problems encountered by the bulk power system.

3.3. Functional Comparison Between a Commercially Available ESS and the Developed ESS with Fault Aware Soft Restart Capability

Table 3.1 compares a commercially available energy storage system with the developed energy storage system in terms of their offered functionalities.

Table 3.1: Functional comparison between a commercially available ESS and the ESS with Fault-Aware-Soft-Restart capability introduced in this research [39],[44],[45],[48].

Functions	Commercially Available ESS	ESS with Fault-Aware-Soft-Restart Capability	Comments
Electric energy time shift	**Yes**	**Yes**	This is also known as Time of Use Management, or Peak Shaving.
Power quality. Including voltage support and frequency regulation	**Yes**	**Yes**	
Transmission capacity deferral and congestion relief	**Yes**	**Yes**	
Emergency back-up or UPS operation	**Yes**	**Yes**	Usually can support the EPS for less than an hour.
Connection with the utility maintained, in the event of a fault	**No**	**Yes**	ESS with FASR goes to current limiting mode rather than disconnecting through a breaker.
Detects the fault to prevent possible fault-feeding.	**No**	**Yes**	ESS with FASR uses voltage measurement from its terminals to detect the fault and prevent feeding power into the fault.
Controls starting inrush current when restoring power to the EPS (or island).	**No**	**Yes**	Uses a controllable V/Hz ramp to avoid starting transients and inrush currents. Since inrush current is controlled by the ESS inverter, the power density requirements for the storage elements are not as stringent as in the case for commercially available ESS.
Fault detection to prevent unnecessary close-open operations of system circuit breakers on to faulted circuit using communication channels.	**No**	**Yes**	A fast fault detection method incorporated into the inverter controls, allows it to assume a power limiting / turn-off mode and prevent current infeed to the system.
Synchronize with the utility / main source following the restoration	**Yes**	**Yes**	

CHAPTER 4

4. RESEARCH GOALS AND CHARACTERIZATION OF FACILITY LOADS

4.1. RESEARCH GOALS

The key aspects of this research are:

1. Demonstrate that the Fault-Aware-Soft-Restart method enables a grid-tied energy storage system to comply with the power quality requirements that would be acceptable from existing customers, and without the need for re-engineering the protection settings of the protection equipment in the area electric power system t which it is connected to.

2. To develop controls for the energy storage inverter so that it will be able to restore power to the facility in a controlled and "transient-free" manner so that the bulk system can be restored quickly without stressing the thermal and electrical limits of line equipment.

3. Demonstrate that the method is effective for different types of facility: industrial, residential and an offshore autonomous power system such as that of an electric ship.

4.2. LOAD CHARACTERISTICS

A system model characterizing the electrical characteristics of a grid-tied energy storage system - powered facility island during power restoration will be discussed in chapter-8. In this chapter we will characterize a residential, industrial and a shipboard medium voltage AC power system based on their load distribution. This characterization

is important, to validate the effectiveness of the soft-restart method for application in different systems – residential/industrial/off-shore power systems.

The IEEE Std. 1547.4 provides the guidelines for design, operation and integration of distributed resource island systems with electric power systems (EPS) [48]. Figure 4.1 shows the scope of intentional islanding in the distribution subsystem described in the standard.
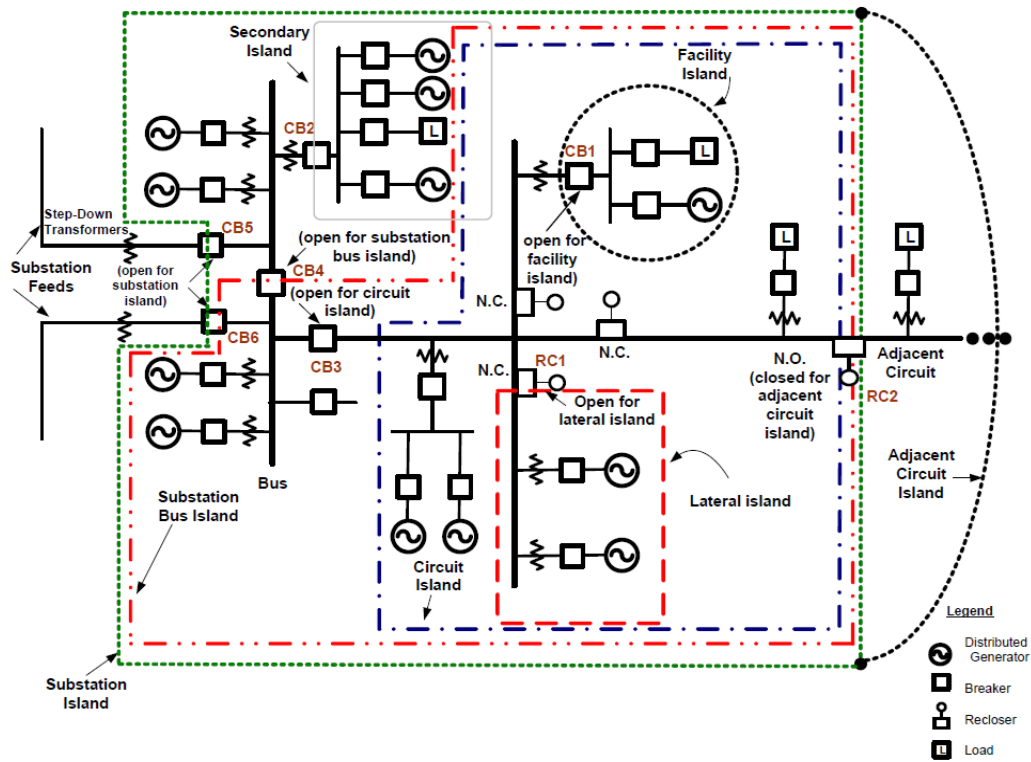

Figure 4.1: Examples of DG island systems described in IEEE Std. 1547.4 (Reproduced from [48])

We consider a single facility island within the distribution susbsystem. The facility island with its assorted loads is shown in Figure 4.2.

The basic difference between a residential and an industrial or an off shore facility is the percentage of motor loads. Since an electrical characteristic of motors characterizes the transient behavior of the system, so the percentage of motor loads in the island power

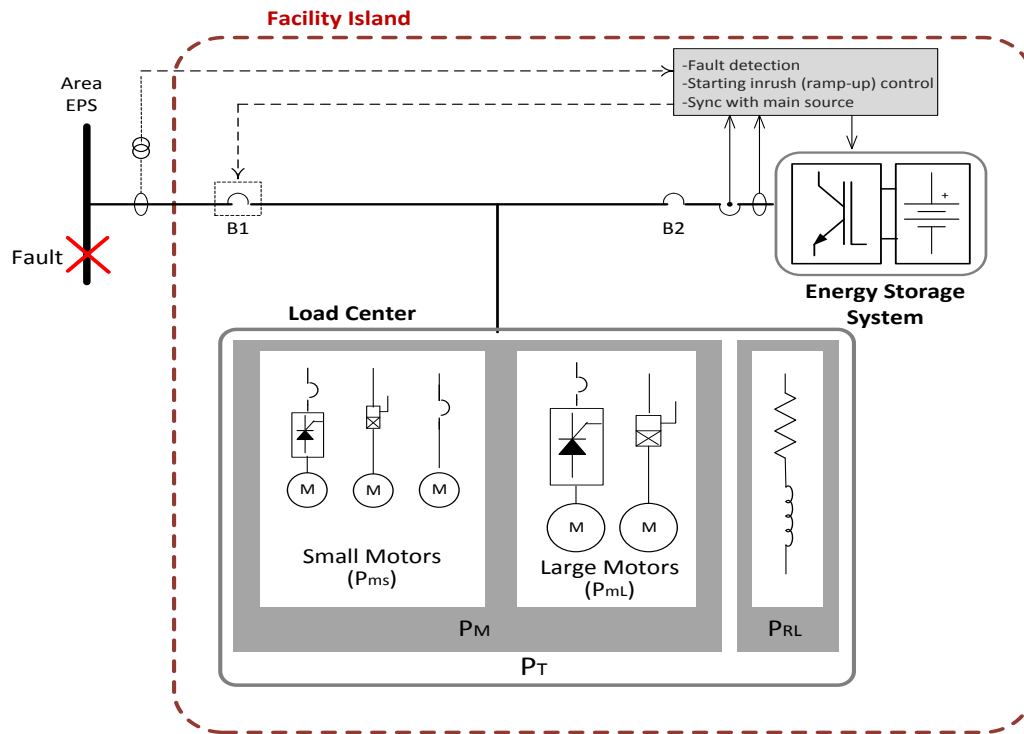system can be used to characterize the type of facility.

Figure 4.2: Facility Island with assorted loads.

Referring to Figure 4.2, we broadly classify the facility loads into the following:

1. **P_{RL}:** These are the loads that represent applications such as: area lighting, space heating, cooking, etc.

2. **P_M:** These loads consists of both small (<50 hp) and large motors. Distribution, sizes and connection of these motors to the circuit varies widely according to:

   a. Applications

   b. Size

   c. Process reliability.

   d. Restarting process which is generally dominated by personnel safety

28

and their impact on power quality.

All motor loads are broadly categorized into large (P_{mL}) and small (P_{ms}) motors. It is readily understood that an industrial and a shipboard power system will have a substantial number of large motor loads, many of which are line connected. Some of the typical applications of these motors are shown in Table 4.1 :

Table 4.1: Typical applications of motors in a facility load island.

Motors	Connection Type	Typical applications
Large (industrial) motors **(P_{mL})**	**Line Connected**	Chillers, Air -Compressors, Granulators, Boiler Feed, Cooling Tower Fan In Ships: Fire pumps.
	Electronically Controlled (Motor Drives)	Extruders, Conveyors. In Ships: Propulsion, Thrusters.
Small motors **(<50 hp)** **(P_{ms})**	**Line Connected**	Chilled water supply, Backing motors in process control, Air Blower, Dryers. In Ships: Recirculating pumps.
	Electronically Controlled (Motor Drives)	Pullers, Extruders. Air-conditioning, Heat pumps.

Motors are generally equipped with contactors that allow them to drop-off when the voltage drops below a certain threshold and then reconnect using:

a. Timer to delay restoration (known from actual tests) or

b. When the voltage at the motor terminals decay to a low enough value (typically 25% of rated voltage) [19],[20].

The above methods are used to block any restart attempts until the motor residual voltage has dropped below some threshold, so that an asynchronous reclosure on to the motor residual voltage can be avoided.

Many large and small industrial motors are also manually restarted. A large percentage

of such motors are found in production facilities such as: plastic/rubber manufacturing plants. Manual restart procedure is preferred by these industries to ensure personnel safety and avoid power quality problems.

We define a characterization parameter X_M to characterize the type of facility that is to be powered by the energy storage system:

$$X_M = \frac{P_M}{P_M + P_{RL}} \tag{4.1}$$

Where:

$$P_M = P_{ms} + P_{mL} \tag{4.2}$$

Table 4.2 shows the range of values of X_M for three different types of facilities estimated from the data available in [21],[49],[50],[51]:

Table 4.2: Range of X_M for different type of loads:

Type of facility	Estimated value of X_M
Residential Facility	0.1 – 0.2
Hotel	0.2
Industrial Facility (few MWs)	0.8-0.9
Ship Power System	> 0.9

Clearly a higher value of X_M means that the number of motor loads in the facility island is higher, thus signifying the use of a soft-restart in that facility.

Some of the major power quality issues in a residential, industrial and a ship MVAC load zone is discussed in the following sections, followed by a summary of the benefits obtained from using a fault-aware-soft-restart.

4.3. SIGNIFICANCE OF FAULT-AWARE-SOFT-RESTART FOR DIFFERENT FACILITIES

4.3.1. INDUSTRIAL FACILITY

Industrial processes such as plastic or rubber production can suffer large financial losses following power disruptions. In the USA there are about a hundred factories that produce consumer plastic products in plants which are of the size of few megawatts [52]. A factory of this size have about 200 motors ranging from $0.5 - 300$ hp, 35% of which are line connected. In addition to direct production losses, there may also be costs associated with wear and tear on power distribution equipment as a result of large inrush currents (in motors, transformers, capacitors) during service restorations. Yang in [53] has shown that system transients are also responsible for the highest number of failures of electronic components. From a cash flow viewpoint, a rough estimate of the direct cost of a power failure [54] is:

$$\textbf{Cost} = \textbf{E} + \textbf{H} + \textbf{I} \tag{4.3}$$

Where,

E = cost of labor for employees affected

H = scrap loss due to process failure

I = cost of startup.

From a strictly technical point of view, reducing the number of startups can minimize this cost. In a manufacturing plant, generally there are separate buses for the line-connected motors used for applications such as hot/cold water supply, chillers, dryers etc. These motors are restarted manually following an outage to ensure safety, avoid voltage dips, and equipment damage from starting inrush currents. However, the manual restart (MR) process generally takes about 30-45 mins. Also, it requires careful consideration of

the turning-on sequence and increased labor involvement which adds to the cost of power failure. Installment of soft-starters is a possible solution to avoid penalties imposed by power companies on the amount of current drawn and maximum number of starts per hour or day [21],[55]. But, additional investments and the potential of injecting harmonic currents which may aggravate the already-low power factor, discourages installment of soft-starters for the line connected motors [23],[55].

The fault-aware-soft-restart can mitigate the aforementioned problems in an industrial plant by avoiding motor starting inrush, startup costs, labor safety and additional penalties imposed by the utility from voltage and power factor fluctuations.

4.3.2. RESIDENTIAL FACILITY

Impacts of power interruption are of different significance for a residential facility as compared to an industrial facility. Restrictions and additional charges on peak current draw and startup costs do not apply for residential customers as in the case for an industrial plant. Also there is no requirement for "synchronized" operation of multiple loads within the residential facility. Restoration of power to a residential facility following an interruption is the biggest challenge for the power industry. With the growing power demand, the bulk power systems are operated close to their design limits making it more vulnerable to potential blackouts caused by system disturbances. The two most commonly used restoration approaches are: the "bottom-up" and the "top-down" restoration strategies. For the "top-down" approach the bulk power transmission system is established first, using interconnection assistance or hydro-plants, followed by subsequent energization of substations and resynchronization of generators. For the "bottom-up" approach, the system is restored by islands first, and then mutually

32

interconnected [34]. With increasing number of small-scale (few kWs for residential PV systems) and utility-scale energy storages ($1-50$ MW) the "bottom-up" approach is an effective way to restore power to residential loads. Using the fault-aware-soft-restart method the "bottom-up" approach can be tailored to implement a seamless restoration and reconnection to the utility within a few seconds without overloading the bulk power system. The application of this method in a residential facility minimizes the effects of starting inrush currents which leads to a delayed-voltage-recovery effect.

4.3.3. SHIPBOARD MVAC SYSTEM

Problems with power quality are of different significance as compared to the ones on a continental power grid. Impacts on pricing relations (e.g. tariffs applied and penalties) between utility and its clients do not apply for a ship system, where the most important issue is the continuous operation of the system and its redundancy. A possible malfunction or failure of line equipment carrying power to critical loads may lead to a total loss of the vessel [50]. Present approach for reconfiguration and restoration in a ship system involves fault isolation using directional overcurrent protection, followed by a routine operation of some automatic bus transfer (ABT) switches to restore power quickly to critical equipment. Load shedding system is incorporated into the power management algorithm to ensure that loss of an operating paralleled generator will not cause a possible black-out. This is generally done by remotely opening the breakers connected to non-vital loads when generator overload is sensed. With this approach, a fixed set of loads are shed which in most cases means that more loads are disconnected than necessary to meet the reduced generation capacity and prevent possible motor-stalling in nearby load-zones. Reclosing transients and starting inrush in many cases

33

causes unwanted generator trip-offs and stalling of motors driving critical loads such as steering equipment and fuel transfer pumps and may cause a substantial accident as the one reported in [56].

New techniques to increase reliability of continuous service through automation of functions in a ship electrical system are of high priority in the work plan of ESRDC in the All Electric Ship Buildings sponsored by the US Navy [57]. Distributed energy storage systems, in commercial cruise ships to protect critical applications such as emergency lighting, navigation equipment, ship automation and HVAC applications against disruptive power interruptions are in use for the last few years [58]. A distributed energy storage configuration where energy storage units are available for individual load-zones, gives much more reconfiguration flexibility and a robust restoration capability in the case where a part of the ship has been damaged or hit. To demonstrate the effectiveness of the fault-aware-soft-restart method, the zonal energy storage system is used to re-energize the load zone, and then transfer the loads back to the main generator when the zone is phase- and voltage-matched to the main generator.

Table 4.3 summarizes the significance of using the fault-aware-soft-restart method for the three major types of facility island.

Table 4.3: Significance of Fault-Aware-Soft-Restart for different types of facilities.

System / Facility Type	Significance of Fault-Aware-Soft-Restart Method
Residential Facility	− Provides a method to implement the "bottom-up" power restoration strategy. − Controls the inrush current into the circuit while energizing, to improve system reliability. − Avoids delayed voltage recovery effect, which may lead to a voltage collapse.
Industrial Facility	− Controls the inrush current to avoid charges by the utility on peak current draw. − Avoid start-up costs and labor involvement.
Ship Power System	− Automated process, restore power within seconds. − Safely restores power to the load zone without overloading the generators, improving system reliability and survivability.

CHAPTER 5

5. TESTING OF THE SOFT-RESTART METHOD USING LARGE INDUSTRIAL MOTORS

This chapter discusses the process of soft-restart for three large (>200 hp) industrial motors of different sizes connected to the same bus as that of the energy storage system. The energy storage system inverter is controlled in an open-loop configuration to produce a linearly increasing V/Hz supply to pre-energize the motor load bus before transferring the loads to the utility. The effect of the soft-restart method on the bus voltage, load-current, torque and speed behavior of the motors is discussed. The speed and torque evolution of each motor are also shown when they are fed from the same inverter-controlled energy source. This exemplifies the effectiveness of this method for application in a load-zone / load-center containing assorted sizes of motor loads.

5.1. SOFT-RESTARTING ALGORITHM

We consider an industrial power network (IPN) that has a separate bus (IPN_Bus) powering only the large motors and having a local ESS for emergency power as shown in Figure 5.1. Islanded operation of this network is entertained in compliance with the standard 1547-2008 [13],[18]. Three induction motors (IMs) with different inertia constants are considered to study the effectiveness of the method. PMCU1 is located at Bus-1 which supervises the relay operation for CB1 and 2. While the computing and communication delays associated with the SVP are important, we assume that these can

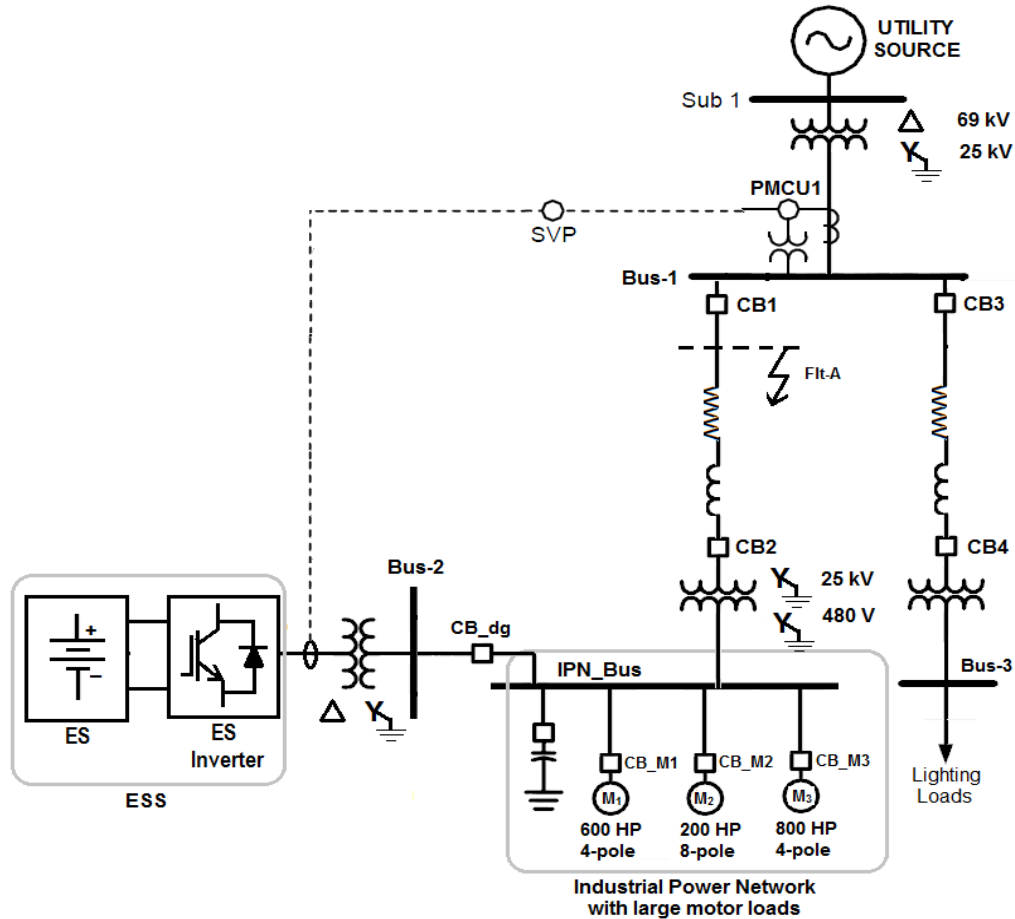be fast enough to not adversely affect our results.

Figure 5.1: Industrial power network with energy storage system and remote communication link.

5.1.1. CIRCUIT BREAKERS OPERATING SEQUENCE

We consider an external three-phase-to-ground fault (Flt-A) occurring somewhere between CB1 & 2. It is assumed CB1, CB2 and CB_dg operating requirements have been jointly developed by the utility and the ESS owner. The tripping operation of line protection equipment complies with Std. 1547, and the motor load contactors CB_M1, CB_M2 and CB_M3 comply with the requirements described in Std C37.96-2000 and Std 242-1986. The following steps take place during SR operation:

- CB1 and CB2 trips following Flt-A in response to overcurrent relay (67).

- CB_dg also trips within 0.16s in response to either the undervoltage relay (27) or the fault back-feed detection relay (67, 51V or 51N) [19],[25].

- With the SR mode activated, CB1 & 2 operation will be dictated by the control signals from PMCU1 thus preventing their automatic reclose. Following the tripping operation (described in 1 and 2), only CB_dg will be reclosed and the ESS inverter will power-up the IPN_Bus using an open-loop constant V/Hz control with the ESS inverter. This is in contrast to the conventional operating sequence where CB1 and CB2 will each attempt to reclose after 0.3s (considering the typical operating duty of medium voltage circuit breakers [14] and in accordance to ANSI c37.09).

- When IPN_Bus frequency and voltage is within the tolerance levels to reconnect with the grid, the ramp-up process ends. The IPN_Bus frequency (and voltage) is maintained at its final value for a few cycles to allow the motors to settle down to their nominal speeds.

- Synchronization process is then started by stepping up the frequency of the ESS inverter. The voltage phase from PMCU1 (Φ_1) and inverter terminals (Φ_2) are now used to detect $\Delta\boldsymbol{\Phi} = \boldsymbol{\Phi_1} - \boldsymbol{\Phi_2}$ through SVP. When $\Delta\Phi$ becomes zero, SVP generates a the signal for PMCU1 which drives the service restoration relay 25 to reclose CB1 & 2 and trip-off CB_dg. This transfers the load on the IPN_Bus to the utility source.

Figure 5.2 shows the operational flowchart for the soft-restart algorithm based on the system shown.

5.1.1. OPERATING SEQUENCE OF CBS FOR THE TEST CASES:

Following are the steps that take place during the SR method (also shown in Figure 5.2): A self-clearing 10 cycle 3-phase-to-ground fault (Flt-A) is applied between CB1 and CB2 at $t_{flt} = 3$ s.
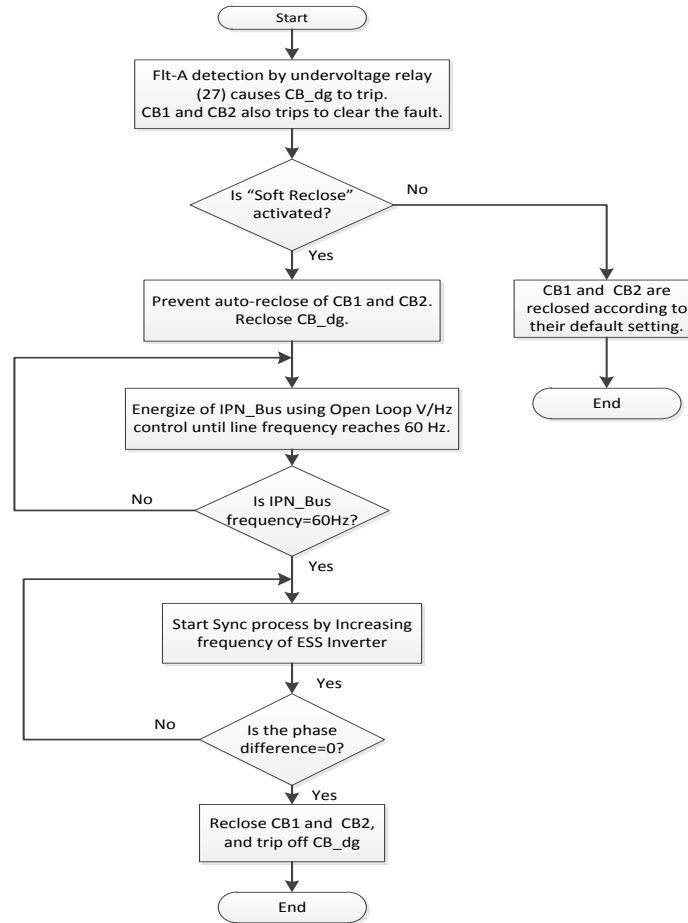

Figure 5.2: Operational flowchart for the Soft-Restarting process.

- Considering an interrupting time of 3 cycles for CB1 & 2, Flt-A is cleared at t_{CBss_open} = t_{flt} + 3/60 = 3.05 s.

- With conventional reclosing method CB1 & 2 are reclosed after 0.3 s i.e at 3.3 s.

- When SR mode is selected, CB_dg is closed and power ramp-up of IPN_Bus starts after 3 s, at $t_{sr\_start} = t_{CBss\_open} + 3\ s = 6.05\ s$.

- A ramp-up time of $T_{ramp} = 2\ s$ is selected for the SR method. This produces a linearly increasing V/Hz source with 196 V/s and 30 Hz/s, voltage and frequency slopes respectively. The IPN_Bus reaches 60 Hz and rated voltage of $V_{LL} = 480\ V$ at $t_{sr\_end} = t_{sr\_start} + T_{ramp} = 8.05\ s$.

- The synchronizing process starts by stepping up the inverter frequency (f_{ESS}) by 0.5 Hz at $t_{sync} = t_{sr\_end} + 0.1\ s = 8.15\ s$.

- Depending on the phase difference between V_{bus1} and V_{IPN_bus} phase-synchronization will occur within:

$$T_{max} = \frac{1}{f_{ESS} - f_{grid}} s = 2\ s \qquad (5.1)$$

Where $f_{grid} = 60$ Hz and $f_{ESS} = 60.5$ Hz.

- In our simulation the matched phase occurs at 8.76 s for case 1 and case 2. A true value for a matched phase drives the relays to reclose CB1 & 2 and trips off CB_dg to transfer the load to utility source.
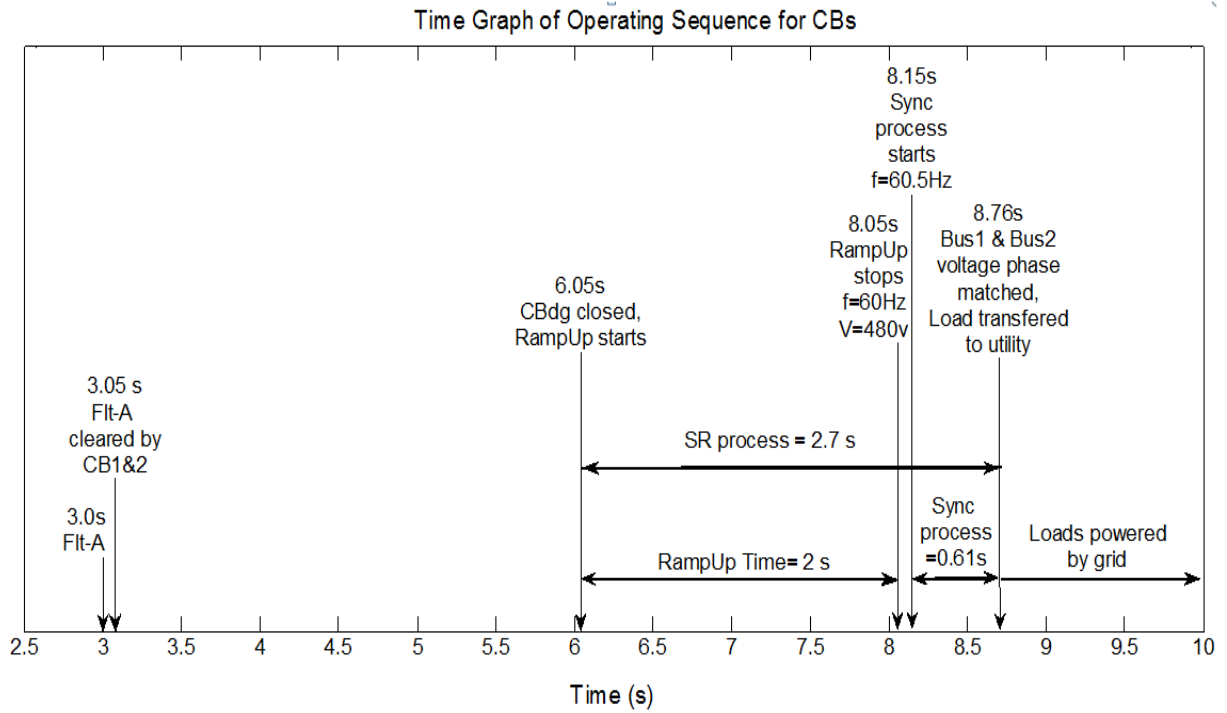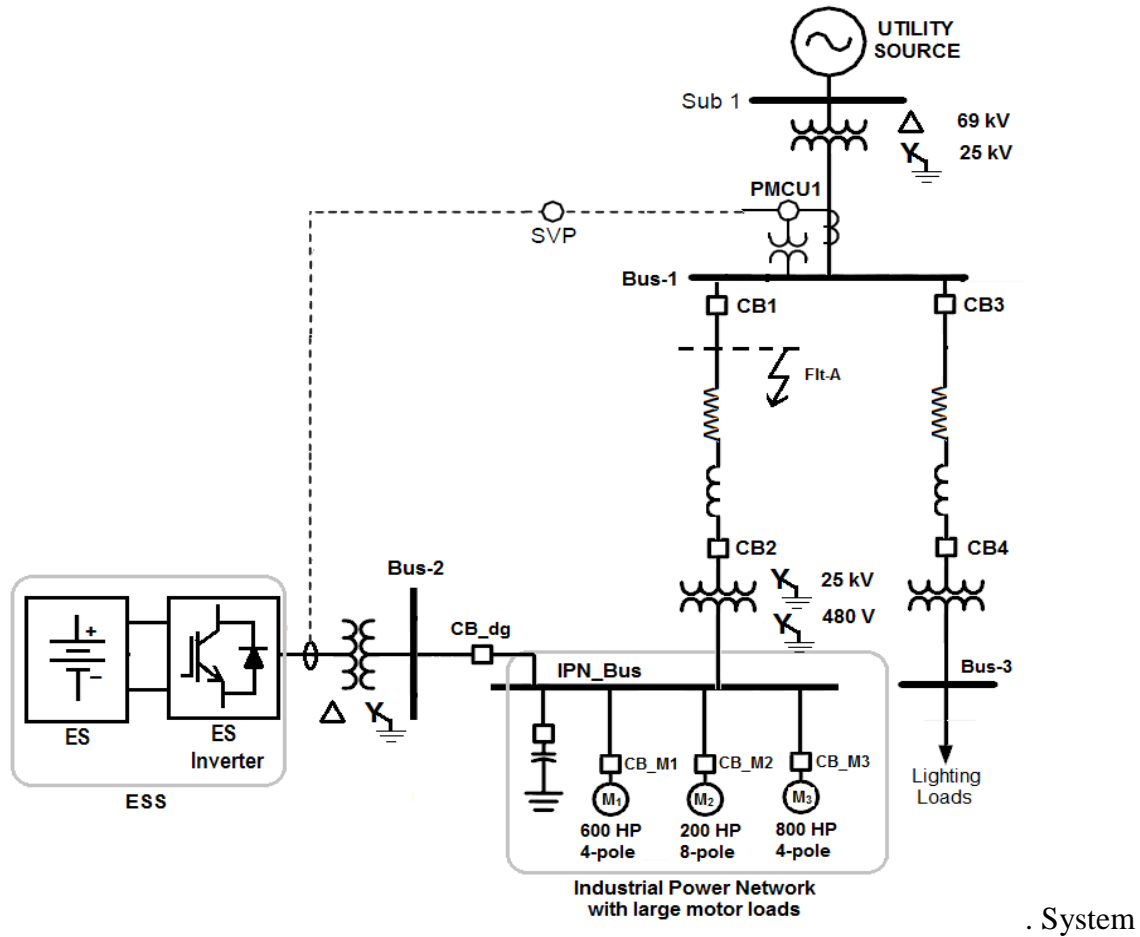
Figure 5.3: Time graph of operating sequence for CBs.

5.2. SIMULATION RESULTS

All simulations are done in Matlab Simulink to validate the SR method using the system shown in Figure 5.1

41

. System

and motor parameters are given in Table 5.1.

Three industrial grade squirrel cage IMs in the same bus with typical load inertias are used for simulation tests [59]. The following two test cases are considered to understand system behavior and advantages of SR method over the conventional method:

Case-I: Using only motor M3 (800 HP, H=0.164 s) as load, conventional and SR method are compared, and motor speed, torque, stator current and bus voltage are studied.

Case-II: Only M1 (600 HP, H=0.145 s) and M2 (200 HP, H=0.1086 s) are used and started at the same time using conventional and SR methods. Motor

speeds, torque oscillations, line current and bus voltage are studied.

Table 5.1: System and Motor Parameters

Parameters	Values		
Base Power (kVA)	600		
Base Voltage (V)	480		
Motors	M1	M2	M3
Rated power (HP)	600	200	800
PF (at rated speed)	0.8	0.8	0.8
Voltage (V)	480	480	480
Frequency (Hz)	60	60	60
Rated Current (A)	1732	577	2308
Rated Speed (rpm)	1780	890	1786
Number of poles	4	8	4
Rotor+Load Inertia (kg-m^2)	6	4	6
H (s)	0.145	0.1086	0.164
Load Constant B_l (N.m/(rad/s)^2)	0.07618	0.192	0.1097
R_s (Ω)	0.0076	0.0229	0.0057
R_r (Ω)	0.006	0.018	0.0045
L_{Ls} (H)	0.000178	0.000534	0.000371
L_{Lr} (H)	0.0001	0.000313	0.0000078
L_m (H)	0.0049	0.0147	0.0037

5.2.1. LOAD MODEL

A simple pump type load is considered. The load torque on the shaft is defined by

$$T_L = B_l \omega_m^2 \quad \text{N-m} \tag{5.2}$$

Where, ω_m : rotor speed in rad/s,

B_l : Load constants in N.m/(rad/s)^2, with values given in Table 5.1.

5.2.2. M3 START UP WITH CONVENTIONAL AND SOFT-RESTARTING

Figure 5.4 and Figure 5.5 shows start-up characteristic of M3 with conventional and soft reclosing.
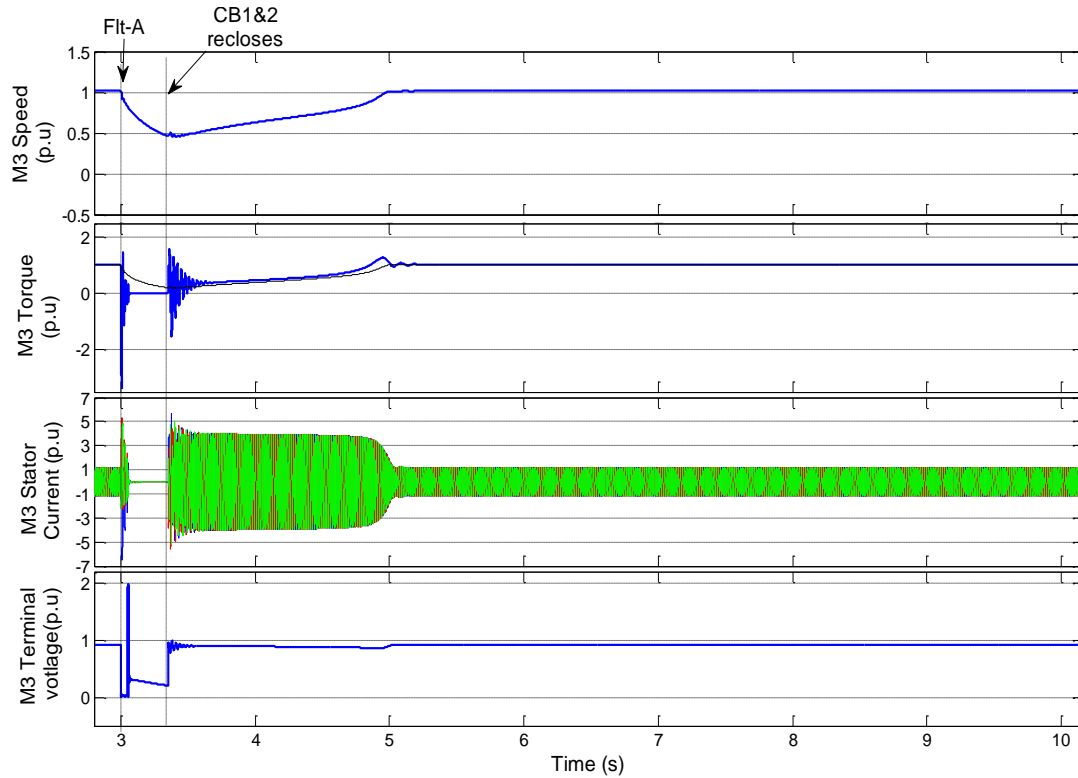
Figure 5.4: Motor M3 restart with conventional reclosing causing high starting inrush currents and torque transients.

Figure 5.4 shows the large inertia does not allow the motor to reach zero speed before the first reclosing of CB1 and CB2 is attempted. The starting current inrush of about 5 p.u is also accompanied by a 2 p.u torque pulsation during reclosing.

Figure 5.5 shows the same motor starting up with SR method. As described in the algorithm, CB1 & 2 are not allowed to reclose automatically, and instead CB_dg is closed at 6.05 s.

The ESS inverter starts operating in the open loop V/Hz control and drives the line frequency to 60 Hz. With a 2 s ramp-up time the stator current never exceeds 1 p.u except at the very first cycle where it is about 2 p.u.

Voltage dip at the motor terminals (also the IPN_Bus in this case) drops below 0.9 p.u as shown in Figure 5.6..
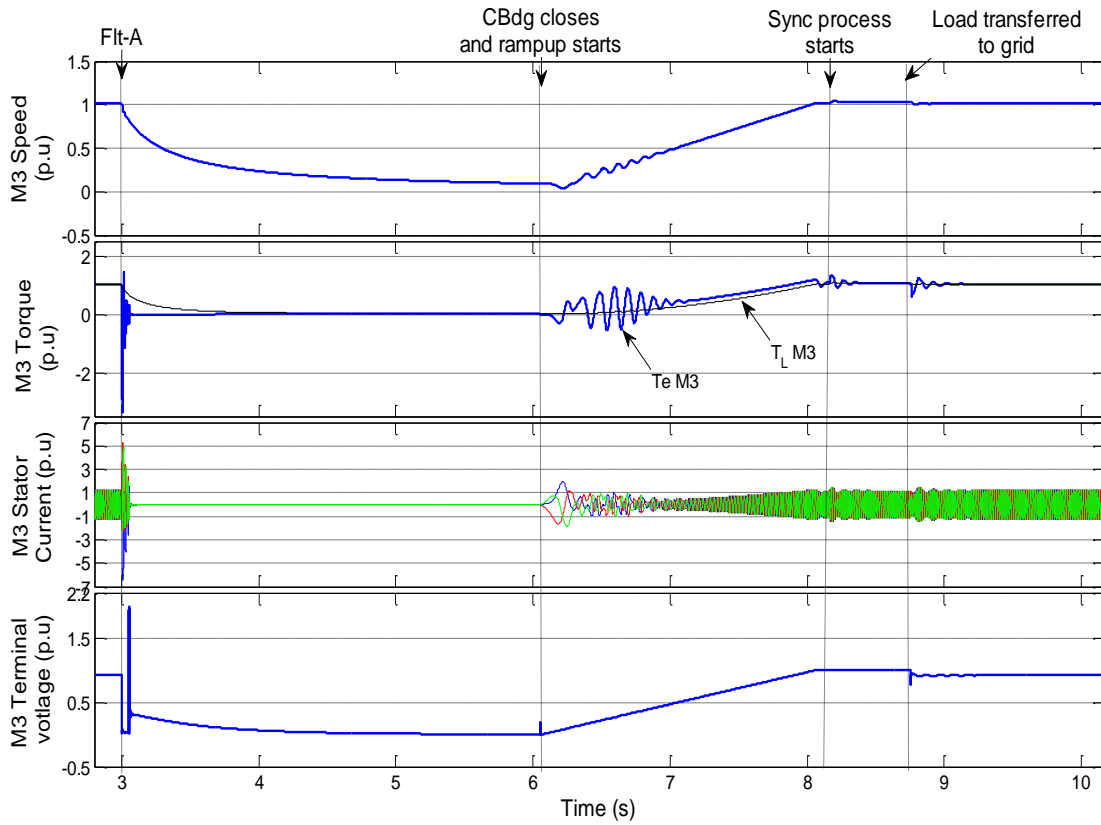
Figure 5.5: M3 starting-up using soft-restarting, following Flt-A. ($T_{e\,M3}$ and $T_{L\,M3}$ are motor and load torques respectively).
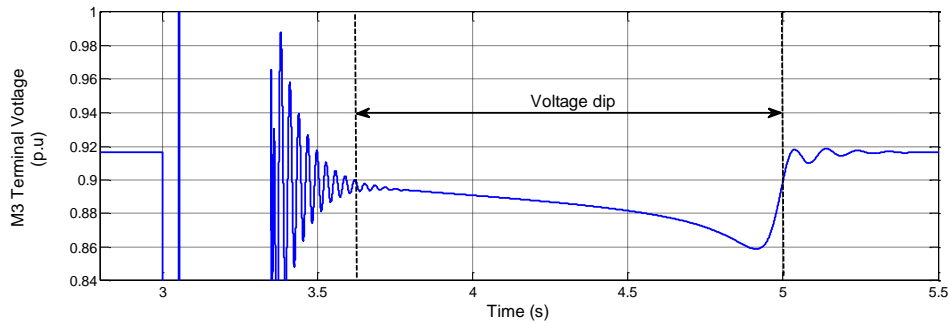

Figure 5.6: Voltage dip during M3 start-up following Flt-A using conventional reclosing.

5.2.3. M1 AND M2 START UP WITH CONVENTIONAL AND SOFT-RESTARTING

5.2.3.1. CURRENT TRANSIENTS AND VOLTAGE DIP

In Figure 5.7 and Figure 5.8 line current and IPN_Bus voltage is shown when CB1 & 2 are reclosed automatically and, using the soft-restart method.

Comparing the line currents in Figure 5.7 and Figure 5.8 for both methods, we find that for the case when soft-restart is used the line currents never actually increase beyond 1 p.u, except during the first cycle where it reaches about 2 p.u.
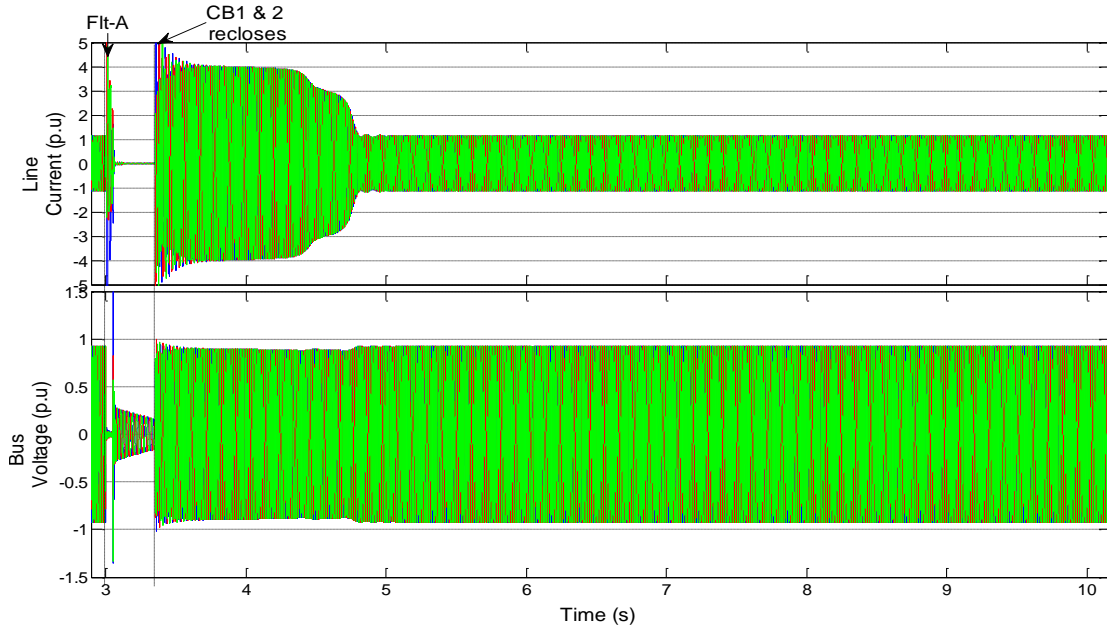

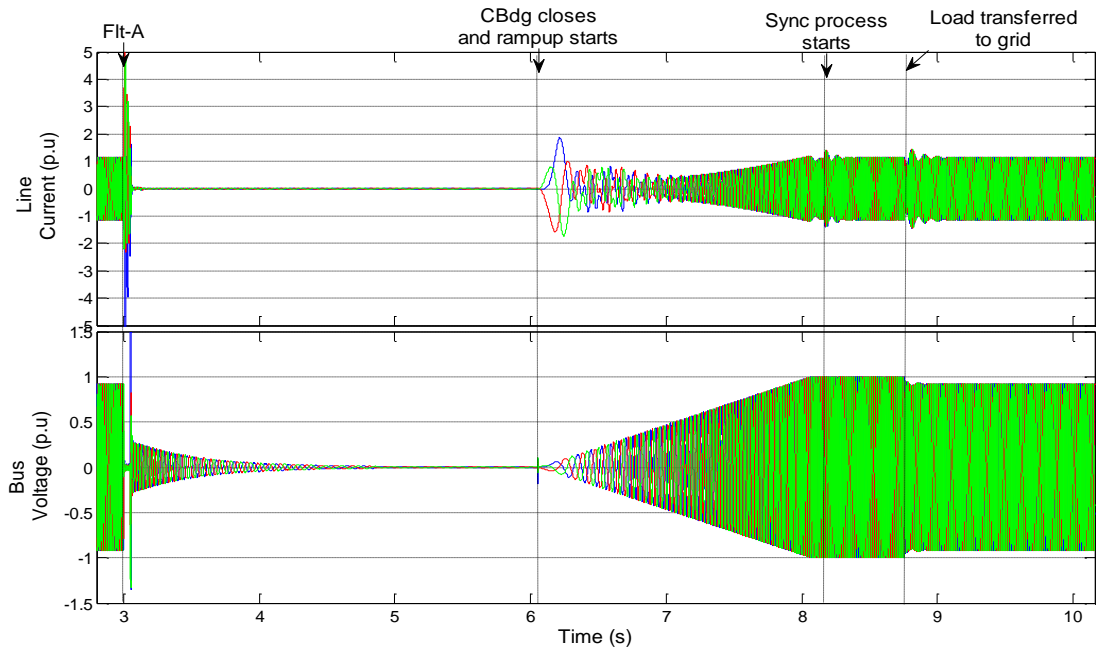Figure 5.7: Line current and IPN_Bus voltage during conventional start-up of M1 and M2.

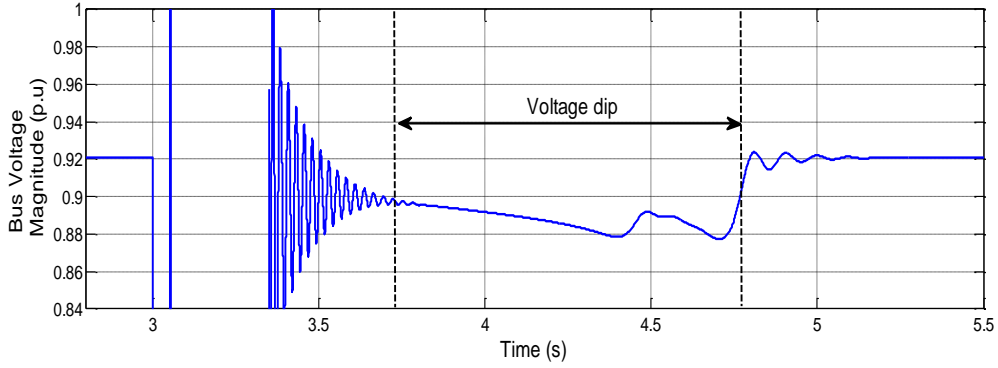Figure 5.8: M1 and M2 start-up using Soft-Restarting, following Flt-A.

Figure 5.9: Voltage dip during start-up of M1 and M2 following Flt-A.

Associated with the starting current transients the IPN_Bus voltage also goes below 0.9 p.u as shown in Figure 5.9 which is not a problem when SR method is used. Although the acceleration time is extended (2.71 s for SR method compared to about 2 s for conventional method) the motors will not suffer from heating problems. This is because, the reduced current does not lead to increased heating, but rather to a cooler acceleration for the motor [55].
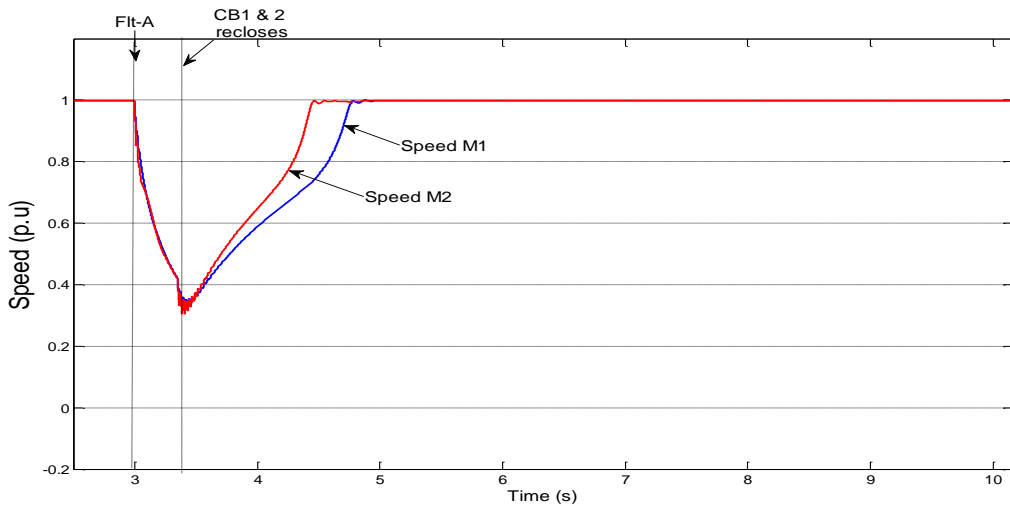

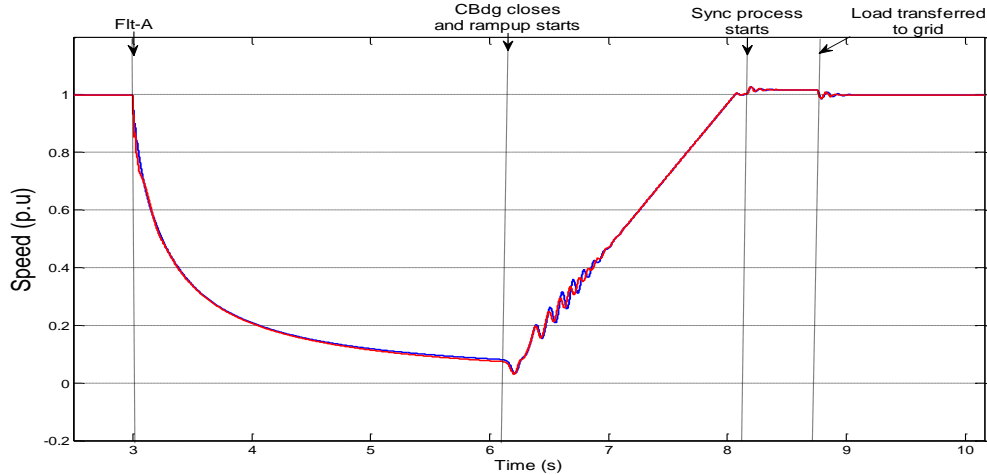Figure 5.10: Speed of M1 & M2 during conventional reclosing.

Figure 5.11: Speed of M1 & M2 during soft-restarting.
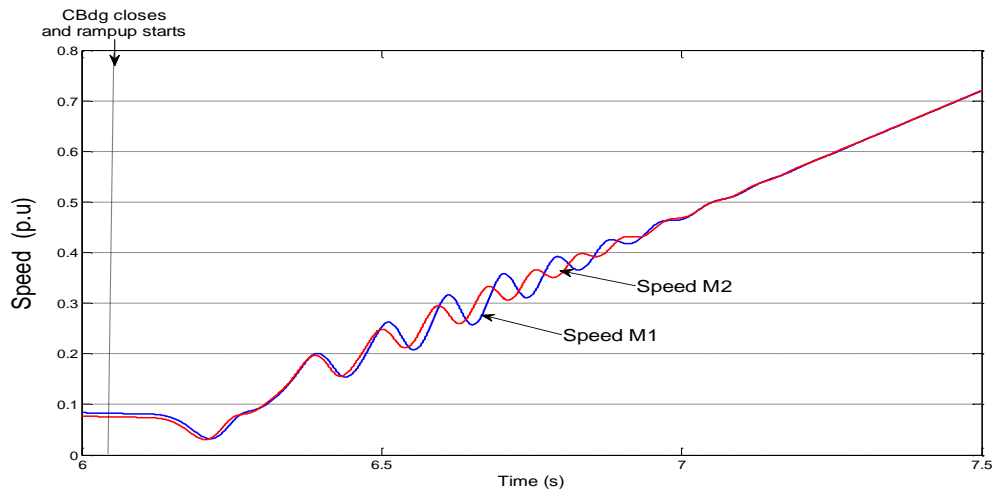
Figure 5.12: Speed of M1 & M2 during soft-restarting.

5.2.4. SPEED CHARACTERISTICS

Speed of M1 and M2 following Flt-A is shown in Figure 5.10 and Figure 5.11 for both methods. In Figure 5.11, for conventional method the speed of M1 & M2 decays together to about 0.4 p.u when CB1 & 2 are reclosed. During the speed up process, M2 having a lower inertia reaches nominal speed faster than M1 as expected.

Figure 5.10 and Figure 5.11 also shows the effect of different inertias on motor speed. During the first half of the start-up process (6.05 s to about 7.05 s) speeds of M1 and M2

48

evolve differently due to the difference in their torque angles (see Figure 5.12). The magnitude of this difference will be higher for motors with higher inertia constants.

5.2.1. MOTOR TORQUES

From comparison of Figure 5.13 and Figure 5.14, we see large torque oscillations at the instant of auto-reclose of CBs. The oscillations die down quickly but the magnitudes of these oscillations are enough to cause damaging forces on the mechanical systems connected to the motors.

When SR method is used the torque oscillations are clearly much lesser as seen in Figure 5.14. These oscillations will cease to exist after the first half of the start-up process has elapsed, which is after 1 s in this simulation. The following provides an explanation of this phenomenon:

Angle θ_r of rotor field current I_r with respect to the stator (airgap) voltage E_{ag} can be written as:

$$\cos \theta_r = \sin(90^0 + \theta_r) = \sin \delta \qquad (5.3)$$

Where, δ is the torque angle.

The relation of δ with the produced torque is given by:

$$T_{em} = K_1 \Phi_{ag} I_r \sin \delta \qquad (5.4)$$

Where, Φ_{ag} is the airgap flux and K_1 is a proportionality constant [60].

So unless the rotor speed (or the rotor field) is at least equal to the speed of the stator field, T_{em} will continue changing its direction producing the oscillations. In other words, for the torque oscillations to die down, δ has to be lower than 180^0 (or $\sin \delta > 0$). Clearly motor M1 with higher load inertia produces higher torque pulsations as expected.
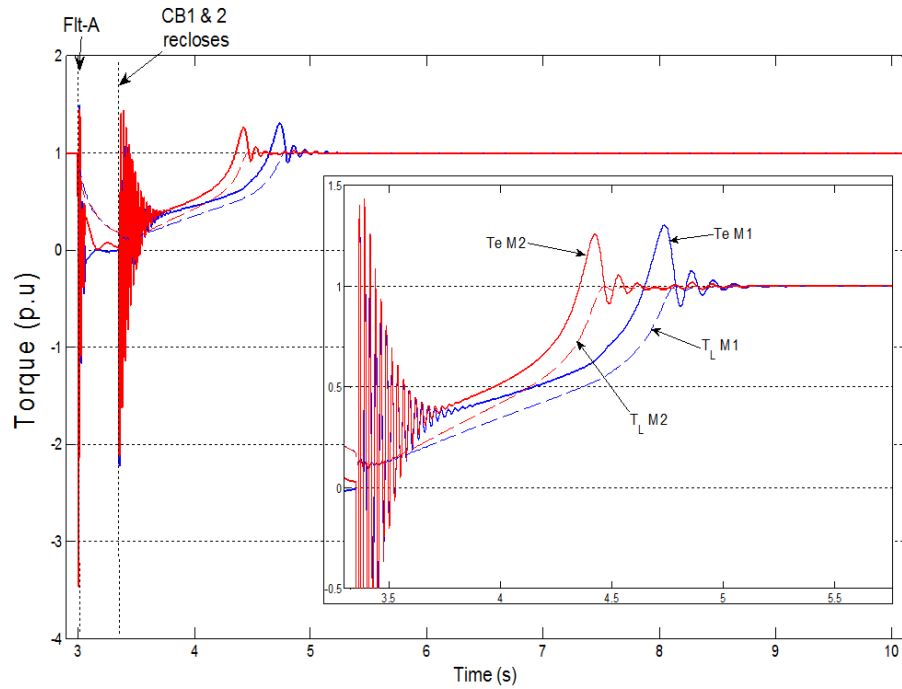
49

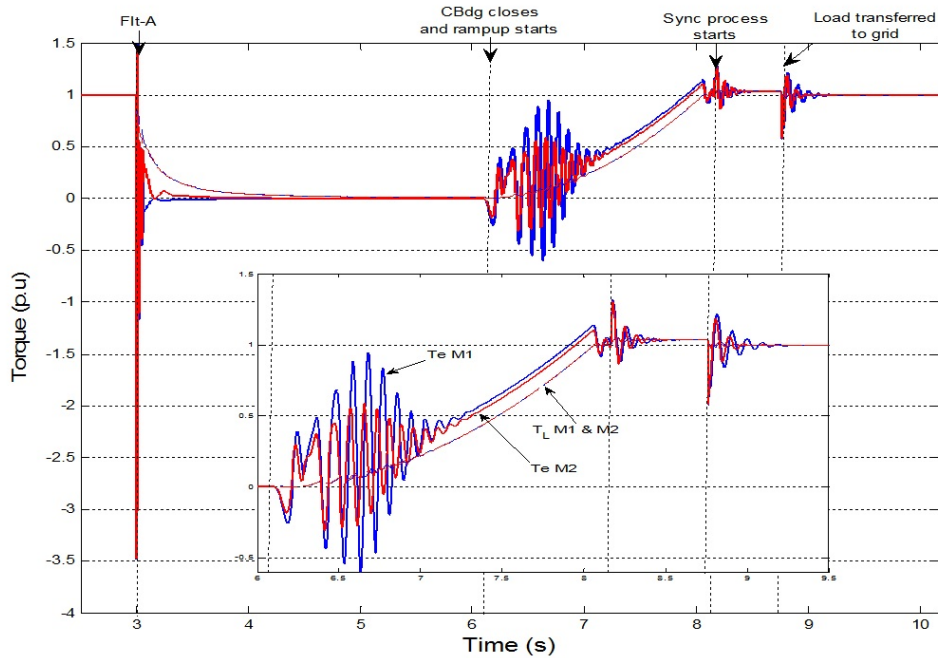Figure 5.13: Produced torques (TeM1 and TeM2) and Load torques (TL_M1 and TL_M2) during conventional reclosing.

Figure 5.14: Produced torques (T_{eM1} and T_{eM2}) and Load torques (T_{L_M1} and T_{L_M2}) during soft restarting.

5.3. CONCLUDING REMARKS

The transient-free service restoration for a variety of large industrial motors is presented in this chapter. Induction motors which has the most serious operational challenges during service restoration is considered for the study cases. State-of-the-art protection relays and communication links are utilized to supervise the operation of CBs and ensure successful and a seamless load-transfer to the utility. Simulation results show the transient-free operation during *energization* and *transfer* of loads. With the open-loop V/Hz control, the total time required for completion of the SR process is about 2.71 s. This value is much less than the typical time setting (~10 s) in the commercially available soft-starters installed for single motors [61]. With large scale energy storages gaining popularity and new standards continue to develop for parallel operation of DGs, soft-restart method will have a wide application area in the near future.

CHAPTER 6

6. EXTENSION OF THE SOFT-RESTART METHOD FOR APPLICATION IN AN INDUSTRIAL POWER SYSTEM USING A CURRENT-FED VOLTAGE CONTROLLED INVERTER

In this chapter the effectiveness of the Soft-Reclosing method is studied using a power system network which is representative of a plastic/rubber manufacturing plant. The process eliminates a number of problems and minimizes the losses due to power outages and momentary interruptions through fast and automated service restoration. Aggregated models of both line-connected and motor drives are considered along with building services loads. The results show significant reduction in current spikes, voltage dips, motor torque, speed, power factor fluctuations and most importantly, process downtime compared to a conventional manual restart process.

In the previous chapter, successful implementation of this method to provide a soft-restart for some large industrial motors has been shown using an open-loop control for the inverter. This chapter extends the method by using a current-fed voltage control-loop to provide a faster service restoration and load-transfer, with negligible current transients utilizing a closed-loop current control for the inverter. The starting inrush current into the loads is controlled by adjusting the voltage and frequency acceleration during the restoration process.

6.1. THE INDUSTRIAL POWER SYSTEM

The industrial system is shown in Figure 6.1. The system is a simplified and scaled-down version of a typical plastic product manufacturing plant. The power system shows line-connected motors in Bus_L1 which requires manual restart, and motors in the production line in Bus_P2 with their typical applications. The ESS is connected to the service entrance bus as an auxiliary source and is able to power the motors in Bus_L1, Bus_P2 and building services loads in Bus_S4.

6.2. OPERATING PRINCIPLE

The sequence of operation that takes place during the process is shown in Figure 6.2. Referring to Figure 6.1, we consider a 3 phase to ground fault (Flt-A) of 15 cycle (0.25 s) duration occurring on the feeder line between CBs 1 and 2. Fault clearing time for CBs 1, 2 and CB_main is 3 cycles (typical duty of medium voltage CBs). The operating duty for the CBs is as follows: O - 0.3 s - CO – 3 min –CO, [14]-[15].

The sequence of operation is described below:

1. t_0: A 3-phase-to-ground fault occurs at location Flt-A.

2. t_1: CB1 and 2 trips to clear the fault in 3 cycles. CB_main also trips in response to the undervoltage relay. As SR is enabled, CB_main stays open even after the utility voltage has been restored (i.e successful reclose of CB1 and 2).

3. t_2: voltage magnitude (V_0) and frequency (f_0) at Bus-1 is measured. CB_ES is closed and the inverter energizes Bus-1 with a constant V/Hz ramp starting at a magnitude of V_0 and f_0. The load current supplied by the inverter is controlled by adjusting the slope of the voltage V(t) and frequency f(t) ramps, until they reach 1 p.u. and 1.02

p.u. respectively. The inverter frequency of 1.02 p.u is chosen to achieve synchronization with the utility votlage.
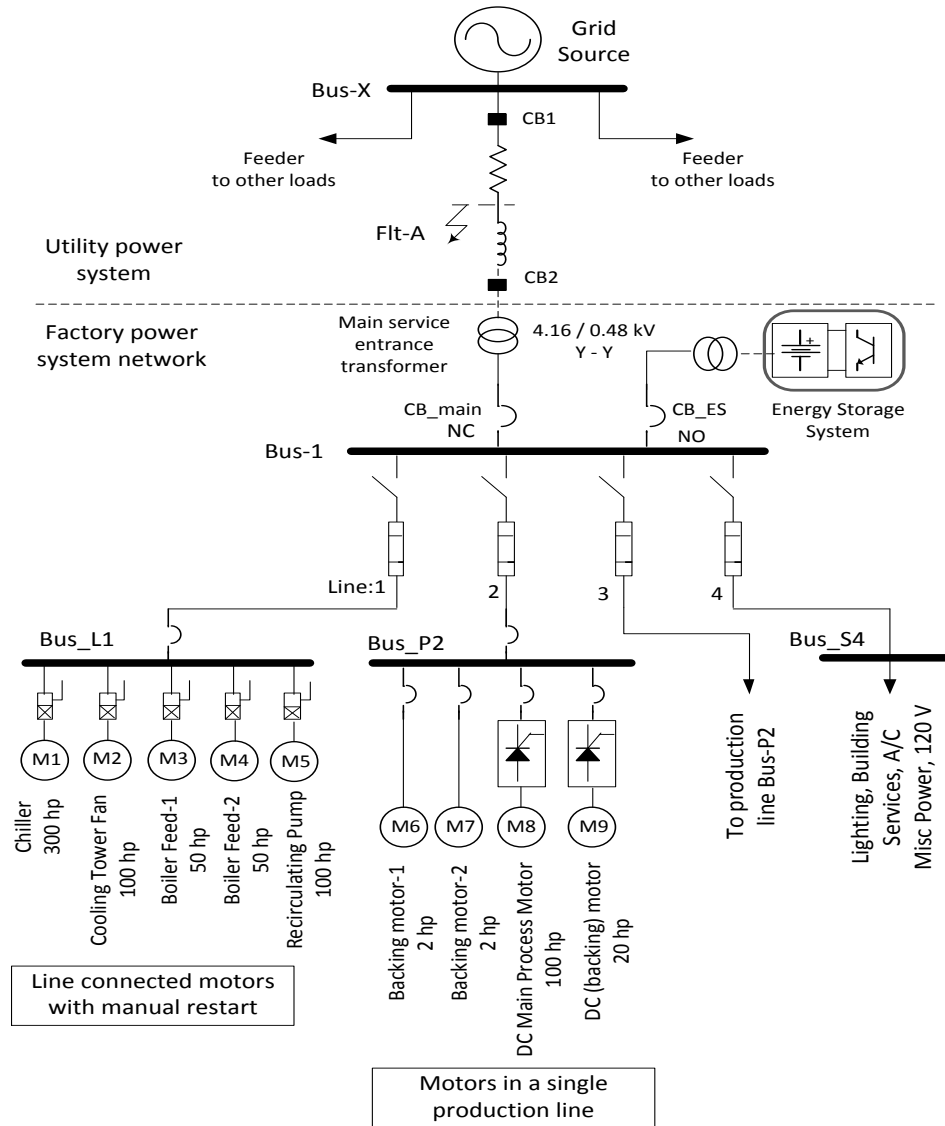

Figure 6.1: Typical industrial power system with line-connected and electronically-controlled motors.

4. **t₃**: voltage at Bus-1 reaches 1.0 p.u and the sync-check relay is activated to check for a voltage phase match across CB_main.

5. **t₄**: frequency at Bus-1 reaches 1.02 p.u.

6. **t₅**: voltage phase across CB_mains are equal, and the sync-check relay initiates the load transfer to the grid by reclosing CB_main and tripping off CB_ES.
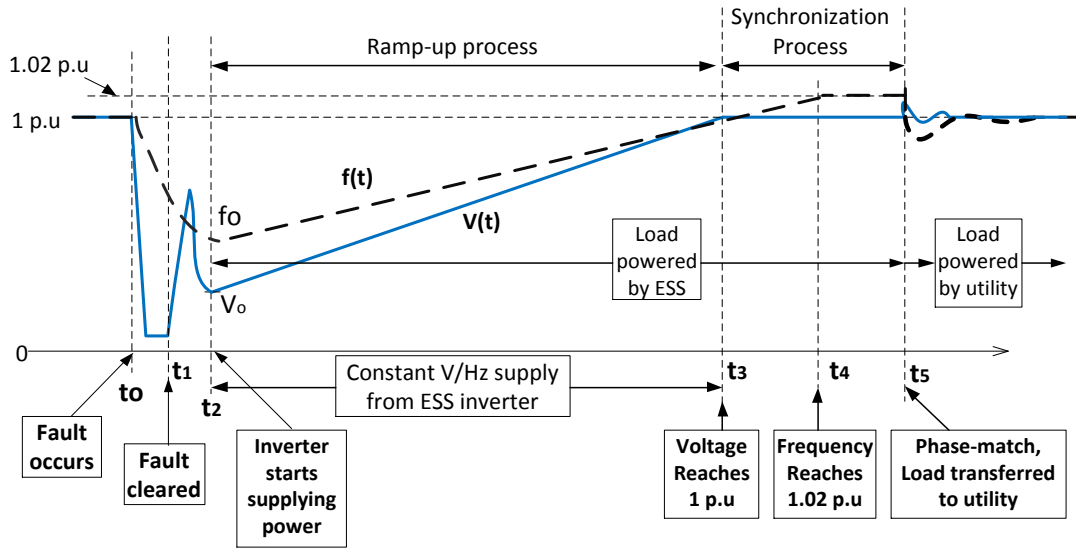

Figure 6.2: Principle of Soft-Reclosing.

6.3. CONTROL DEVELOPMENT

Figure 6.3 shows the control schematic for the ESS inverter and Figure 6.4 shows a simplified power system of the plant shown in Figure 6.1, with the required measurements.

It is necessary to detect the residual motor voltage (V_{abc_line}) and frequency (ω_{line}) at Bus-1 in order to drive the loads appropriately and prevent the motor from decelerating further in the post-fault condition.

The voltage at V_{abc_line} is the residual motor voltage as all motors are connected to the same bus. The method is highly dependent upon the accurate detection of the post-fault frequency ω_{line}. A synchronous reference frame PLL (SRF-PLL) can be employed for this purpose which is well suited for this variable frequency application and because it better rejects harmonics, notches and other kinds of disturbances [62].
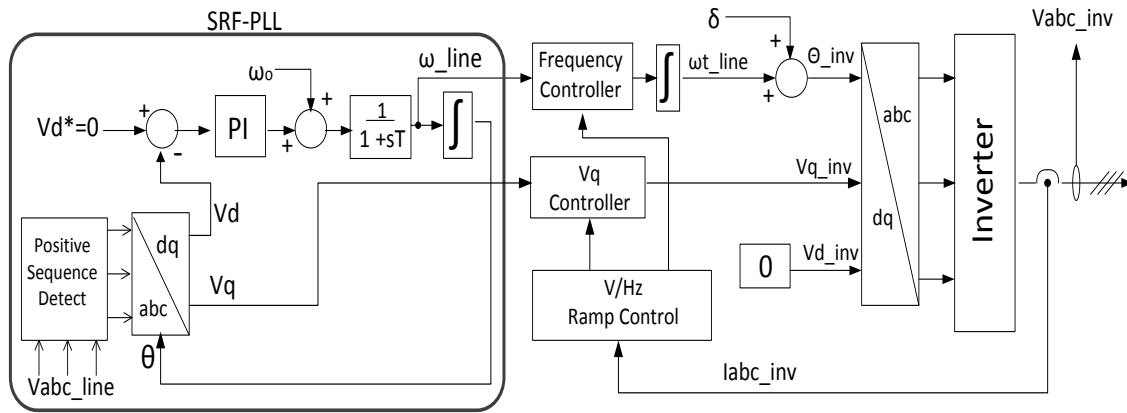
Figure 6.3: Energy Storage System Control Schematic.
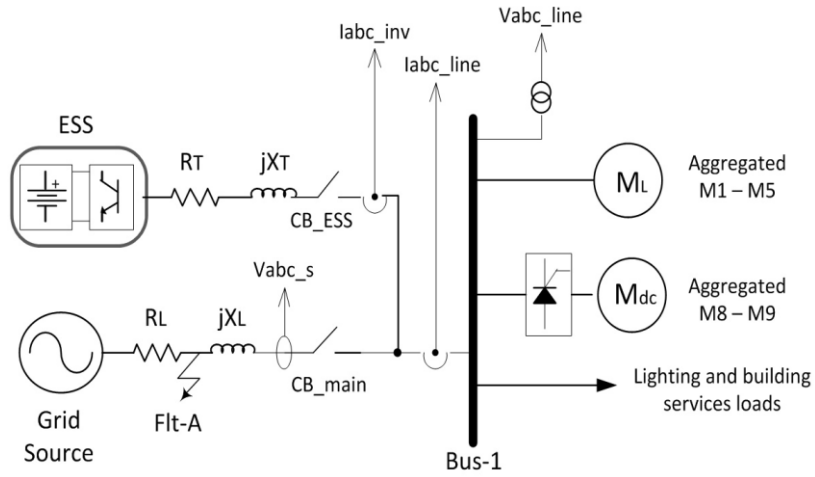
Figure 6.4: Simplified test system of the industrial power network (shown in Fig.1) and required measurements.

A positive sequence detection of the line voltage V_{abc_line} is used in conjunction with the PLL to overcome grid unbalance [63]. V_d^* is set to zero, to obtain exact phase match condition as required by the SRF-PLL.

The coupling transformer impedance R_T+jX_T causes a small phase shift δ between V_{inv} and V_{abc_line}.

6.3.1. CONTROL VARIABLES

As shown in Figure 6.3, the current feedback is only used to adjust the V/Hz ramp. An open loop V/Hz supply is generated by the ESS inverter to power up Bus-1. The control variables are obtained by abc→dq transformation. V_q and ω_{line} obtained from the PLL and used as the inputs to the frequency and V_q controller. V_d is not used to adjust the magnitude and frequency of the V/Hz ramp and is set to zero

$$V_{d\_inv} = 0 \tag{6.1}$$

We can then define the inverter output voltage magnitude as:

$$|V_{inv}| = V_{q\_inv} \tag{6.2}$$

Park's transformation gives the line voltages in dq variables:

$$V_{q\_line} = \sqrt{2}\,V_{\mathbf{abc\_line}}\cos[(\omega_{line} - \omega_{inv})t + \theta_{line0} - \theta_{inv0} + \delta] \tag{6.3}$$

$$V_{d\_line} = \sqrt{2}\,V_{\mathbf{abc\_line}}\sin[(\omega_{line} - \omega_{inv})t + \theta_{line0} - \theta_{inv0} + \delta] \tag{6.4}$$

Where, $V_{\mathbf{abc_{line}}}$: (rms) magnitude of line-to-neutral voltage at Bus-1.

ω_{line} and ω_{inv} are the detected line frequency and inverter output frequency respectively.

θ_{line0} and θ_{inv0} are (phase-angle) constants, determined from initial values.

δ is the voltage angle between V_{abc_line} and V_{inv} with phase angle of 0^0 referred to the ESS bus. We select time zero such that $\theta_{line0} = 0$ and $\theta_{inv0} = 0$

And let

$$\sqrt{2}\mathbf{V}_{\textbf{abc\_line}} = V_m \tag{6.5}$$

So (6.3) becomes:

$$V_{q\_line} = V_m \cos[(\omega_{line} - \omega_{inv})t + \delta] \tag{6.6}$$

And, since the d-axis voltage will not be used as a control variable, we will only use (6.6) for further analysis.

Referring to the generalized diagram in Figure 6.4, V_m is obtained from the measurements at Bus-1 and fed to the ESS PLL to obtain ω_{line}. In the PLL-locked condition, i.e when ω_{line} is being accurately tracked:

$$\omega_{line} = \omega_{inv} \tag{6.7}$$

(6.6) can then be written as the following phasor during steady-state operation:

$$\overrightarrow{V_{q\_line}} = \mathbf{V}_m \, e^{j\delta} \tag{6.8}$$

The inputs to $\mathbf{V}_q$ and frequency controller are $\mathbf{V}_{q\_line}$ and ω_{line}. And

$$\theta_{inv} = \omega t_{line} + \delta \tag{6.9}$$

(6.8) and (6.9) are the control variables for the inverter.

The phase angle (δ) is known from the transformer coupling impedance $R_T + jX_T$.

Figure 6.5 shows the power flow direction when the ESS energizes Bus-1. Voltage phasors for the Bus-1 voltage ($\mathbf{V}_m$), and $\mathbf{V}_{inv}$ during the steady-state (when bus-1 is supplied by the utility source) and when the ESS inverter is used to power the segmented network, are shown in Figure 6.6.
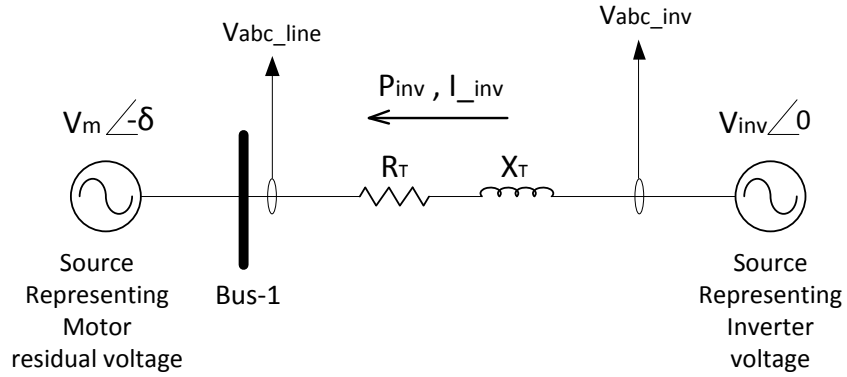
Figure 6.5: Single line diagram showing the relationship between voltage phasors for motor residual voltage and inverter output voltage.
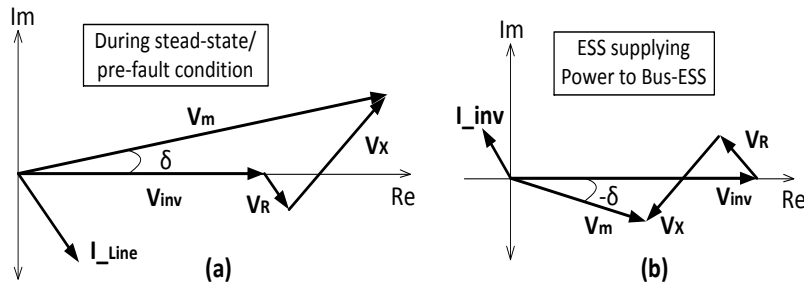

Figure 6.6: Voltage phasors for V_{inv} and V_m when ESS supplies Bus_ESS. (not to scale, phase angles are exaggerated).
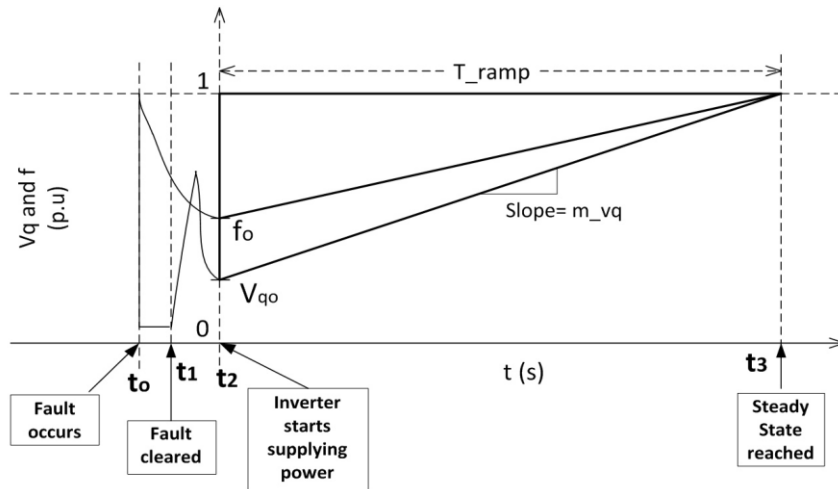
Figure 6.7: Constant V/Hz ramp applied to bus-1.
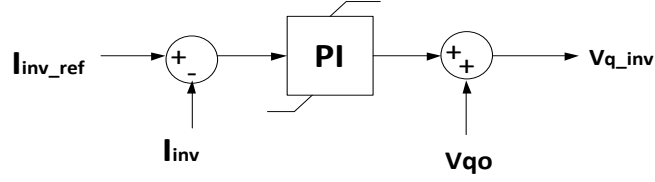
Figure 6.8: V_q controller.

(6.8) gives the voltage phasor measured at Bus-1 seen from the inverter terminals during steady state (pre-fault) condition.

6.3.2. START OF ESS SUPPLY

When ESS starts to supply power to Bus-1, the inverter voltage phasor is written as:

$$\overrightarrow{V_{inv0}} = \mathbf{V_{m0}} \, e^{-j\delta} \tag{6.10}$$

Where, $\mathbf{V_{m0}}$: (rms) magnitude of line-to-neutral voltage at Bus-1 at time t2. And, with (6.2) being true, the reference voltage for the inverter drive at t_2 will be:

$$V_{q\_inv}(t_2) = \mathbf{V_{m0}} = \mathbf{V_{q0}} \tag{6.11}$$

And the angle input to the inverter,

$$\theta_{inv}(t_2) = \omega t_{line} - \delta \tag{6.12}$$

Between the times t_2 and t_3 (during T_{ramp}), $V_{q_{inv}}$ and θ_{inv} are controlled using the V/Hz Ramp Control only, which is described next.

6.3.3. OPERATION DURING T_{RAMP} (V/HZ RAMP CONTROL)

The voltage and frequency ramps initiated by ESS inverter following the fault is shown in Figure 6.7. The decaying voltage and frequency at time t_2, given by V_{q0} and f_0 respectively, have a non-linear relationship that will highly depend on the inertia of the motor load(s) connected.

60

Acceleration of $V_q(t)$ is controlled by a simple PI controller shown in Figure 6.8 and driven by the current error between I_{inv_ref} and I_{inv}. I_{inv_ref} is set by the user. So $V_q(t)$ is defined by:

$$V_q(t) = V_{q_{inv}}(t) = V_{q0} + m_{Vq}t \qquad (6.13)$$

$$for: t_2 < t \leqslant t_3$$

Where, m_{Vq} is the slope of the voltage ramp and adjusted by the PI controller. T$_0$ ensure a constant V/Hz operation and for

$$V_{q\_inv}(t_3) = f_{inv}(t_3) = 1\, p.u \qquad (6.14)$$

we develop the following relationship:

$$f_{inv}(t) = 1 - \frac{1}{K_0}\left[1 - V_{q_{inv}}(t)\right] \qquad (6.15)$$

$$for: t_2 < t \leqslant t_3$$

Where, f_{inv}: inverter output frequency in p.u.,

$$K_0 = \frac{1 - V_{q0}}{1 - f_0} = constant \qquad (6.16)$$

Eq (6.15) is used to determine $f_{inv}(t)$ which is used to determine the angle input (θ_{inv}) to the inverter from:

$$\omega t_{line} = 2\pi \int f_{inv}(t)\, dt \qquad (6.17)$$

6.3.1.   ENERGY REQUIREMENT FOR THE ESS

The total energy required to carry out the SR process depends upon T$_{ramp}$, and the

time required to achieve a phase-matched condition with the live bus (T_{sync}) as shown in Figure 6.9. During the ramp-up process, inverter output current magnitude (I_{inv}) is kept to a constant value I_{ref}. We neglect the transients in the current magnitude $I_{inv}(t)$ and approximate a linear power ramp during T_{ramp}. The energy required during the ramp-up period T_{ramp} is given by:

$$E_{ramp} = \int_{t_2}^{t_3} P_{inv}(t)dt = 3I_{ref} \int_{t_2}^{t_3} V_{inv}(t)dt \tag{6.18}$$

And, the energy required during the synchronization period T_{sync} can be calculated as:

$$E_{sync} = P_{inv} * T_{sync} \tag{6.19}$$

The total energy requirement for the SR process is:

$$E_{ESS} = E_{ramp} + E_{sync} \tag{6.20}$$

In (6.20) Tsync shall have an arbitrary value and depends on the phase difference:

$$|\Phi_{inv}(t_5) - \Phi_{Vs}(t_3)| \tag{6.21}$$

Where, $\Phi_{inv}(t_5)$ is the phase of $V_{inv}(t)$ at time t_5 and

$\Phi_{Vs}(t_3)$ is the phase of $V_s(t)$ (voltage at the live bus) at time t_3.

The maximum energy required before a phase match occurs can be calculated from:

$$E_{sync\_max} = P_{inv} \left[\frac{1}{f_{inv\_max} - f_{inv}(t_3)} \right] \tag{6.22}$$

Where f_{inv_max} is the maximum frequency generated by the inverter at time t_4 to obtain synchronization, and

$$f_{inv}(t_3) = rated\ frequency = 60\ Hz \tag{6.23}$$

Neglecting the losses in the inverter, and to carry out the soft-reclosing process, the required power rating of the ESS (P_{inv}) must be at least equal to the total loads at Bus-1.
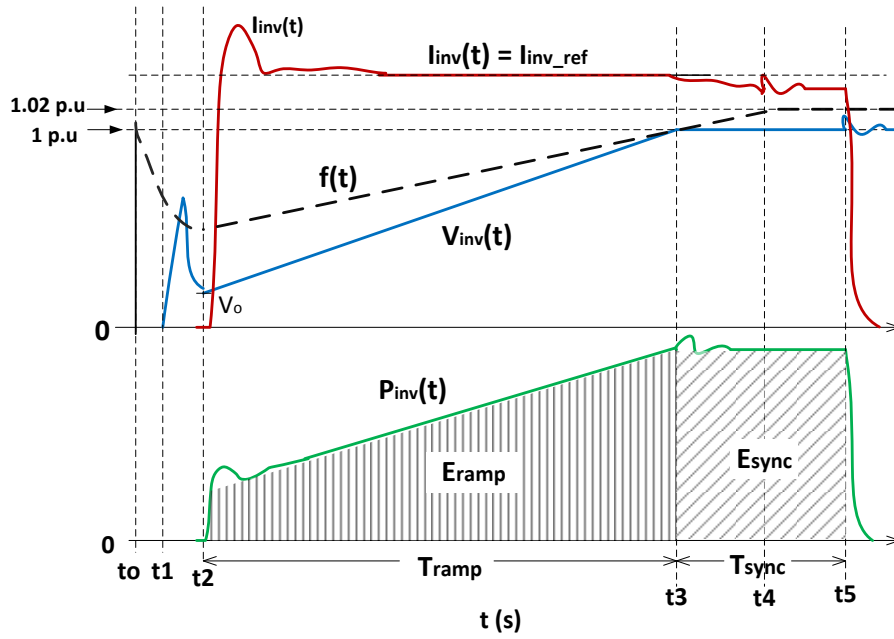
Figure 6.9: Energy calculation during T_{ramp} and T_{sync} (Not to scale).

So the maximum energy requirement to complete the process can be given by:

$$E_{ESS\_max} = E_{ramp} + E_{sync\_max} \qquad (6.24)$$

Considering a total load of 500 kW (= P_{inv}), to be driven by the ESS during the SR process, we can calculate the maximum energy requirement to be: $E_{ESS\_max} \approx 0.2$ kW-h, using the following and typical values:

T_{ramp}= 0.5 s, Iref = 1.5 p.u, V_{q0} = 0.3 p.u, f_0 = 0.65 p.u, E_{ramp} = 0.07 kW-h, and

f_{inv_max} = 61.2 Hz (=1.02 p.u), E_{sync_max} = 0.12 kW-h.

All simulations are done in Matlab Simulink to validate the effectiveness of SR method. Two cases are considered for comparison with conventional restarting methods.

6.3.2. SIMULATION PARAMETERS AND TEST CASES FOR VALIDATING EFFECTIVENESS OF THE SOFT-RECLOSING PROCESS

Five industrial grade induction motors of Bus-L1 (M1-M5 in Figure 6.1) are lumped

together and represented as an aggregated motor model M_L (600 hp). The two dc drive motors M_8-M_9 of Bus-P2 are also aggregated into an equivalent 120 hp dc motor M_{dc}, driven by a single thyristor rectifier. Lighting loads are represented by constant impedance load (Z_{RL}) of 20 kW. All load data and cable parameters are taken from [59]. The motor-aggregation method used is described in [64].

6.3.3. COMPARISON CASE-I

In this case, the loads used are:

a. The aggregated model (M_L) of the induction motors M1-M5.

b. The aggregated model (M_{dc}) of the dc drive motors M8-M9.

c. A 20 kW constant impedance load (Z_{RL}) representing the building services and lighting loads.

The parameters used for the system measurements and the loads are given in Table 6.1. The simulation tests done for this case are:

a. M_L, M_{dc} and Z_{RL} are started across-the-line, and using soft-restart following the fault to compare current draw and bus-1 voltage for both methods.

b. M_L, M_{dc} and Z_{RL} are started across-the-line, and using soft-restart following the fault to compare torque and speed evolution of M_L and M_{dc} for both the processes.

Different values of I_{inv_ref} are used for the SR process, and the ramp-up time (T_{ramp}) and energy requirement during ramp-up process (E_r) is plotted against I_{inv_ref} .

6.3.4. COMPARISON CASE-II

In this case, the loads used are:

a. Motors M_1 (300 HP) and M_2 (100 HP)

b. Aggregated model (M_{dc}) of the dc drive motors M8-M9.

Table 6.1: System and Motor Parameters for Comparison Case-I

c.

Parameters		Values	
kVA$_{base}$		700	
V$_{LL\_base}$ (V)		480	
Line Impedance: R$_L$ + jX$_L$ (Ω)		0.015 + j006	
Lumped Model of Induction Motor: M$_L$		**Lumped Model of DC Motor: M$_{dc}$**	
P$_{rated}$ (hp)	600	P$_{rated}$ (hp)	120
PF (at rated speed)	0.85	V$_{rated}$ (V)	500
V$_{L\_rated}$ (V)	480	J (kg-m^2)	10
f (Hz)	60	V$_f$ (V)	300
I$_{rated}$ (A)	385	R$_a$ (Ω)	0.1499
N (rpm)	1750	L$_a$ (H)	0.00288
J (kg-m^2)	7.8	R$_f$ (Ω)	51.14
F (N.m.s)	0.0065	L$_f$ (H)	5.968
R$_s$ (Ω)	0.0073	F (N.m.s)	0.0138
R$_r$(Ω)	0.0055		
L$_{Ls}$ (H)	0.00016		
L$_{Lr}$(H)	0.00009		
L$_m$ (H)	0.0045		
Lighting Loads		20 kW, PF=0.9	

Table 6.2: System and Motor Parameters for Comparison Case-II

System Parameters	Values	
kVA$_{base}$	500	
V$_{LL\_base}$ (V)	480	
Motor Parameters	**M$_1$**	**M$_2$**
P$_{rated}$ (hp)	300	100
PF (at rated speed)	0.85	0.8
V$_{L\_rated}$ (V)	480	480
f (Hz)	60	60
I$_{rated}$ (A)	105	36
N (rpm)	1750	1160
J (kg-m^2)	4	3
F (N.m.s)	0.0065	0.0005

The parameters used for this test case is given in Table 6.2.

The simulations performed for this case are:

a. Motors M_1, M_2 and M_{dc} are started sequentially following the fault to mimic a manual restart process. Current draw, voltage magnitude and power factor at bus-1are measured.

b. Motors M_1, M_2 and M_{dc} are re-energized using soft-restart method following the fault. Current draw, voltage magnitude and power factor at bus-1are measured and compared with the sequential manual restart process.

6.3.5. THE ENERGY STORAGE SYSTEM

The energy storage is assumed to be made up of flooded lead-acid batteries which are popularly used for grid-tie applications for providing ancillary and power quality services [65]-[67].

Details of the battery configuration and inverter are not described in this work, but the storage requirement is addressed using the energy requirement for the SR process.

The transformer coupling impedance is: $R_T + jX_T = 0.004 + j0034 \ \Omega$.

6.3.6. MOTOR LOAD TORQUE MODEL

A pump type load is considered for all the motor loads. The load torque on the shaft is given by [68] as:

$$T_L = (T_{init} + (T_F - T_{init})\omega^2) * T_B$$

(6.25)

Where,

T_{init} : Initial load torque during starting in p.u.

66

T_F **:** Final load torque in p.u.

ω **:** Motor speed in rad/s

T_B **:** Base torque in N-m.

The values for eq. (6.25) used in this work are: T_{init}= 0.1 p.u, T_F = 0.9 p.u and T_B = 2873 N-m.

6.4. SIMULATION RESULTS

6.4.1. SIMULATION RESULTS FOR COMPARISON CASE-I

The simulation tests assume the following:

- 3-phase-to-ground fault at 2.5 s at location Flt-A. (t_0 = 2.5 s).

- The fault is cleared by CB 1, CB2 in response to overcurrent, and CB_main in response to undervoltage relay, in 3 cycles (i.e t_1 = 2.5 + 3/60 = 2.55s).

- When SR is enabled, CB_main stays open until synchronization is achieved between votlages V_{inv} and V_S. CB_ESS is closed 4-cycles after CB_main has tripped (i.e, t_2 = t_1 + 4/60 = 2.62 s).

- The maximum load current allowed during the ramp-up process is: I_{inv_ref} = 1.5 p.u.

6.4.1.1.   LINE CURRENT AND BUS-1 VOLTAGE

Figure 6.10 shows the instantaneous voltage at bus-1, and line currents when an across-the-line-start (ATLS) is attempted for the loads.

Figure 6.11 shows the instantaneous voltage, and line currents when a soft-reclose is done using the ESS.

It is easy to notice the significant reduction in starting inrush current. The ATLS causes a 4.7 p.u inrush current through the line, while the SR method ensures a starting current

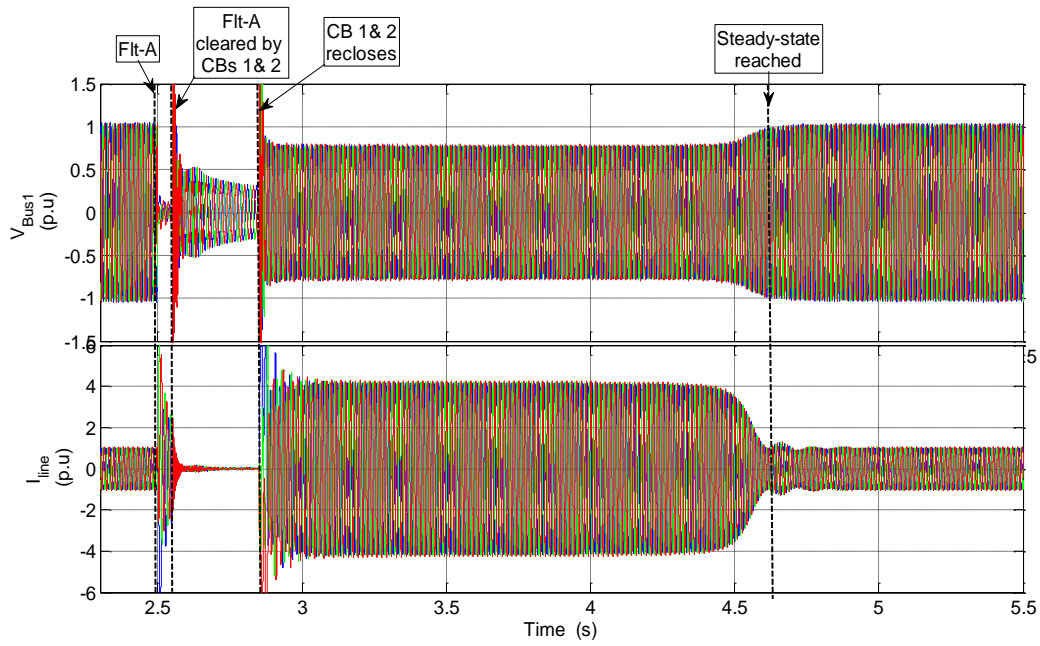of 1.5 p.u. This gives a 67% decrease in starting current.

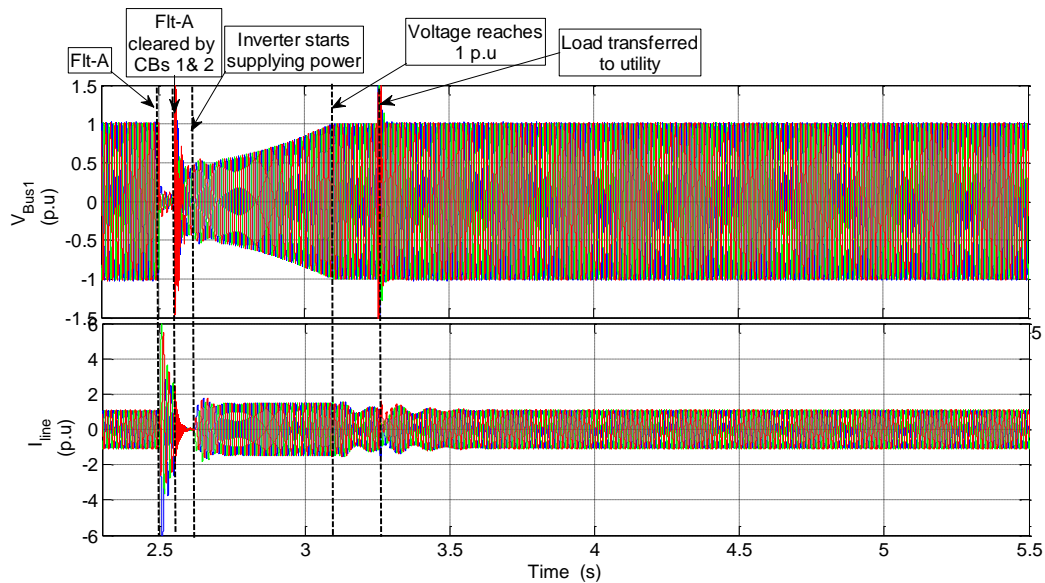Figure 6.10: Bus-1 voltage and line current during across the line start of the loads in bus-1.

Figure 6.11: Bus-1 voltage and line currents when soft-reclosing is enabled ($I_{inv\_ref} = 1.5$ p.u).

Associated with this high inrush, is the voltage depression of about 0.8 p.u at Bus-1

that lasts for almost 2 s. When SR method is used (see Figure 6.11), the voltage V_{bus-1} reaches 1 pu at around 3.1 s, compared to 4.6 s when ATLS is done. The load transfer to the utility occurs at 3.25 s, with negligible current transient.
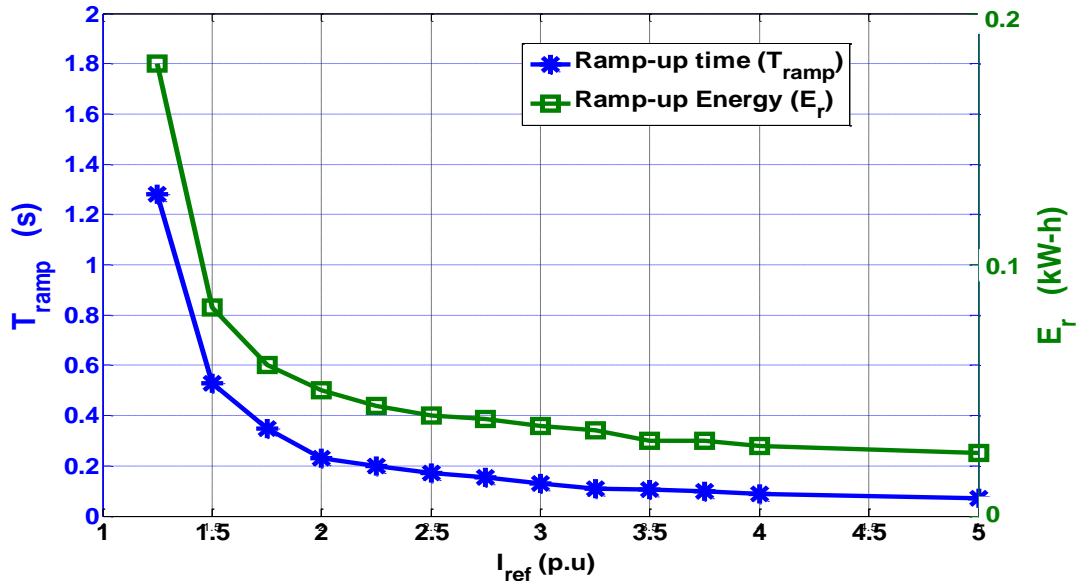
Figure 6.12: Ramp-up time (Tramp) and Ramp-up energy (Er) for different values of Iinv_ref.

Figure 6.12 (blue line) shows the reduction in T_{ramp} with increasing values of I_{inv_ref}. If a higher line current is allowed, the ramp-up time (T_{ramp}) can be reduced. For values lower than I_{inv_ref}=1.2 p.u, the ESS is unable to reaccelerate the motors. No significant reduction in Tramp is observed for Iinv_ref values greater than 2.25 p.u. Also, with higher values of Iinv_ref motor torque oscillations may be unacceptable.

Figure 6.12 also shows the energy requirement during the ramp-up process (Er) in kW-h for different values of Iinv_ref.

Table 6.3 compares a utility scale ESS in Vernon, CA (Flooded lead-acid, 3 MW, 4.5 MWh), with the requirements and estimated costs of an ESS for performing soft-

reclosing operation [39]. The comparison gives an idea about the size and cost of the energy storage if it has to perform the SR operation only. It is also important to realize that the additional cost for power electronics may not be needed if the SR method is incorporated into an existing ESS functioning as an auxiliary source.

Table 6.3: Energy Requirement and Cost Comparison for Implementing Soft-Reclosing with a Utility-Scale ESS [39]

	Typical utility scale ESS	**ESS for soft-reclosing (Load = 700 kW)**
Energy requirement	4500 kW-h	0.18 kW-h
Storage cost ($305/kWh)	$1,372,500	$55
Power Electronics ($275/kW)	$825,000	$192,500
Storage space requirement ($0.058m^2$/kWh)	261 m^2	0.01 m^2

For the results shown in Figure 6.10 and Figure 6.11, the energy required during T_{ramp} is 0.08 kW-h (=2.88 MJ). The energy requirement E_{ramp} vs I_{inv_ref} characteristic is similar to T_{ramp} vs I_{inv_ref}.

6.4.1.2.   TORQUE AND SPEED BEHAVIOR OF M_L AND M_{DC}

Although, synchronized processes in a factory are controlled by ASDs, it will be worthwhile to investigate the speed and torque behavior of the motors M_L and M_{dc} when SR process is used. Figure 6.13 and Figure 6.14 illustrate this behavior.

For the induction motor ML, the torque transients are completely avoided when SR method is used. Comparing the speed pick-up behavior of ML for both cases, it is easy to observe that when SR method is used, ML reaches its nominal speed much faster as compared to the case when ATLS is done. The time taken to reach the nominal speed, for SR method is about 0.58 s compared to about 2.18 s when ATLS is done.

The torque build-up for the dc drive motor (Mdc) is slower for SR method due to the

70

additional charging time-constant of the dc bus capacitor. However, the speed build-up is much faster compared to the ATLS operation.
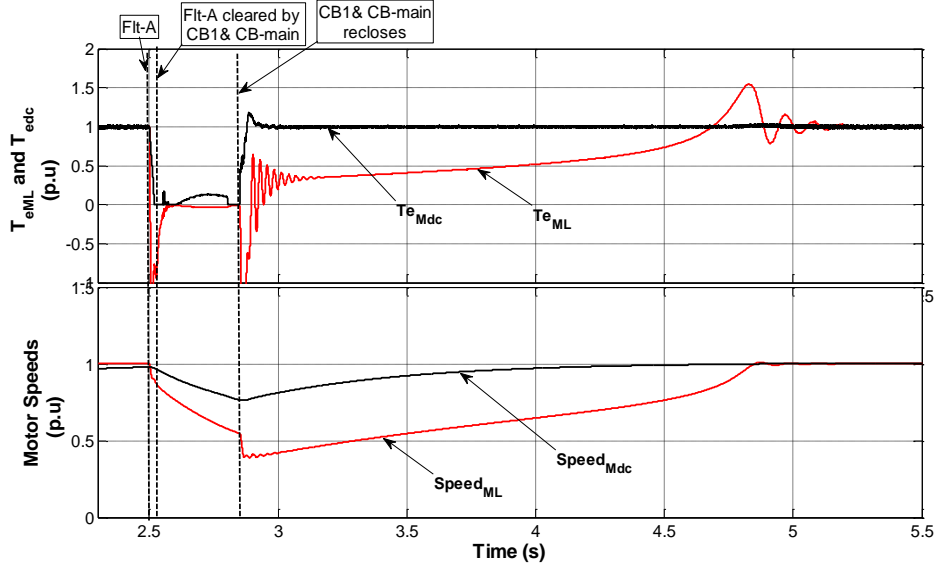

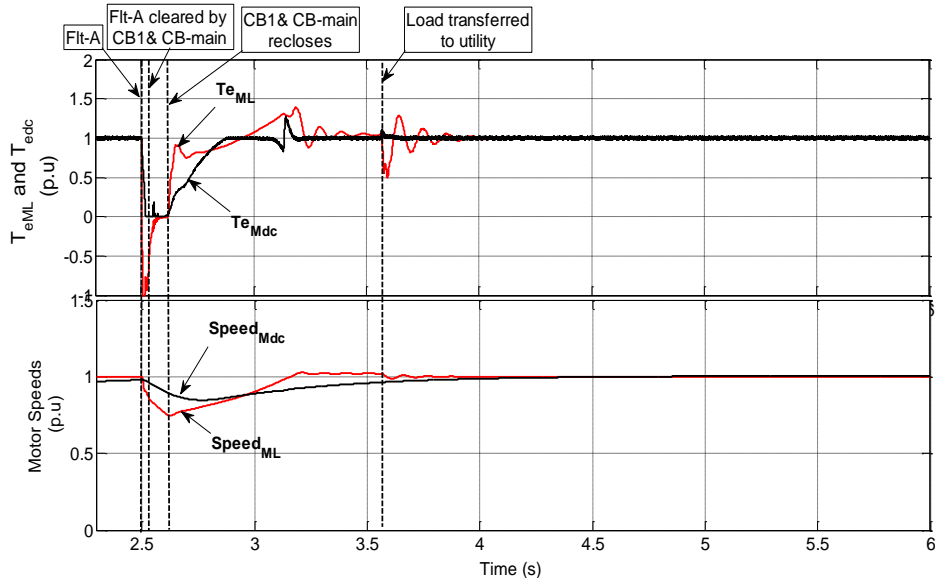Figure 6.13: Speed and torque behavior of ML and Mdc when across-the-line-start is done following Flt-A.

Figure 6.14: Speed and torque behavior of M_L and M_{dc} when soft-reclosing is done following Flt-A.

The speed pick-up behavior gives an idea about the effectiveness of SR method if it is to be applied to processes which may require synchronization between motors. Clearly,

from the speed behavior of ML and Mdc in Figure 6.13 and Figure 6.14, we find that the difference in speed is much more pronounced when ATLS is done. When SR is used, not only speeds of ML and Mdc reach their nominal value faster but are in "near-synchronism" during the ramp-up time. This behavior is especially important for understanding the effectiveness of SR method to minimize "scrap-losses" in industrial process. Simulation Results for Comparison Case-II

The manual restart assumes the following time values for operation of the equipment:

- 3-phase-to-ground fault at 3.5 s at location Flt-A. ($t_0 = 3.5$ s).

- The fault is cleared by CB 1 and CB_main in 3 cycles (i.e $t_1 = 3.5 + 3/60 = 3.55$s). All loads M_1, M_2 and M_{dc} are dropped off.

- Voltage is restored at Bus-1 with the automatic reclosing of CB1 and CB_main at 3.85 s.

- M1 is turned on across-the-line at: 4.55 s.

- M2 is turned on across-the-line at: 6.55 s.

- M_{dc} is turned on across-the-line at: 9.05 s.

For the soft-reclosing process, the time values for operation of the equipment are:

- 3-phase-to-ground fault at 3.5 s at location Flt-A. ($t_0 = 3.5$ s).

- The fault is cleared by CB 1 and CB_main in 3 cycles (i.e $t_1 = 3.5 + 3/60 = 3.55$s).

- CB_main stays open until synchronization is achieved between votlages V_{inv} and V_S. CB_ESS is closed 4-cycles after CB_main has tripped (i.e, $t_2 = t_1 + 4/60 = 3.62$ s).

- The maximum load current allowed during the ramp-up process is: $I_{inv\_ref} = 1.5$ p.u
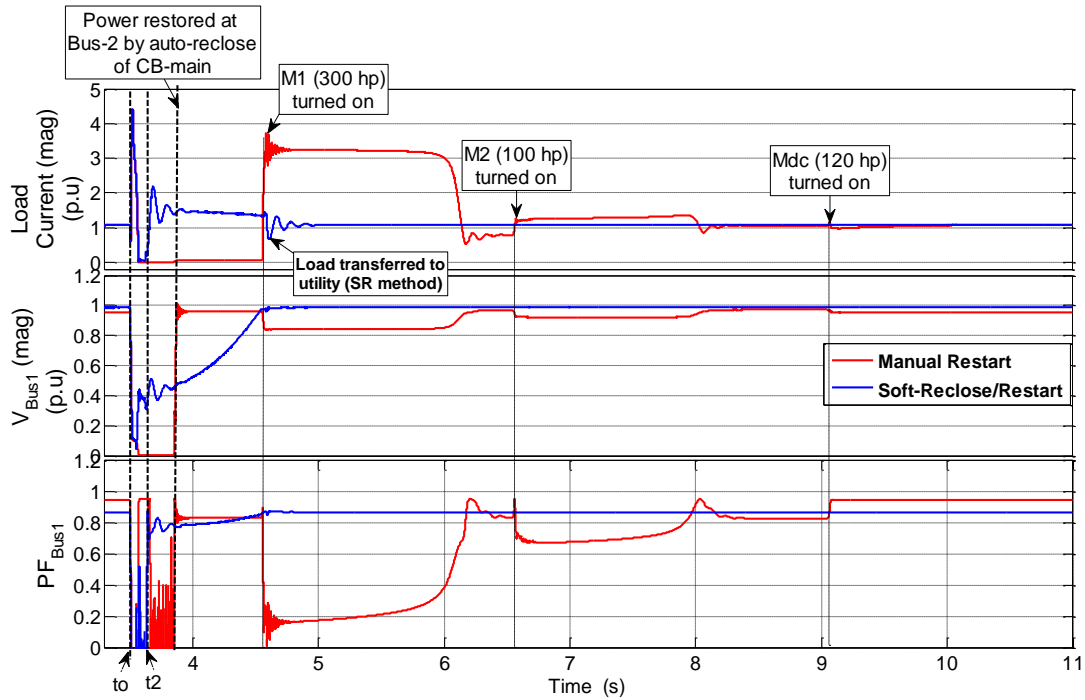
Figure 6.15: Load current and voltage magnitude, and power factor at bus-1, during manual restart (red line) and soft-restart (blue line).

6.4.1.3. VOLTAGE AND POWER FACTOR FLUCTUATIONS DURING MANUAL RESTART AND SOFT RECLOSING (COMPARISON CASE-II)

Figure 6.15 (red line) shows the current, voltage and power factor (PF) fluctuations at the service entrance bus (Bus-1) during a manual restart. The blue line shows the behavior during soft-restart.

Clearly, the current, voltage and PF do not show any fluctuation during the soft-reclosing process. Although in the simulation of the MR process, the system p.u value is calculated using only the 3 motors, SR process clearly shows the following advantages over the MR process:

1. Load current is controlled and stays within the preset value of 1.5 p.u. This is especially beneficial for factories having a large number of line-connected motors, which are started manually to comply with the grid regulations of maximum current

73

draw during process restarts.

2. No voltage fluctuations at the service entrance bus occur due to sequential across-the-line-starting of motors.

3. No PF fluctuations. This is a very important benefit for most manufacturing plants as they are subjected to additional penalties for not maintaining the minimum PF required by the grid codes.

4. Time required for the SR process is only about 1 s compared to the time required for manual restart, which may take up to 45 mins.

5. As there is no process downtime, process operator safety can be ensured.

6. Restarting sequence does not have to be considered and timed.

7. Possible "scrap-losses" are minimized, and "clean-up" costs are avoided.

6.5. CONCLUDING REMARKS

Benefits of soft-reclosing for a consumer product manufacturing plant are shown in this chapter. The example system is representative of a plastic/rubber manufacturing plant which has a large number of line-connected motors. The major benefits of soft-reclosing method, compared to the conventional method of service restoration are summarized in Table 6.4.

Table 6.4: Benefits of Soft-Reclosing Method Compared to a Conventional Service Restoration Method

Conventional Method for Post-Fault Service Restoration	Benefits of Soft-Reclosing Method
Manual restart is done to ensure safety during process restarts.	No process downtime, so erroneous assumption of a "dead-line" condition (by labor operator) is not plausible.
Manual restart process may take up to 45 mins.	Automatic and continuous process.
Restarting sequence has to be considered and timed to minimize inrush current.	The method ensures a predefined inrush current.
Extended process downtime may cause increased "scrap-losses" and "clean-up" costs if the process involves line-connected motors.	No process downtime, so such costs are avoided.
Voltage fluctuations at the motor bus, due to sequential across-the-line-starts done manually.	Voltage fluctuations do not exist, since the motor bus operates in islanded mode during the process.
Disconnection of DER prior to reconnection to the utility is required to avoid asynchronous reclosing between live networks.	Synchronization is achieved by the inverter to perform a "transient-free" load transfer to the utility source.

Apart from voltage dip problems additional penalties due to power factor fluctuations are also avoided. The soft-restart method is able to decrease the starting inrush current by 67%. The total time required for completion of the process is about 1 s compared to 30-45 mins required for a manual restart. Since process downtime is avoided, associated costs and complications such as safety, "clean-up" time, etc. arising due to manual restarts are also avoided. Consumer product manufacturing plants which generally have a large number of line-connected motors will benefit greatly from this method, as additional penalties due to voltage and power factor fluctuations can be avoided.

The energy requirement for performing the soft-reclosing method is also very small and can easily be incorporated with an existing grid-tied ESS.

CHAPTER 7

7. THE FAULT-AWARE-SOFT-RESTART METHOD

In this chapter we extended the soft-restart method using the current-fed voltage control described in the previous chapter by introducing a fault-detection algorithm into the inverter controls.   In this method the magnitude of phase voltages at the inverter terminals are measured to confirm a fault condition. The applicability and reliability of this simple fault detection algorithm is analyzed and proved to be effective when applied to a MVAC system in an electric ship. The fault-aware-soft-restart method is able to a) prevent current feed into the fault, b) avoid close-open operations of the breakers producing current transients, and c) perform a safe and controlled power restoration for the load zone followed by a synchronous reclosure of the load-zone islanding-breaker on to the distribution bus. The method utilizes the voltage-frequency modulation capability of the inverter with an energy storage system (ESS) to pre-energize a load zone and then reconnect the loads back to the main generator(s) or distribution bus.

This new approach is in contrast to the existing approach for reconfiguration and restoration in a ship system which involves isolation of faults by using directional overcurrent protection, followed by a routine operation of automatic bus transfer switches to quickly restore power to critical equipment. A load-shedding algorithm is typically incorporated into the power management algorithm to ensure that loss of an operating parallel generator will not cause a possible black-out.This is generally done by remotely

opening the breakers connected to non-vital loads when generator overload is sensed. With this approach, a fixed set of loads are shed which in most cases means that more loads are disconnected than necessary to meet the reduced generation capacity and prevent possible stalling of line-connected electric motors in nearby load-zones. The reclosing transients and inrush currents associated with restarting of machines may cause unwanted generator trip-offs and stalling of motors that drive critical loads such as steering equipment or fuel transfer pumps and may cause a substantial accident such as the one reported in [56].

Problems with power quality are of different significance as compared to the ones associated with land-based power grids. Impacts on pricing relations (e.g. tariffs applied and penalties) between utility and its clients do not apply for a ship system, where the most important issue is the continuous operation of the system and its redundancy. A possible malfunction or failure of line equipment carrying power to critical loads may lead to a total loss of the vessel [56]. The preceding works [69] and [70] proves the effectiveness of the soft-restarting method for restoring service in an industrial power network. We extend the work reported in [69] to incorporate a fault-detection capability into the ESS to provide a complete "fault-aware" restoration process for a shipboard or an off-shore MVAC system.

7.1. PRINCIPLE OF FAULT-AWARE-SOFT-RESTART

To explain the principle of fault-aware-soft-restart (FASR) we will refer to the section of a ship MVAC power system as shown in Figure 7.1. The configuration shows a "zonal" energy storage system that has a primary purpose of providing load support and UPS functionality for the loads in zone-1.
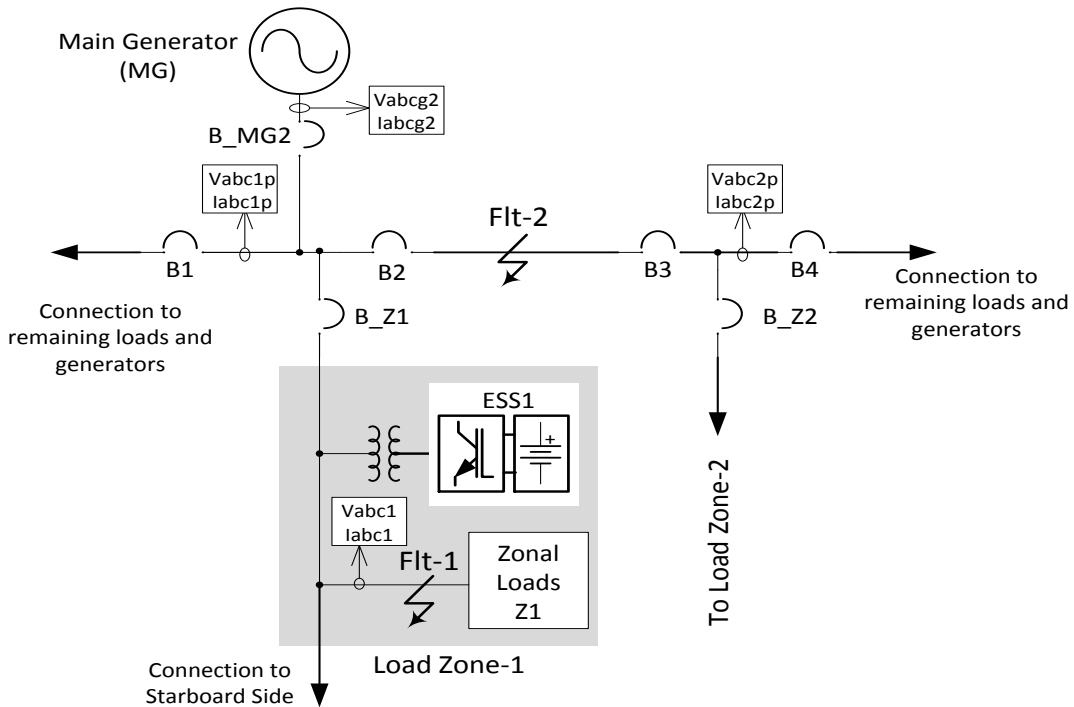
Figure 7.1: Section of the Ship MVAC power system showing an energy storage system (ESS1) for load zone-1.

Operation of the system is explained using Figure 7.2 with reference to the sequence of events following a fault: "Flt-2" between breakers B2 and B3 in the system shown in Figure 7.1.

- t_0: Fault occurs at any place between the breakers B2 and B3. The duration and type of fault are unknown.

- t_1: The fault detected within one-half cycle by measuring the phase-voltage magnitude at the inverter terminals. The power reference for the inverter assumes a zero reference value to prevent feeding power into the fault.

  t_2: The fault is cleared by tripping off breakers B2 and B3 by the overcurrent protective

Figure 7.2: Principle of fault-aware-soft-restart (not to scale).
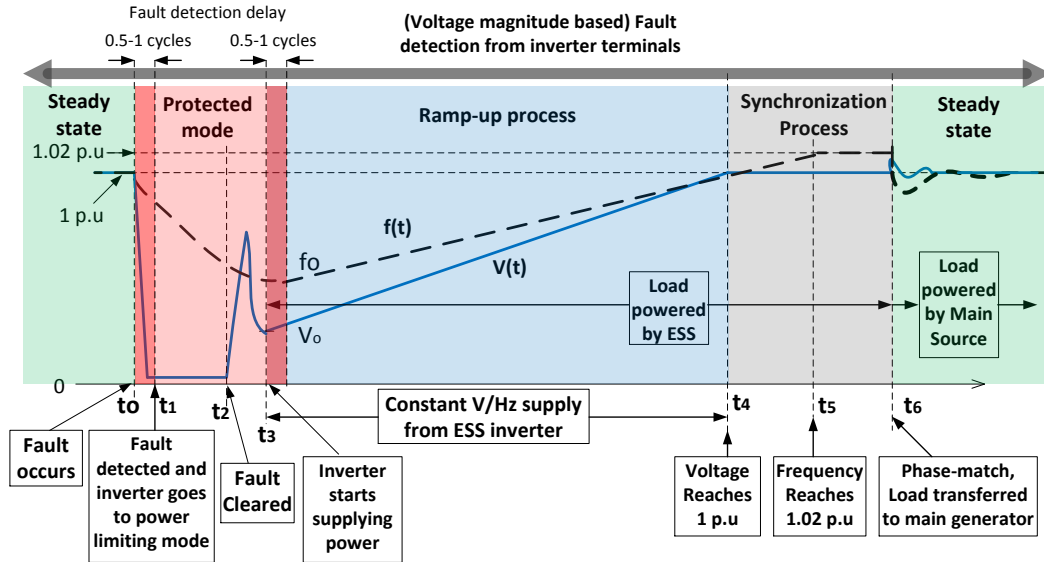
relays in about 3-5 cycles (typical duty of medium voltage CBs) [15]. Breaker B_Z1 is also tripped to create a load-zone island that can be powered by ESS1. (Breakers B2 and B3 will carry out their scheduled close-open operations, depending on the duration of the fault).

- t_3: Voltage transient that may occur due to motor residual voltages or stored energy in the line, usually dies down in 2-3 cycles. The voltage magnitude (V_0), and the decaying frequency (f_0) at time t_3 are measured within a cycle using a PLL. The inverter energizes the load zone with the voltage and frequency ramping up at a constant rate and under a constant V/Hz characteristic starting at a magnitude of $|V_{abc1}|=V_0$, and f_0. During this time (T_{ramp}: from t_3 to t_4) the load current supplied by the inverter I_{abc1} is controlled by adjusting the slope of the voltage and frequency ramps $V_{abc\_inv}(t)$ and $f(t)$, until they reach 1 p.u. and 1.02 p.u. respectively. The upper limit of inverter frequency is set as 1.02 p.u in order to achieve synchronization with the main source.

- t_4: V_{abc1} reaches 1.0 p.u and the sync-check relay is activated to check for a voltage phase match between V_{abc1} and the main source voltage V_{abc1p}.

- t_5: frequency of $V_{abc\_inv}(t)$ reaches 1.02 p.u.

- t_6: Sync-check relay produces a TRUE value, and the loads are transferred to the main source by reclosing B_Z1.

The major difference between the fault-aware-soft-restart and the conventional fault management procedure is that unlike the conventional process the load zone is islanded by opening breaker B_Z1 to avoid reclosing current transients produced by the scheduled close-open operations of B2 and B3. Figure 7.3 and Figure 7.4 compares the fault-aware-soft-restart process with the conventional restoration process generally followed in a ship MVAC system.
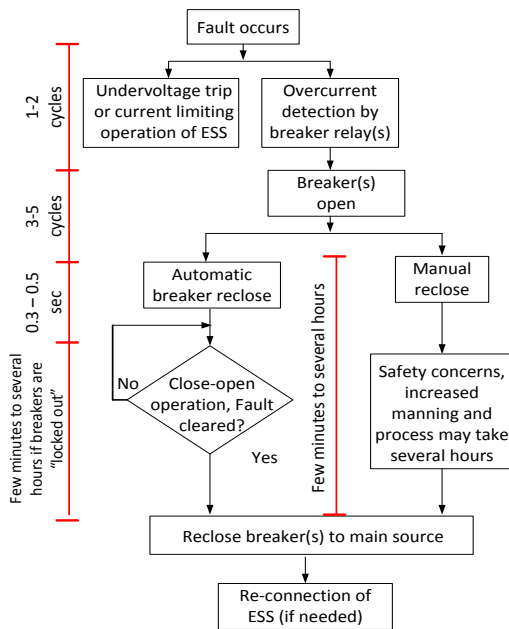

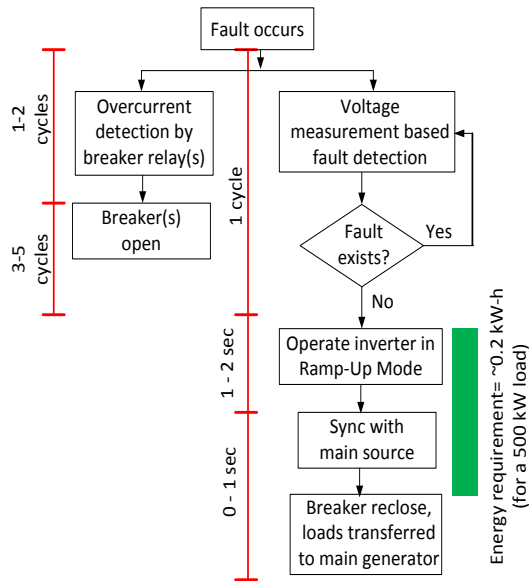Figure 7.3: Flowcharft for conventional fault management process in a ship MVAC system.

Figure 7.4: Flowchart showing the fault-aware-soft-restart method for fault management in a ship MVAC system.

Robustness of the method is easily realized from the comparison, as the process is

always completed within a few seconds. The energy requirement for restoring power to a 500 kW load, is estimated to be 0.2 kW-h.

7.2. TEST SYSTEM AND LOAD CHARACTERIZATION

7.2.1. TEST SYSTEM

Figure 7.5 shows a reference system topology known as the "Notional Baseline System Model" defined by ESRDC, for the exploration, testing and validation of new ship power system technologies [57]. Distributed energy storage systems have been used, to protect critical applications such as emergency lighting, navigation equipment, ship automation and HVAC applications against disruptive power interruptions in commercial cruise ships [58]. One of the study cases considered by the ESRDC consists of a single (4 MW, 100 MJ) energy storage unit for the purpose of providing power protection for the MVAC system in case of the loss of one of the 4 MW generators. Also, the case studies include the use of ESS for service restoration to act as a UPS unit until regular power is restored to vital loads [57]. A distributed energy storage configuration where energy storage units are available for individual load-zones, gives much more reconfiguration flexibility and a robust restoration capability in the case where a part of the ship has been damaged or hit.

Figure 7.5 shows the configuration of each load zone, comprising of a variety of loads which can be powered by an inverter-coupled energy storage system located on the same bus of that of the loads. The test system used in this work is developed from this configuration.
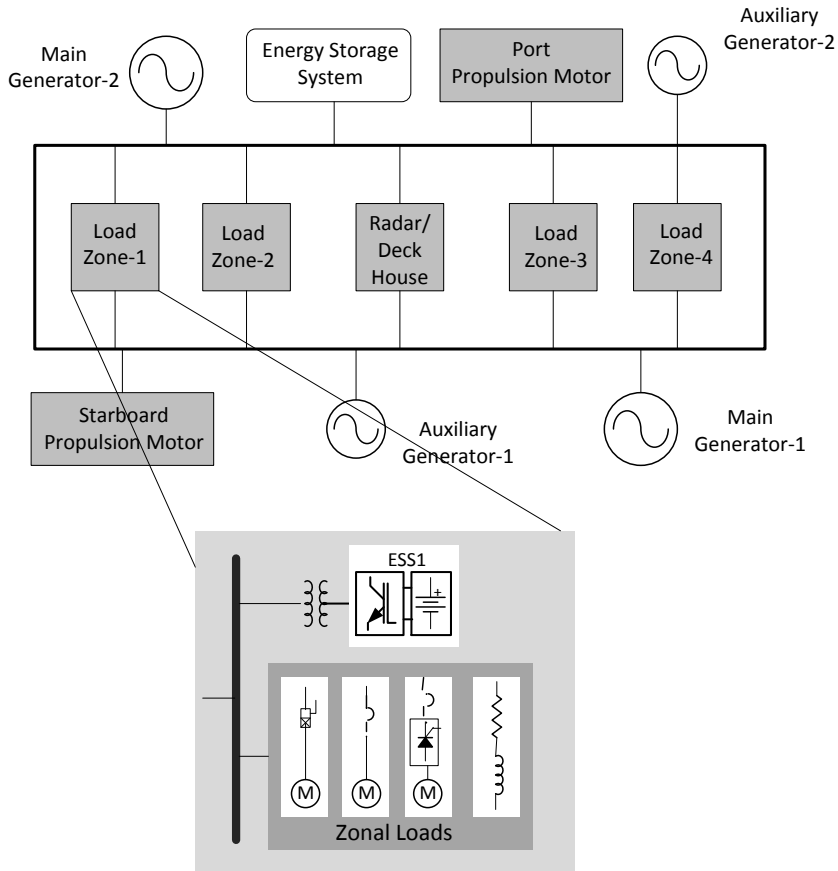
Figure 7.5: Ship MVAC test system with zonal loads [57]

7.2.2. Zonal Loads and their Operational Characteristics

Characterization of the zonal loads is important to accurately simulate the electrical behavior of the subsystem in the event of a fault. Figure 7.5 shows the assorted load types in a single load zone consisting of line-connected and electronically connected motor drives, as well as lighting/ship service loads represented by resistive-inductive elements. In a ship power system the percentage of motor loads are much higher (>90%) than a typical residential facility in a utility distribution circuit, which characterizes the transient behavior during service restoration. To simulate the correct loading condition during power restoration in a load-zone, the pickup and drop-off voltages are evaluated as follows: For a line-connected motor the minimum voltage required to prevent a running

motor from stalling is given by [23]:

$$V_{min} = \sqrt{\frac{\tau_L}{\tau_{pull-out}}} \times \mathbf{100} \text{ \%} = \mathbf{70} \text{ \%} \tag{7.1}$$

Assuming $\boldsymbol{\tau_L} = \mathbf{100}$ % : fully loaded shaft, and $\boldsymbol{\tau_{pull-out}} = \mathbf{200}$ %: pull-out torque for commonly used design-B motors.

For an ASD, driving a typical motor 460 V, 100 hp (= P_0), the trip-off time can be calculated as:

$$t_{trip} = \frac{1}{2} C_{dc} \frac{V_{dc}^2 - V_{dc-trip}^2}{P_0} = \mathbf{9.17} \ \boldsymbol{ms} \tag{7.2}$$

here, $\boldsymbol{C_{dc}}$= 10000 μF is the typical dc bus capacitance, and $\boldsymbol{V_{dc-trip}}$, is the dc trip-off voltage which can be calculated using the widely recognized CBEMA curve which shows a trip-off voltage value of 0.87 p.u. For ASDs that do not necessarily match the exact minimal thresholds of the CBEMA curve, and set to lower values of ~80%, the trip-off time will be 13.6 ms, which translates into 0.8 cycles for a 60 Hz system [71]. The above implies that, even for a one cycle voltage dip below 0.8 p.u. caused by a breaker reclosing transient, will cause the drop-off of almost all critical motor loads which are fed through ASDs.

The standard: MIL-Std-1399 [72] and technical manual [73] defines the pickup voltage for motor contactors and ASDs between 85-95%. We will use V_{pickup}= 85% as the voltage pickup value for the ASDs. We assume that the group of small line-connected motors and the ship service loads are not tripped offline during a fault.

7.3. FAULT DETECTION METHOD

The fault detection method similar to the one described in [50] to classify voltage dips

in a ship system that may occur due to faults, pulse load operation, or motor starting is used in this work. In this method the magnitude of phase voltages (Va1, Vb1 and Vc1) are measured and a fault condition is confirmed if the voltage magnitude is below a certain threshold.

7.3.1. RELIABILITY OF THE FAULT DETECTION METHOD

Reliability and speed of the fault detection method is extremely important to prevent a possible damage of the protection equipment and safety hazards due to current infeed from the inverter in the event of a fault. To investigate the reliability of the detection method we analyze the inverter response to a voltage dip and its current contribution during the subtransient period. Inverters have no inertia in their output except for the synthetic inertia built into their control algorithm. This causes it to respond immediately to voltage dips in the ac power system by injecting power into the system.

Referring to Figure 7.6, which shows a typical control scheme for an inverter the outer power control loop which is a function of the measured system voltage (V_g), and the commanded reference power (P_{ref}, Q_{ref}), generates the current reference (I_{ref}) for the inner current loop.
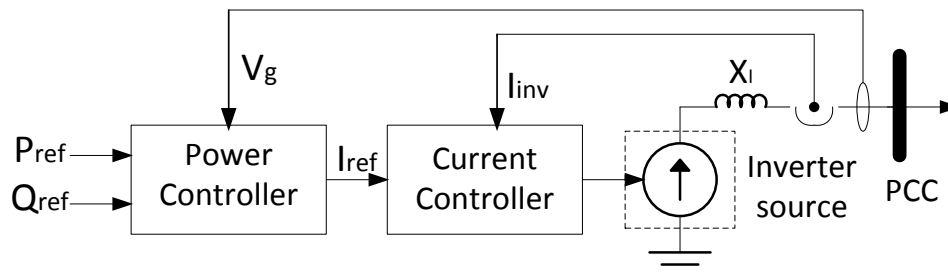

Figure 7.6 : Inverter control scheme.

$$I_{ref} = f(V_g, P_{ref}, Q_{ref}) \qquad (7.3)$$

Although P_{ref} and Q_{ref} can be set to a constant value externally, I_{ref} depends on the voltage measurement. So the immediate response to a voltage sag at the inverter terminals is to inject current into the system which is only limited by the controller saturation limits. For the inverter to trip off successfully or assume a power-limiting mode before the current output from the inverter reaches its peak, the terminal voltage (V_{gf}) has to drop off fast enough within half a cycle. This is because there is a half-cycle measurement delay for updating the inverter internal voltage (reference voltage, E) [2]. This condition will be satisfied if the time constant determined by the Thevenin impedance seen by the main source is less than 8 ms (=1/2 cycle). i.e.

$$\tau_f < \frac{L_{th}}{R_{th}} < 8\ ms \qquad (7.4)$$

Where: ωL_{th} and R_{th} are the Thevenin impedance components. For the reference system, this value comes out to be 2.4 ms using the cable impedance values: $31 + j28.65$ $\mu\Omega$/ft.

We can also estimate the peak current during the subtransient period using:

$$I_{inv}^p = \frac{|E_{f0} - V_{gf}|}{X_l} \qquad (7.5)$$

Where V_{gf} is the measured voltage at PCC during the subtransient period, and E_{f0} is the pre-fault inverter internal voltage calculated as:

$$E_{f0} = V_{f0} + jX_l I_{inv}^0 \qquad (7.6)$$

With V_{f0} : pre-fault voltage at the PCC which can be calculated from inverter rated

power and x_l : the link reactance. Typically the maximum momentary current rating for inverters is twice its rated current (I_{inv}^0). So if $I_{inv}^p > 2I_{inv}^0$ (measured using (7.5)) the inverter may also trip off even before the current reaches its peak.

7.3.2. VOLTAGE DIP MAGNITUDES

Finally the voltage dip magnitudes have been estimated. For a 3-phase fault the dip magnitude has an appreciably low value to distinguish itself from the high power load start-up. A startup power of 50 MW, only produces a voltage dip of about 0.9 p.u. this is illustrated in Figure 7.7 and Figure 7.8.

In this work (for a 3-phase fault only) we considered a phase-to-neutral voltage magnitude of 0.5 p.u. measured for each phase at the inverter terminals, as the threshold to detect a fault condition. For a line-to-line fault, the measured voltage may be higher, in which case the threshold can be changed accordingly.
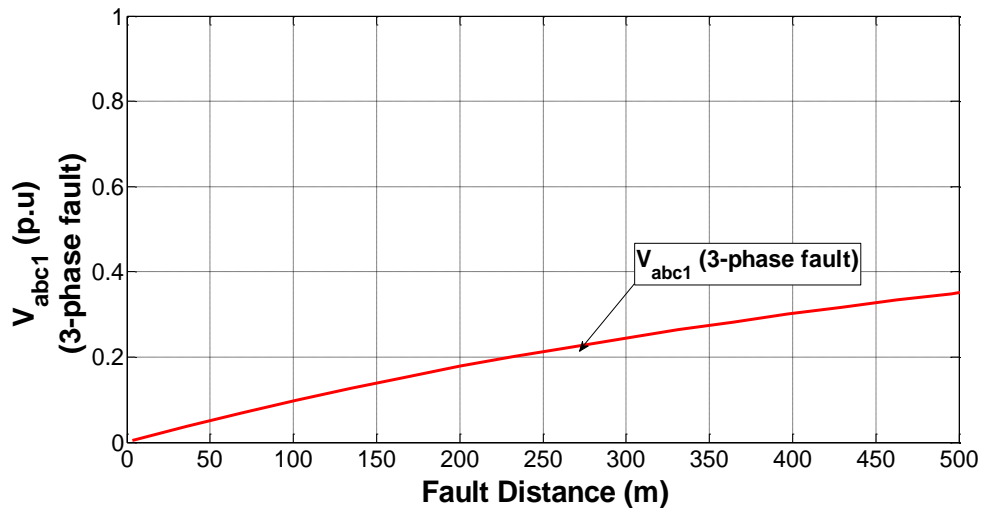
Figure 7.7: Voltage sag magnitude vs fault distance for a ship MVAC power system.
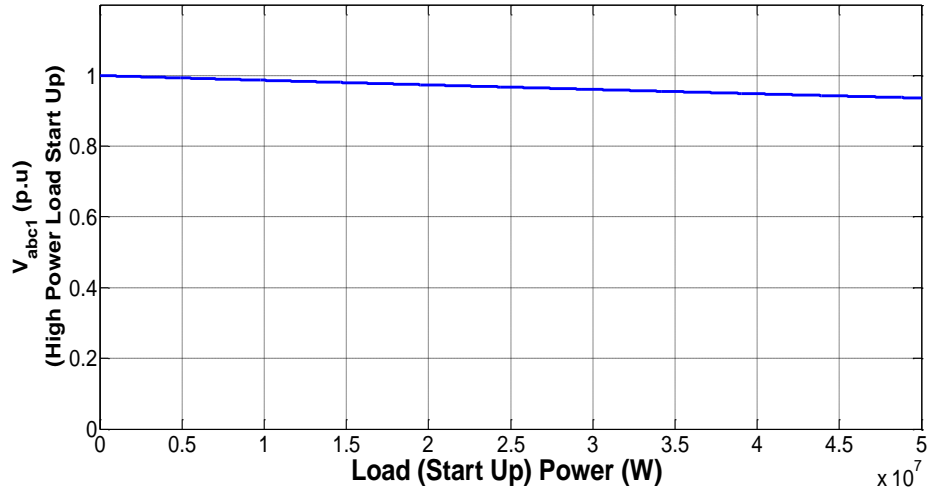
Figure 7.8: Voltage dip magnitude vs load startup power.

7.4. ENERGY STORAGE SYSTEM CONTROLS

Figure 7.9 shows test system with the required measurements. The control schematic is shown in Figure 7.10.

7.4.1. CONTROL VARIABLES

As shown in Figure 7.10, the current feedback (I_{abc_inv}) is used to adjust the ramp of the V/Hz supply generated by the ESS inverter to power up Bus-1. The control variables are obtained by abc→dq transformation V_q and ω_1 obtained
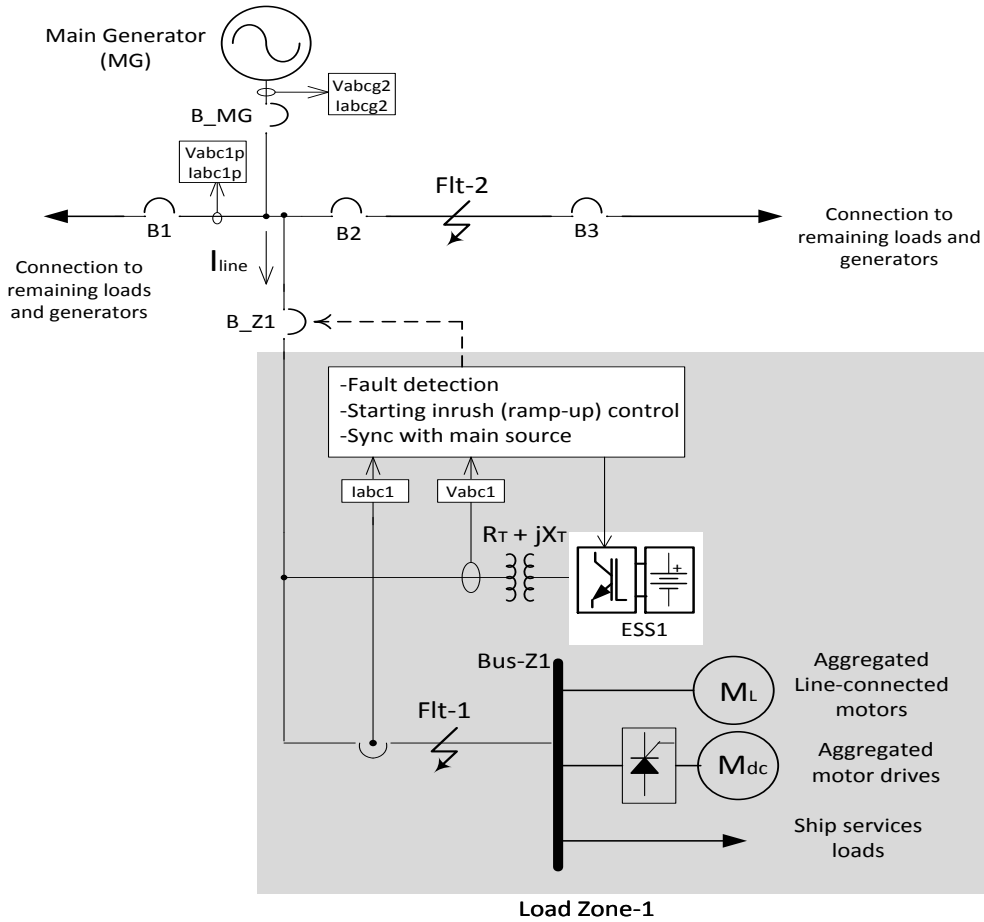
Figure 7.9: Test System with aggregated models of line-connected motors, ASDs and ship service loads

Figure 7.10: ESS control schematic.

from the PLL and used as the inputs to the frequency and V_q controllers. V_d is not used to

adjust the magnitude and frequency of the V/Hz ramp and is set to zero: $V_{d\_inv} = 0$. So, the

inverter output voltage magnitude:

$$|V_{inv}| = V_{q\_inv} \tag{7.7}$$

The input signal to the V_q controller during steady-state (pre-fault condition) can be written in phasor form as:

$$\overrightarrow{V_{q1}} = |V_{abc1}| e^{j\delta} \tag{7.8}$$

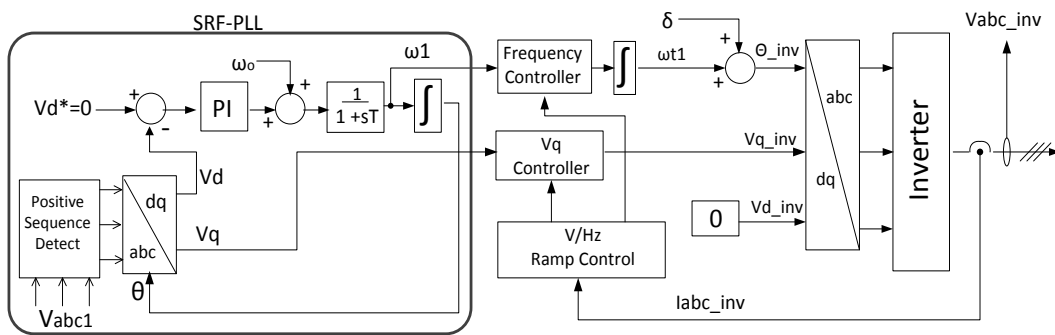with a phase angle of 0^0 referred to the load bus. The phase angle (δ) is known from the transformer coupling impedance $R_T + jX_T$. And

$$\theta_{inv} = \omega t_1 + \delta \tag{7.9}$$

The decaying voltage (V_{q0}) and frequency (f_0) measured at time t_3 (see Figure 7.2), has a non-linear relationship that will highly depend on the inertia of the connected motor load(s).

Table 7.1: System and Motor Parameters

Parameters		Values	
kVA$_{base}$		1000	
V$_{LL\_base}$ (V)		480	
Line Impedance: R$_L$ + jX$_L$ (µΩ/ft)		31 + j28.65	
Lumped Model of Line-Connected Inductionn Motors: M$_L$		**Lumped Model of ASDs: M$_{dc}$**	
P$_{rated}$ (hp)	400	P$_{rated}$ (hp)	400
PF (at rated speed)	0.85	V$_{rated}$ (V)	500
V$_{L\_rated}$ (V)	480	J (kg-m^2)	10
f (Hz)	60	V$_f$ (V)	300
I$_{rated}$ (A)	422	R$_a$ (Ω)	0.1499
N (rpm)	1750	L$_a$ (H)	0.00288
J (kg-m^2)	9	R$_f$ (Ω)	51.14
F (N.m.s)	0.0065	L$_f$ (H)	5.968
R$_s$ (Ω)	0.0078	F (N.m.s)	0.0138
R$_r$(Ω)	0.0062		
L$_{Ls}$ (H)	0.00018		
L$_{Lr}$(H)	0.0001		

L_m (H)	0.005		
Lighting Loads		150 kW, PF=0.9	

Table 7.2: Energy Storage System Parameters

Parameters	Values
Rated power (kW)	2000
Rated current (A)	832
Minimum energy capacity (kW-h)	0.25 (~1 MJ)
Transformer coupling impedance: $R_T + jX_T$ (Ω)	0.004+ j0034

7.5. SIMULATION PARAMETERS

System and motor parameters are given in Table 7.1. M_L (400 hp) and M_{dc} (400 hp),
are the aggregated models for all line-connected and the ASDs respectively in the load
zone. The motor-aggregation method used is described in [64]. Other ship service loads
are modeled as a resistive-inductive element (Z_{RL}) of 150 kW.

For the both the fault cases (for Flt-1 and Flt-2) the operating duty of the breakers is
considered as follows: O - 0.3 s - CO – 1 s –CO, instead of: O - 0.3 s - CO – 3 min –CO
[15]. This means that the breakers will attempt their first reclose in 0.3 s, and if the fault
exists, another "close-open" (CO) operation will take place after a 1 s delay instead of a 3
min delay. This is done to observe the electrical behavior in a shorter simulation time.

7.5.1. MOTOR LOAD TORQUE MODEL

All motors are considered to drive pump type loads, so that the load torque on the shaft
is given by as:

$$\tau_L = (\tau_{init} + (\tau_F - \tau_{init})\omega^2) * \tau_B \tag{7.10}$$

Where,

τ_{init}: Initial load torque during startup in p.u.,

τ_F : Final load torque in p.u.,

ω : Motor speed in rad/s, and

τ_B: Base torque in N-m.

The values for eq. (7.10) used in this work are: τ_{init} = 0.1 p.u, τ_F = 0.9 p.u and τ_{BL} = 1915 N-m (for M_L) and τ_{Bdc} = 2350 N-m (for M_{dc}).

7.5.2. THE ENERGY STORAGE SYSTEM

We assume that the energy storage has a rated capacity which is at least equal to the required startup energy of the load zone. The parameters for the energy storage system are given in Table 7.2. For a maximum allowable startup current of 2.0 p.u. the inverter has to be rated as twice the load power i.e 2 MW.

7.6. SIMULATION RESULTS

Both the simulation test cases (Flt-1 and Flt-2) assumes the following:

- A 3-phase-fault of duration 0.5 s occurs at 30.0 s at location Flt-1. (t_0 = 30.0 s).
- The fault is cleared by B_Z1 (or B2 and B3 for Flt-2) in response to overcurrent relay, in 4 cycles (i.e t_1 = 30.0 + 4/60 = 30.06 s).
- The inverter takes 0.5 cycle to measure the rms phase voltages at its terminals, and assumes a protected mode of operation at t_0 + 0.5/60 = 30.008 s.

7.6.1. SIMULATION RESULTS FOR THE CASE: FLT-1

Figure 7.11 - Figure 7.15 and Figure 7.16 - Figure 7.19 shows the simulation results for the conventional reclosing and for FASR scheme respectively for the case: Flt-1.

From comparison of the instantaneous current plots in Figure 7.11 (I_{line}) and in Figure 7.12 (I_{abc1}), we see the current transients due to the scheduled reclosing attempts by B_Z1 are completely avoided when FASR is used.

B_Z1 attempts its first reclose at 30.0+4/60+0.3=30.36s producing current transients, the magnitude of which is unobservable, since the p.u. current is measured using the base load value of 1000 kVA.

Figure 7.11: Instantaneous voltage at the load bus-Z1 (V_{abc1}), line current (I_{line}), phase voltage magnitudes (V_{a1}, V_{b1}, V_{c1}) at inverter terminals, and inverter current magnitude (I_{inv}) during conventional "hard reclosing".
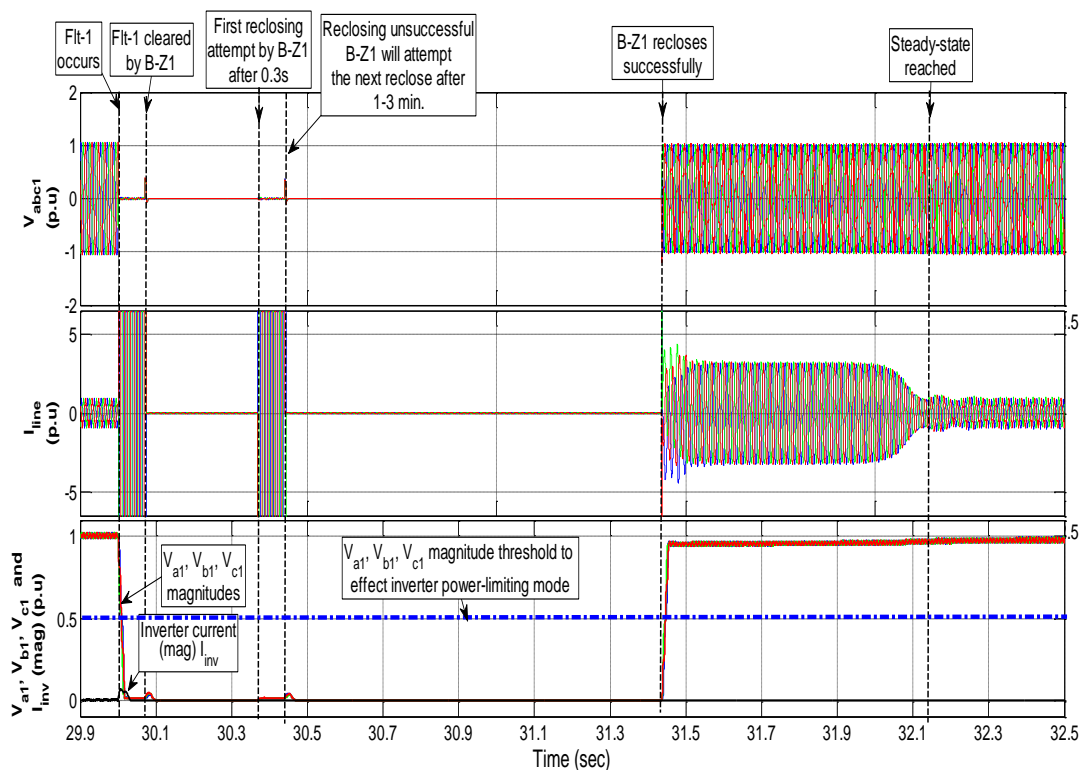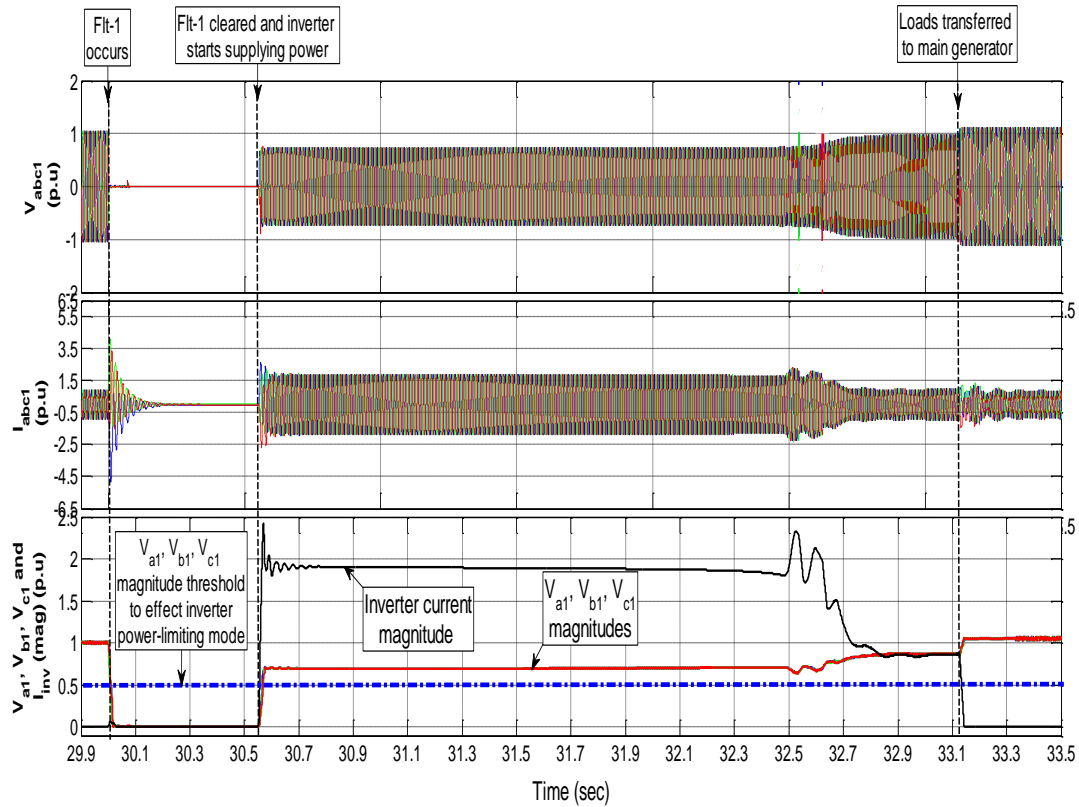
Figure 7.12: Instantaneous voltage at the load bus-Z1 (V_{abc1}), load current (I_{abc1}), phase voltage magnitudes (V_{a1}, V_{b1}, V_{c1}) at inverter terminals, and inverter current magnitude (I_{inv}) during fault-aware-soft-restart.
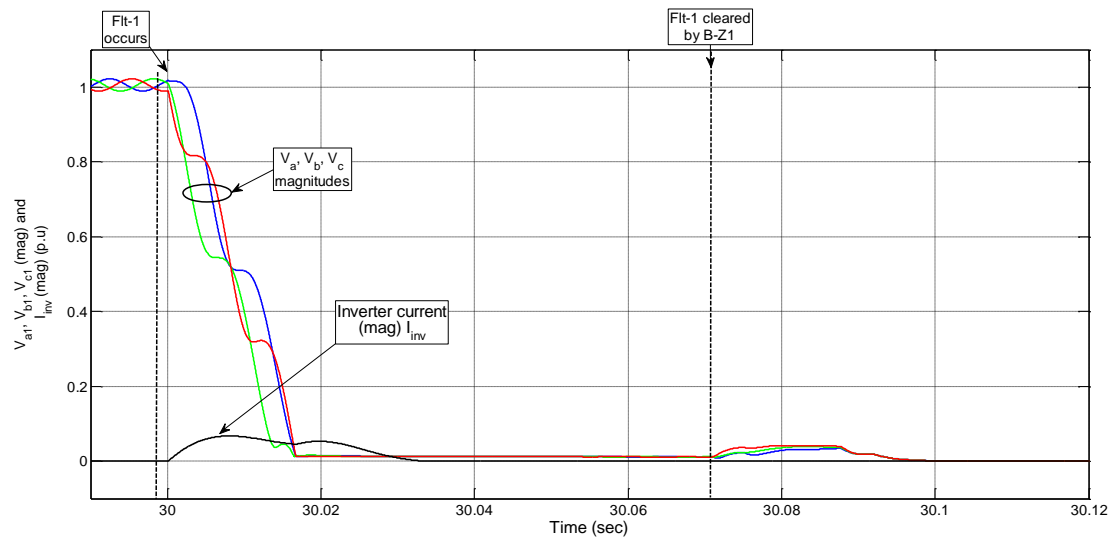
Figure 7.13: Zoomed in figure, showing current feed from the inverter during the fault.
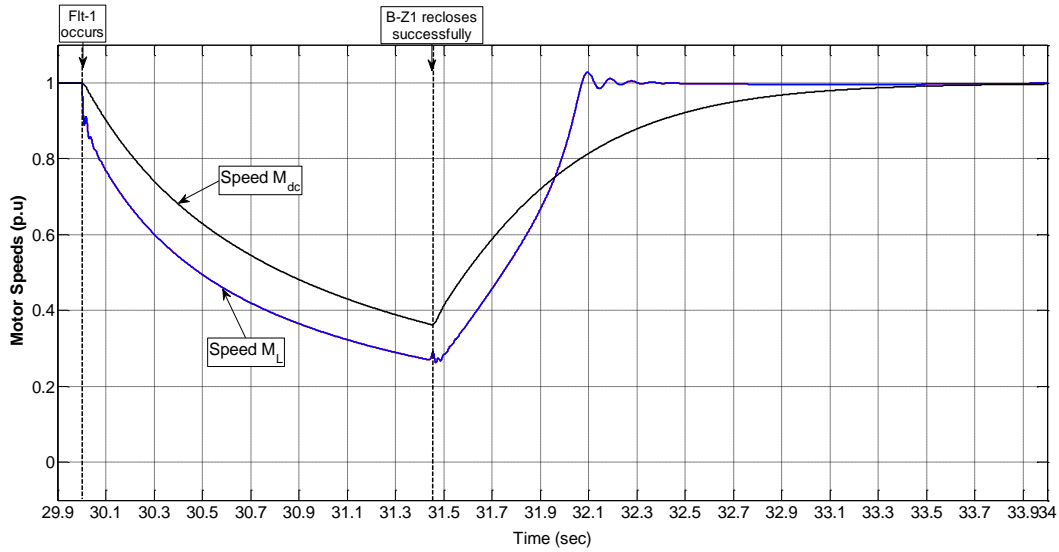
Figure 7.14 : Speed of motors M_L and M_{dc} during the fault case: Flt-2 with conventional reclosing
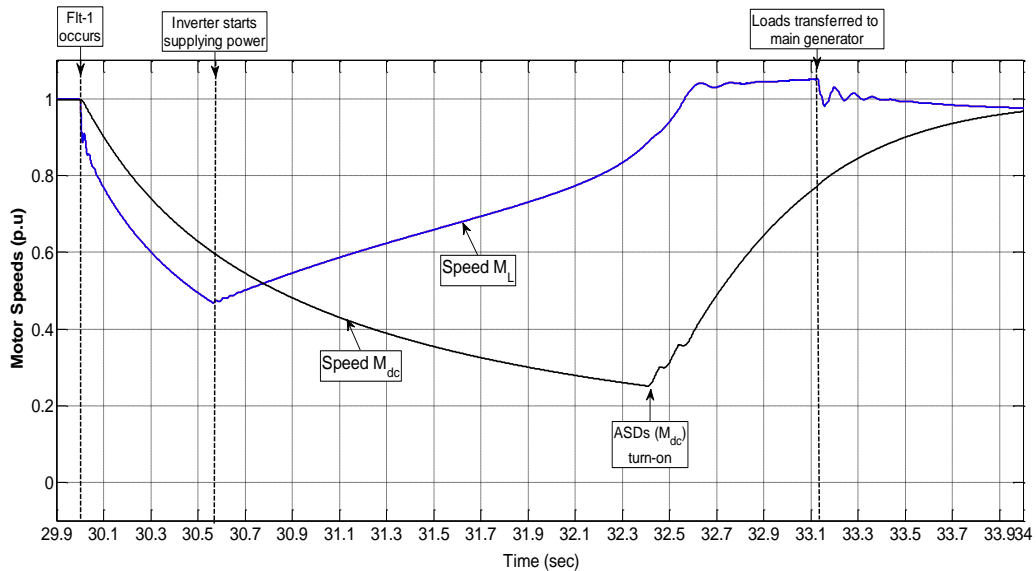
Figure 7.15: Speed of motors M_L and M_{dc} during the fault case: Flt-2 with fault-aware-soft-restart.

Since the fault is cleared at 30.5 s, the second reclosing attempt after 1 s, (i.e at 31.43 s) energizes the load bus, with the motors drawing about 3.5 p.u. starting inrush currents.

In the FASR process the scheduled reclosing attempts of B_Z1 is blocked, and the load-zone-1 is islanded with ESS1 supplying the power to restore its loads. The initial

94

subtransient current when the inverter starts the ramp-up process is about 2.5 p.u, after which the current is controlled to remain below 2.0 p.u. The current reaches steady-state at 32.75 s and the loads are transferred to the main generator at 33.2 s.

Figure 7.13 shows the magnitude of the current infeed from the inverter (I_{inv_mag}). As predicted, the voltage magnitudes V_{a1}, V_{b1} and V_{c1} drops below the threshold of 0.5 p.u. within half cycle, allowing the inverter to turn itself off with negligible (~0.08 p.u) current feed into the fault.

Speed behaviors of M_L and M_{dc} for both the processes are shown in Figure 7.14 and Figure 7.15. In this fault case the motor speed behavior is not affected by the multiple reclosing attempts by B_Z1. The motors are able to re-accelerate at the second (successful) reclosing at 31.43 s and reaches nominal speed at about 33.5s. When FASR is used it takes a longer time for the speed of M_{dc} to reach nominal speed since the pickup voltage is set at at 0.85 p.u.

The FASR process takes about 3.2 s from the instant when the fault occurred.

7.7. Simulation Results for the Case: Flt-2

Figure 7.16 and Figure 7.17 compares the instantaneous voltage at the load bus-Z1 (V_{abc1}), load current (I_{abc1}), phase voltage magnitudes (V_{a1},V_{b1},V_{c1}) at inverter terminals, and inverter current magnitude (I_{inv}) during conventional "hard-reclosing" and during a fault-aware-soft-restart. Clearly from the plot of instantaneous currents I_{line} and I_{abc1} in Figure 7.16 and Figure 7.17respectively we see that the reclosing transients caused by the scheduled reclosing of B2 and B3 are completely avoided when FASR is used. The inverter current is controlled to remain below 1.5 p.u. after the initial transient peak of 2.0 p.u. when it starts supplying power.
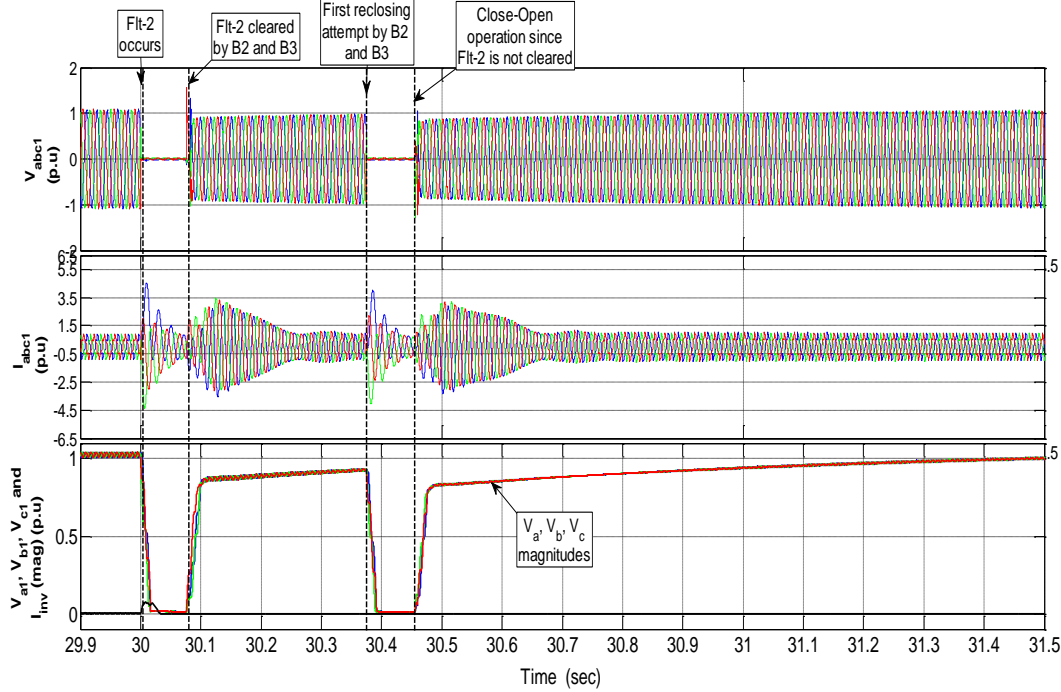
Figure 7.16: Instantaneous voltage at the load bus-Z1 (V_{abc1}), load current (I_{abc1}), phase voltage magnitudes (V_{a1}, V_{b1}, V_{c1}) at inverter terminals, and inverter current magnitude (I_{inv}) during conventional "hard reclosing" of B2 and B3.
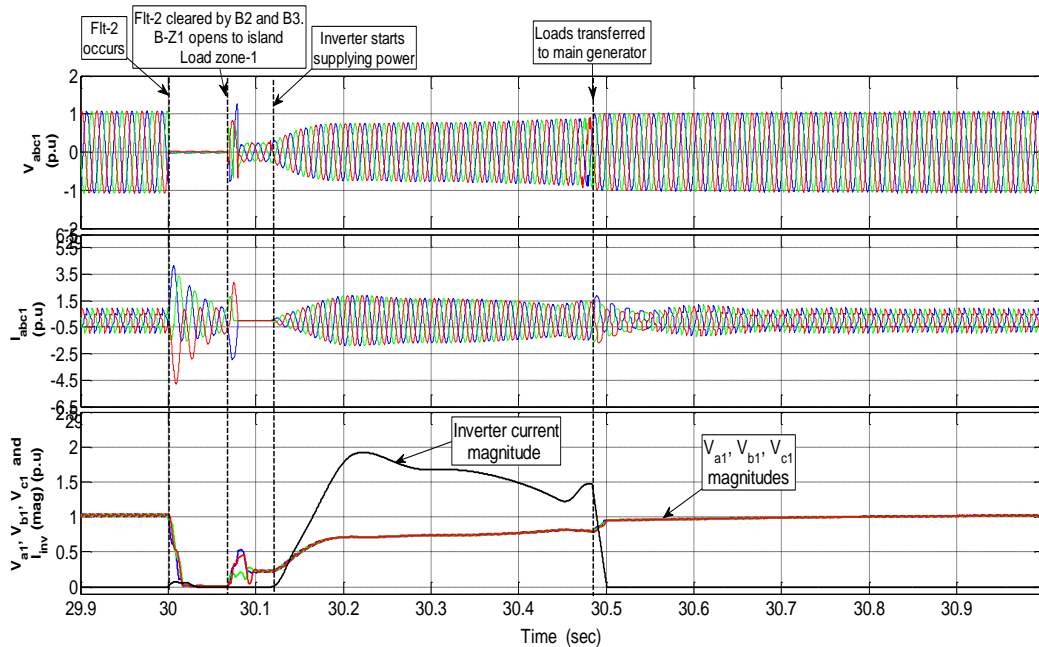
Figure 7.17: Instantaneous voltage at the load bus-Z1 (V_{abc1}), load current (I_{abc1}), phase voltage magnitudes (V_{a1}, V_{b1}, V_{c1}) at inverter terminals, and inverter current magnitude (I_{inv}) during fault-aware-soft-restart.

Also of significant importance is the voltage magnitude at the load bus (V_{abc1}) during the fault-aware-soft-restart, which is able to sustain the operation for the motor loads. This is an advantage since the motors are not allowed to drop-off and decelerate with each reclosing attempts by B2 and B3 on to the fault. The speed behavior of the motors M_L and M_{dc} during conventional and fault-aware-soft-restart is compared in Figure 7.18 and Figure 7.19.
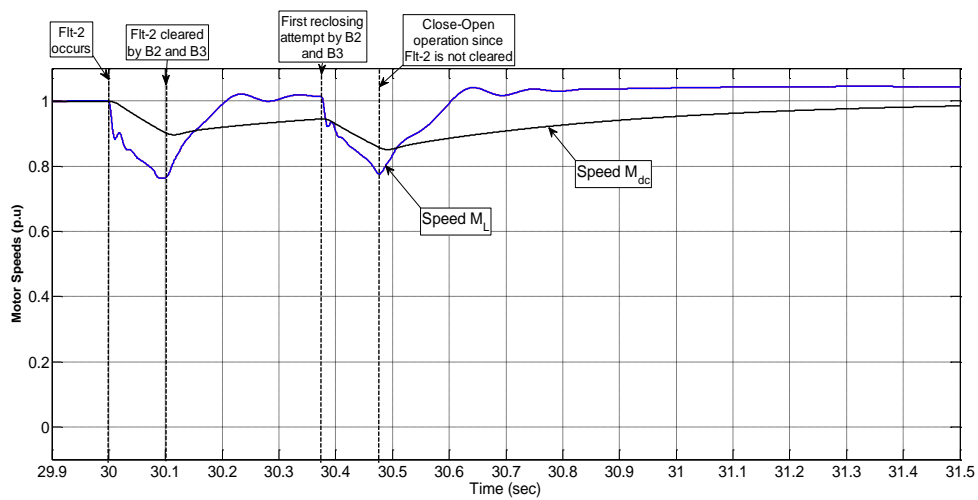
Figure 7.18: Speed of motors M_L and M_{dc} during the fault case: Flt-2 with conventional reclosing.
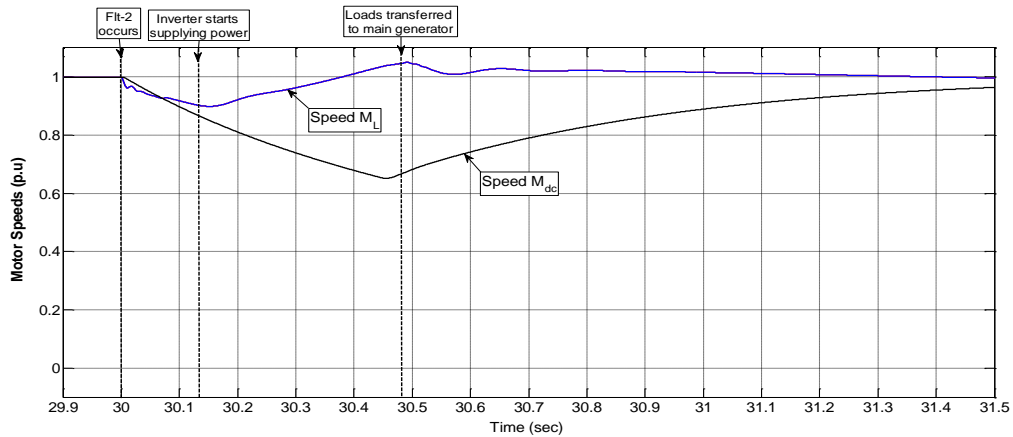
Figure 7.19: Speed of motors M_L and M_{dc} during the fault case: Flt-2 with fault-aware-soft-restart.

7.8. CONCLUDING REMARKS

For a ship system the most important issue is the continuous operation of the system and its redundancy. Replacements and availability of redundant equipment being almost nil in a ship system, damage or loss of line equipment cannot be afforded during the restoration process. A new method for a robust, fast and safe service restoration for a zonal load in the ship MVAC system is presented in this chapter. An energy storage system that is co-located with the zonal loads is used to carry out a controlled energization of the load zone followed by a seamless transfer of the loads back to the main bus. A current-fed voltage control is used to control the inverter current during the restoration process. Two fault locations are considered for the test system which is representative of a section of the ship MVAC system. For the cases: Flt-1 and Flt-2, starting inrush current transients are reduced by over 40% and 50% respectively. By measuring the phase voltage magnitudes at the inverter terminals for detecting the presence of a fault condition, a possible fault-feeding and safety hazard is avoided. For the study cases in this work, the restoration process is completed within a few seconds (0.48 s for Flt-2, and 3.2 s for Flt-1) compared to the conventional restoration process which may take a few minutes to few hours, and may require additional human intervention. Table 7.3 summarizes the benefits of a fault-aware-soft-restart compared to the conventional power restoration method presently in practice in the ship MVAC system [74].

Table 7.3: Benefits of Fault-Aware-Soft-Restart Compared to the Conventional Service Restoration Method in a Ship System

Conventional Method for Post-Fault Service Restoration	Fault Aware Soft Restart Method
Reclosing transients and starting inrush currents may cause motor stalling and subsequent restoration failure.	Avoids reclosing current transients and consequent voltage drop. Starting inrush current is kept to a minimum. Service restoration is carried out in a seamless manner.
Multiple reclosing attempts by CBs (close-open operations) degrade equipment reliability and lifetime.	The process only allows a synchronous reclosing of CBs, and close-open operations of CBs are avoided by utilizing a fault detection incorporated in the ESS.
Unnecessary load shedding is imminent since starting inrush currents are not controlled when starting the loads with limited generation capacity.	Robust restoration method and starting inrush currents are controlled.
The process may take up few minutes to several hours to ensure safety of operating personnel and avoid equipment damage.	The method only takes a few seconds and safety is ensured by avoiding reclosing on to a faulted circuit.
Increased manning requirement.	The process is fully automated, and no human intervention is necessary.

Distributed energy storage systems in future electric ships can be exploited to provide a fault-aware-soft-restart of vital loads following a fault, to improve system reliability and survivability.

CHAPTER 8

8. MODELING THE DISTRIBUTED GENERATION POWER SYSTEM DURING SERVICE RESTORATION.

This chapter describes the method to model the electrical characteristics of a microgrid / a facility island / group of islands during service restoration following an interruption. Characterizing the load behavior during different stages of power restoration is very important to estimate the inverter size, energy-storage capacity and consequently its placement in the power system [75]-[76]. An accurate system model which is able to predict the electrical behavior during the different stages of service restoration will enable us to devise the appropriate algorithm for operating the energy storage system. The algorithm will be actuated by the following set of prioritized operation:

1. Feasibility of successful islanding. This will generally depend upon the energy storage capacity and the size of the microgrid / island.

2. Effectiveness and power quality benefits for surrounding customers when the soft-restart process is used for power restoration. This will depend upon multiple factors, mainly: load characteristics, utility generation capacity and load demand during the time of restoration.

The model will also enable us to perform a parametric study to determine the appropriate configuration and algorithm for the energy storage system based on the load (island) size and load characteristics. Load size is also a function of geographical area,

while load characteristics depend on the system type: residential or industrial.

8.1. CIRCUIT LOAD CHARACTERIZATION

In the first stage, load characteristics and the percent of each type of load connected to each distribution circuit must be estimated. Generally, these load levels are for peak load conditions, that is, peak winter-heating or peak summer-cooling loads. Knowledge of diversity factors for each type of load is necessary to characterize the load behavior during power restoration. If it is anticipated that one-half of all air-conditioning loads will be operating during peak load conditions, then a diversity factor of 50% would be assigned to air-conditioning loads [21].

Table 8.1 shows the major types of loads (P_i) in any facility categorized according to their assigned diversity factor (D_i), percentage weight in the circuit (x_i) and the cold load pickup (CLPU) factor C_i. The values given in brackets are the typical values for a distribution circuit with predominately residential type of loads during winter (heating) season.

Table 8.1: Load type, Load Diversity Factor, Cold Load Pickup Factor for a residential type load during winter (heating) season [21].

Load type (P_i)	Load Diversity Factor (D)	% Circuit Load (x)	CLPU factor C = x/D % (With loss of load diversity)
Area Lighting (P_l)	D_l (1.0)	x_l (10%)	C_l (10%)
Resistive Space Heater (P_{sh})	D_{sh} (0.5)	x_{sh} (25%)	C_{sh} (50%)
Heat Pumps (P_{hp})	D_{hp} (0.5)	x_{hp} (25%)	C_{hp} (50%)
Heat Pump Resistive Heater (P_{hpr})	D_{hpr} (0.2)	x_{hpr} (10%)	C_{hpr} (50%)
Air Conditioner (P_{ac})	D_{ac} (0.5)	x_{ac} (0%)	C_{ac} (0%)
Miscellaneous Small Motors (P_{ms})	D_{ms} (0.25)	x_{ms} (10%)	C_{ms} (40%)
Large Industrial Motors (P_{mL})	D_{mL} (1.0)	x_{mL} (10%)	C_{mL} (0%)*
Other Loads (P_0)	D_0 (1.0)	x_0 (10%)	C_0 (10%)
Total		100%	210%

*Generally expected, large industrial motors automatically shut off when power is lost.

The basic distinction between a residential and an industrial (or any other) facility is the total percentage of small and large motors in the system. We define the parameter X_M to denote the percentage of small and large motor loads in the system as:

$$X_M = \frac{x_{ms} + x_{mL}}{\sum_i x_i} * 100\ \%$$

(8.1)

Where:

$$x_i \in \{x_l, x_{sh}, x_{hp}, x_{hpr}, x_{ac}, x_{ms}, x_{mL}, x_0,\}$$

(8.2)

For the residential type load distribution shown in Table 8.1, $X_M = 20\%$.

To characterize the load distribution in a circuit (B), based on a known load distribution in circuit (A), we use the following equation:

$$x_i^B = x_i^A \left(1 + \frac{X_M^A}{X_M^B}\right)(1 - X_M^B) * 100\ \%$$

(8.3)

Where,

$$x_i^A \in \{x_l, x_{sh}, x_{hp}, x_{hpr}, x_{ac}, x_0,\}$$

(8.4)

x_i^B is the percentage of the circuit loads for system B, and

X_M^B is the percentage of small and large motor loads in system B which has to be known primarily.

With the new load distribution calculated, we can then determine the cold-load-pickup factor C_i^B for the new circuit as:

102

$$C_i^B = \frac{x_i^B}{D_i} * 100 \ \%$$

<div align="right">(8.5)</div>

This factor will enable us to estimate the restoration current flowing into the circuit.

8.1.1. CALCULATION OF LOAD PICKUP CURRENT DURING DIFFERENT STAGES OF LOAD RESTORATION

In this step the total circuit current and time dependent current variation are evaluated. In general, four specific time intervals are considered for evaluating the current draw:

- **T_1 :** This period lasts about 10-15 cycles and characterizes initial circuit energization which includes inrush current to all connected loads.

- **T_2 :** This period is a 0.2 s inrush which characterizes circuit load as miscellaneous small motors are transitioning from starting to running.

- **T_3 :** This period of about 2 s characterizes the time at which steady state current has been established.

- **T_4 :** This period is about 15 min, which characterizes a sustained circuit load operation before load diversity of the bulk system begins to recover.

In this research we are only concerned about the first three time periods of T_1, T_2 and T_3, during which the energy storage system is used to establish the steady state current into the circuit load. The inrush current magnitudes during the three time periods vary with the type of loads. We define the current magnitudes during the different time periods with the typical values for a residential type system in Table 8.1.

Table 8.2: Multiple of steady state current for different load types during the three inrush intervals.

Load type (P$_i$)	Multiple of steady state current			
	m_i^{T1}	m_i^{T2}	m_i^{T3}	m_i^{T4}
Area Lighting (P$_l$)	2-8	1	1	1
Resistive Space Heater (P$_{sh}$)	1	1	1	1
Heat Pumps (P$_{hp}$)	5-8	1	1	1
Heat Pump Resistive Heater (P$_{hpr}$)	1	1	1	1
Air Conditioner (P$_{ac}$)	5-8	1	1	1
Miscellaneous Small Motors (P$_{ms}$)	5-8	5-8	1	1
Large Industrial Motors (P$_{mL}$)				5-8
Other Loads (P$_0$)	1	1	1	1

We can now calculate the total circuit current during each period as follows:

$$I_B^{T1} = \sum_i m_i^{T1} C_i^B \tag{8.6}$$

$$I_B^{T2} = \sum_i m_i^{T2} C_i^B \tag{8.7}$$

$$I_B^{T3} = \sum_i m_i^{T3} C_i^B \tag{8.8}$$

Above equations (8.6)-(8.8) allows us to calculate the load pick up current of facility-B for the different stages of load restoration.

Now, it can easily be recognized that, it the soft-restart is used to re-energize the loads in facility-B, the load pick-up current during the 3 stages can be calculated as:

$$I_{BSR}^{Tramp} = \sum_i m_{i1}^{Tramp} C_{i1}^B + \sum_j m_{jref}^{Tramp} C_j^B \tag{8.9}$$

Where:

i: denotes the set of loads that will draw 1 p.u.current during that period

And,

j: denotes the set of loads that will draw more than 1 p. u. current during

that period

Since the inverter current is controlled to a predefined reference (m_{ref} p.u.) so the

loads which generally draws more than 1 p.u. (P_l, P_{hp}, P_{ac}, P_{ms}) current are now defined by

m_{jref}.

8.1.2. POWER AND ENERGY REQUIREMENT FOR EACH STAGES

Once the values of currents are known, the power flow into the circuit at each stage can

easily be calculated. For the conventional reclosing process of facility-B, the power

requirements are:

$$P_B^{T1} = V_B^{T1} * I_B^{T1} \tag{8.10}$$

$$P_B^{T2} = V_B^{T2} * I_B^{T2} \tag{8.11}$$

$$P_B^{T3} = V_B^{T3} * I_B^{T3} \tag{8.12}$$

And for the soft restart, the power flowing into facility-B at different stages:

$$P_{BSR}^{Tramp} = V_B(\text{t}) * I_{BSR}^{Tramp} \tag{8.13}$$

Since the voltage is adjusted using the current flowing into the facility, so unlike the

conventional restoration process, voltage is a function of time, whereas the current (I_{BSR})

is maintained constant. The nominal voltage will be established within the time period

$T_{ramp.}$

The energy requirement for the conventional restoration process can now be easily calculated (for comparison purpose) using the following:

$$E_B^{T1} = \int_0^{T1} P_B^{T1} dt \tag{8.14}$$

$$E_B^{T2} = \int_0^{T2} P_B^{T2} dt \tag{8.15}$$

$$E_B^{T3} \int_0^{T3} P_B^{T3} dt \tag{8.16}$$

Similarly for soft-restart, the energy requirement during re-energization is:

$$E_{BSR}^{Tramp} = \int_0^{Tramp} P_{BSR}^{Tramp} dt \tag{8.17}$$

8.2. POWER SYSTEM MODEL WITH MULTIPLE ISLANDS POWERED BY ENERGY STORAGE SYSTEMS

For the purpose of evaluating power quality indices and subsequently define the operational algorithm for ESSs, the energy storage system – powered facility islands in context with its surrounding power system has to be modeled. Figure 8.1 shows a generic structure of a distributed generation power system comprised of multiple facility islands. The islands (or microgrids) can be powered by a single substation source, or by individual energy storage systems (ESSs).

8.2.1. EFFECT ON SUPPLY VOLTAGE DURING POWER RESTORATION

To estimate the effects on the substation voltage V_{sub}, we can use the following equation:
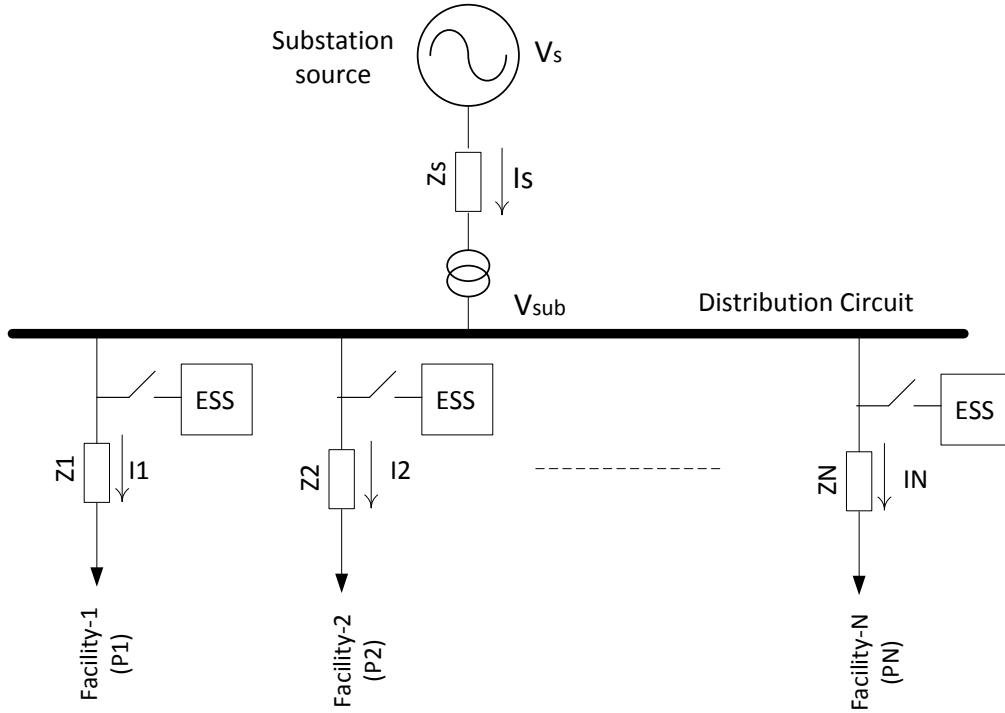
Figure 8.1. N number of facilities connected to the same substation source.

$$V_{sub} = 1 - \left[\frac{I_1^{T1}}{\frac{VA_1}{\sqrt{3}V_{LL1}}} + \frac{I_2^{T1}}{\frac{VA_2}{\sqrt{3}V_{LL2}}} + \cdots \ldots \ldots + \frac{I_N^{T1}}{\frac{VA_N}{\sqrt{3}V_{LLN}}} \right] * Z_s \ \ \mathbf{p.u.} \qquad (8.18)$$

Where, VA_1, VA_2 ….. ; and $V_{LL1}, V_{LL1} \ldots \ldots \ldots ..$ are the facility size and voltage levels of each facility respectively.

$I_1^{T1}, I_1^{T1} \ldots \ldots ..$ are the current drawn by each facility during the time period $\mathbf{T_1}$.

Figure 8.2 shows the voltage magnitude at the substation vs the combined load power of the facilities estimated using (8.18). For this plot we only considered 3 facilities, the load power of which are varied from 0 to 10 MW. The dotted line denotes the commonly used load drop-off threshold $V_{th} = 0.9$ p.u.
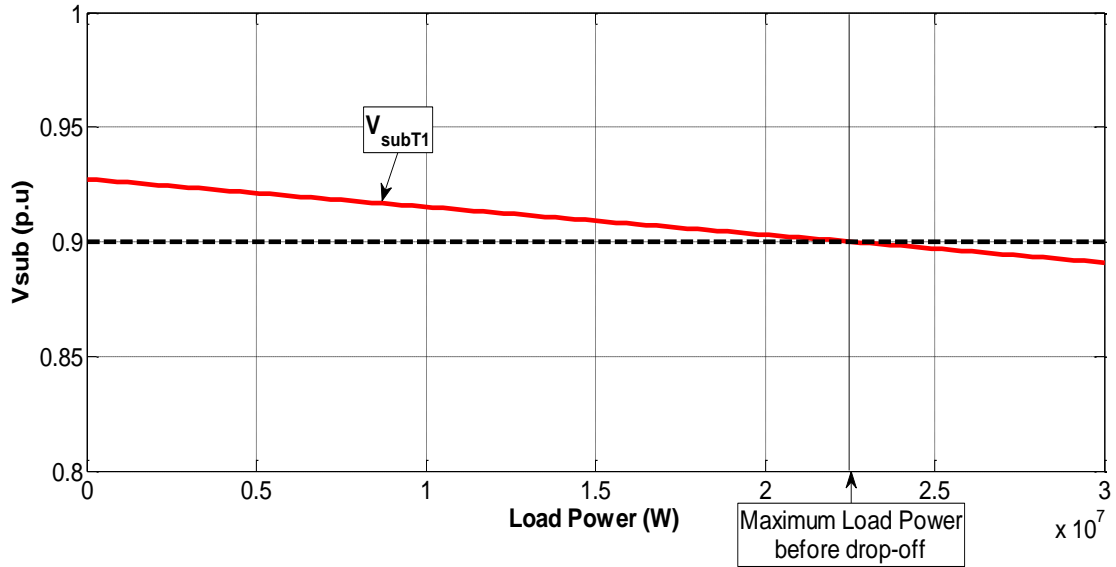
Figure 8.2. Plot of substation voltage during T1 vs total load power of the facilities for the system shown in Figure 8.1, with N=3.

Considering the voltage threshold value V_{th} we can define the maximum load size that can be carried by the substation source without trespassing the threshold as:

$$\sum_{k=1}^{N} VA_k^{T1} = \frac{Z_s}{\sqrt{3}} \frac{\sum_{k=1}^{N} I_k^{T1} V_{LLk}}{(1 - V_{th})}$$

(8.19)

Where k = 1,2,…. N, denotes the number of facilities fed by the substation.

Z_S : is the substation source impedance including the impedance of the step-down transformer.

8.2.2. ENERGY REQUIREMENT

The energy required for carrying out a soft-restart for a single or a group of facilities is given by:

$$E_{SR}^{Tramp} = \int_0^{Tramp} \left(\sum_{j=1}^{n} P_j^{Tramp} \right) dt \tag{8.20}$$

Where P_j^{Tramp} is the total load supported by the energy storage system during restoration period T_{ramp}.

For each facility the required power during start-up can be calculated using (8.13).

For comparison we can also estimate the energy required from the utility for the three different stages of power restoration:

$$E^{T1} = T1 * \sum_{j=1}^{n} P_j^{T1} \tag{8.21}$$

$$E^{T2} = T2 * \sum_{j=1}^{n} P_j^{T2} \tag{8.22}$$

$$E^{T3} = T3 * \sum_{j=1}^{n} P_j^{T3} \tag{8.23}$$

Where $P_j^{T1}, P_j^{T2}, P_j^{T3}$ are calculated using (8.10)-(8.12).

CHAPTER 9

9. CONCLUSION AND FUTURE WORK

9.1. CONCLUSION

This dissertation introduces a new method for operating an inverter interfaced energy storage system to provide a controlled and automated power restoration functionality for restoring power to a facility or a microgrid. One of the biggest drawbacks of operating an ESS in the event of a fault is the regulatory constraints which restricts its operational capabilities. These constraints are put into place:

a) To avoid expensive upgrade of line protection equipment in the bulk power system for every new installment of DERs.

b) To allow reclosers to have "single-shot" type designs to operate in a live-bus/dead-line condition and avoid asynchronous reclosure on to motor residual voltages.

Also DERs power rating being comparatively smaller than that of the substation, are generally not equipped with power restoration functionality to pre-energize a "dead" load-zone in a controlled manner so that the problems associated with starting inrush and load pick-up currents cannot be avoided. This research developed the method to operate an inverter-coupled energy storage as a self-controlled power source capable of providing a fast, safe and controlled power restoration for a facility island. The applicability and effectiveness of this method is shown for an industrial and an offshore power system. The condition to avoid significant current feed into the fault is discussed and used to develop

a simple fault-detection algorithm based on local voltage measurement. An industrial facility and a shipboard power system both of which are comprised of a large number of motors and drives, and are most affected by power disruptions are considered.

Using appropriate controls for the power electronic interface (inverter) the developed energy storage system can effect an automatic and seamless transition between islanded and grid-connected modes of operation. In addition to the protected fault-ride-through operation, the developed algorithm is capable of controlling the starting inrush currents to a predefined value during the restoration process. The controlled restoration is followed by a seamless transfer of the loads / island to the main source or substation.

For the example industrial power system current transients during automatic reclosing of line CBs, starting inrush and corresponding voltage dip effects on system loads and equipment due to motor starting are minimized. A current-fed voltage control is used to control the inverter current during the restoration process. Compared to an across-the-line start, the soft-restart method is able to decrease the starting inrush current by 67%. The total time required for completion of the SR process is about 1 s compared to 30-45 mins required for a manual restart. Since process downtime is avoided, associated costs and complications such as safety, "clean-up" time, etc. arising due to manual restarts are also avoided. The effectiveness of this method and the results are shown in Chapter-6.

The method is then extended to incorporate a fault–detection capability into the inverter to prevent a possible fault-feeding and avoid safety hazards. Phase voltage magnitudes are measured from the inverter terminals to detect a fault condition. The detection scheme is used and applied in the ship MVAC power system to provide a complete "Fault-Aware-Soft-Restart" algorithm. The method and the results are shown in Chapter-7.

Unnecessary close-open operations of circuit breakers that generate current transients and degrade equipment reliability are avoided. Two fault locations are considered for the test system and the starting inrush current transients are reduced by over 40% in both the cases. Also for the study cases, the restoration process is completed within a few seconds compared to the conventional restoration process which may take a few minutes to few hours.

This dissertation also shows the method to model a distribution circuit with multiple facilities by which power quality indices can be estimated with and without the use of energy storage system with soft-restart capability. Transient behavior of a particular load zone or a facility can be characterized using this method. Power and energy requirements can be estimated for the energy storage system connected at a particular location. Optimal sizing, placement and desired benefits can be estimated using this approach.

9.2. FUTURE WORK

This dissertation is able to generate multiple research directions for the future. The major ones are listed as follows:

- Extend the distributed generation system model to estimate energy requirement and inverter size for different types of facilities: residential and industrial. This will also lead to estimating the application range in terms of geographical area / system size.

- Extend the fault-detection algorithm applicable to utility distribution system to be able to detect line-line, line-to-ground and 3-phase-to-ground faults reliably.

- Modify the synchronizing algorithm, to accelerate the synchronizing process. In this case the inverter-controlled voltage will reach the steady-state and a "phase-matched"

condition simultaneously.

- Use the distributed generation system model to estimate power quality and reliability indices for a given set of facilities or microgrids with and without the use of energy storage system with soft-restarting capability. This will be able to predict return-benefits for installation of an energy storage system for a particular facility.

The final goal of developing a self-controlled energy storage system for a distributed generation scenario is to ensure full flexibility in terms of power management as well as to make it appear harmless or "indistinguishable" to its surrounding power system customers and utility. This research has shown the approach to mitigate the two major problems that hinders the widespread installment of inverter coupled DGs, which are: current infeed causing desensitization of protection relays and difficulty in power restoration following an interruption.

REFERENCES

[1]   Math H. J. Bollen, "Understanding Power Quality Problems - Voltage Sags and Interruptions", IEEE Press, 1999.

[2]   Mesut E. Baran, Ismail El-Markaby, "Fault Analysis on Distribution Feeders with Distributed Generators". IEEE Transactions on Power Systems, Vol. 20, No. 4, November 2005, pp 1757-1764.

[3]   M. Baran, "Adaptive Over Current Protection for Distribution Feeders with Distributed Generators".

[4]   T. S. Sidhu, D. A. Tziouvaras, A. P. Aplostolov, C. H. Castro, S. R. Chano, S. H. Horowitz, W. o. Kennedy, Sungsoo Kim, R. J. Martilla, P. G. McLaren, G. L. Michel, K. K. Mustaphi, P. Mysore, M. Nagpal, B. Nelson F. P. Plumptre, M. S. Sachdev, J. S. Thorp and J. T. Uchiyama, "Protection Issues During System Restoration", IEEE Transactions on Power Delivery, Vol. 20, No. 1, January 2000, pp47-56.

[5]   Hassan Nikkhajoei, Robert H. Lasseter, "Distributed Generation Interface to the CERTS Microgrid", IEEE Transactions on Power Delivery, Vol. 24, No. 3, July 2009, pp 1598-1608.

[6]   S. Conti, "Analysis of distribution network protection issues in presence of dispersed generation," Electric Power Systems Research, vol. 79, no. 1, pp. 49–56, Jan. 2009.

[7]   de Britto, T.M., Morais, D.R. ; Marin, M.A. Rolim, J.G. ; Zurn, H.H. ; Buendgens, R.F., "Distributed generation impacts on the coordination of protection systems in distribution networks," Transmission and Distribution Conference and Exposition: Latin America, 2004 IEEE/PES Volume, Issue, 8-11 Nov. 2004 Page(s): 623 – 628.

114

[8]   N. Nimpitiwan, S. Member, G. T. Heydt, and R. Ayyanar, "Machine and Inverter Based Distributed Generators," vol. 22, no. 1, pp. 634–641, 2007.

[9]   A. K. Srivastava, S. Member, A. A. Kumar, S. Member, and N. N. Schulz, "Impact of Distributed Generations with Energy Storage Devices on the Electric Grid," vol. 6, no. 1, pp. 110–117, 2012.

[10]   M. A. Kashem, G. Ledwich, "Multiple Distributed Generators for Distribution Feeder Voltage Support", IEEE Transactions on Energy Conversion., Vol. 20, No.34, September 2005, pp 676-684.

[11]   M. A. Kashem, G. Ledwich, "Energy Requirement for distributed energy resources with battery energy storage for voltage support in three-phase distribution lines", Electric Power Systems Research 77 (2007) pp 10-23.

[12]   Roger C. Dugan, Mark F. McGranaghan, Surya Santoso, H. Wayne Beaty, "Electrical Power Systems Quality", 2nd Ed, McGraw Hill 2004.

[13]   *IEEE Standard for Interconnecting Distributed Resources with Electric Power Systems,* IEEE Std. 1547.2-2008.

[14]   ABB HPA SF6-Circuit Breaker, Specifications: http://www05.abb.com/global/scot/scot235.nsf/veritydisplay/566c61c1379f33ee6 5256f4e001bcd71/$File/Hpa%20Brochure.pdf

[15]   Eaton Corp. Medium Voltage Switchgears: http://www.eaton.com/EatonCom/Markets/Electrical/Products/Switchgear/Mediu mVoltageSwitchgear/index.htm?ssSourceNodeId=5027&ssSourceSiteId=EatonC om.

[16]   Toshiba Medium Voltage Circuit Breaker Datasheet. Available online: http://www.ctiautomation.net/PDF/Toshiba/Toshiba-HV6-Vacuum-Circuit-Breakers.pdf

[17]   R. A (Reigh) Walling, Robert Saint, Roger C. Dugan, Jin Burke, Ljubomir A. Kojovic, "Summary of Distributed Resources Impact on Power Delivery Systems", IEEE Transactions on Power Delivery, Vol. 23, No. 3, July 2008, pp 1636-1644.

[18]   *IEEE Recommended Practice for Design of Industrial and Commercial Power Systems,* IEEE Std. 493-2007. (The Gold Book)

[19]   *IEEE Recommended Practice for Protection and Coordination of Industrial and Commercial Power Systems*, IEEE Std. 242-1986.

[20]   IEEE Guide for AC Motor Protection, IEEE Std. C37.96-2000

[21]   "Cold-Load Pickup Issues", A report to the Line Protection Subcommittee of the Power System Relay Committee of The IEEE Power Engineering Society, prepared by working group D1.

[22]   "Load Representation for Dynamic Performance Analysis", IEEE Task Force on Load Representation for Dynamic Performance, IEEE Transactions on Power Systems, Vol. 8, No. 2, May 1993, pp472-482

[23]   A.Jack Williams, J.R. , M. Shan Griffith, "Evaluating the Effects of Motor Starting on Industrial and Commercial Power Systems", IEEE Transactions on Industry Applications, Vol. 1A-14, No. 4, July/August 1978, pp 292-305.

[24]   "Modeling Stalled Induction Motors", WECC System Modeling Workshop, November 15, 2006. Link: http://www.wecc.biz/committees/StandingCommittees /PCC/TSS/MVWG/111306/Lists/Minutes/1/Validation.pdf

[25]   John A. Kay, Richard H. Paes, J. George Seggewiss and Robert G. Ellis, "Methods for the Control of Large Medium-Voltage Motors: Application Considerations and Guidelines", IEEE Transactions on Industry Applications, Vol. 36, No. 6, November/December 2000, pp 1688-1696

[26]   Charles Mozina, "Undervoltage Load Shedding", Beckwith Electric Co., Inc, Link:http://www.beckwithelectric.com/docs/tech-papers/undervoltage_ loadshedding.pdf

[27]   J. M. Maza Ortega, M. Burgos Payan, J. M. Romero Gordon and M. Pinilla Rodriguez, "Supply Voltage Effects on the Operation of Residential Air Conditioning Appliances: Theoretical Analysis",

[28]   George K. Stefopoulos, A. P. Melipoulos, "Induction Motor Load Dynamics: Impact on Voltage Recovery Phenomena", IEEE PES, Transmission and Distribution Conference and Exhibition, 21-24 May 2006, pp 752-759.

[29]   Martin Geidl, "Protection of Power Systems with Distributed Generation: State of the Art", Power Systems Laboratory, Swiss Federal Institute of Technology (ETH), 20th July 2005.

[30]   John Mulhausen, Joe Schaefer, Mangapathirao Mynam, Armando Guzman and Marcos Donolo, "Anti-Islanding Today, Successful Islanding in the Future". 36th Annual Western Protective Relay Conference, Spokane, WA, October 20-22, 2009.

[31]   Hector J. A. Ferrer, Edmund O. Schweitzer III, "Modern Solutions for Protection, Control, and Monitoring of Electric Power Systems", Schweitzer Engineering Laboratories, 2010.

[32]   Charles J. Mozina, "Interconnection Protection of IPP Generators at Commercial/Industrial Facilities", IEEE Transactions on Industry Applications, Vol. 37, No. 3, pp681-688,May/June 2001.

[33]   Thi Thu Ha Pham, Yvon Besanger and Nouredine Hadjsaid, "New Challenges in Power System Restoration With Large Scale of Dispersed Generation Insertion", IEEE Transactions on Power Systems, Vol. 24, No. 1, February 2009, pp 398-406.

[34]   D. Lindenmeyer, H. W. Dommel, M. M. Adibi, "Power system restoration – a bibliographical survey", Electrical Power and Energy Systems, Vol. 23, 2001, pp 219-227.

[35]   Evert Agneholm and Jaap E. Daalder, "Load Recovery in the Pulp and Paper Industry Following a Disturbance", IEEE Transactions on Power Systems, Vol. 15, No. 2, May 2000, pp831-837.

[36]   Vishal Kumar, Rohit Kumar H.C., Indra Gupta, and Hari Om Gupta, "DG Integrated Approach for Service Restoration Under Cold Load Pickup", IEEE Transactions on Power Delivery, Vol. 25, No. 1, January 2010, pp 398-406.

[37]   Wade, N. S., Taylor, P. C., Lang, P. D., & Jones, P. R. (2010). Evaluating the benefits of an electrical energy storage system in a future smart grid. *Energy Policy*, *38*(11), 7180–7188. doi:10.1016/j.enpol.2010.07.045

[38]   Nexight Group: Organized by Sandia National Laboratory and Sponsored by US Department of Energy. Electric Power Industry Needs for Grid-Scale Storage Applications, (December, 2010).

[39]   Abbas A. Akhil, Lana Lachenmeyer, S. J. Jabbour, H.K. Clark "Specific Systems Studies of Battery Energy Storage for Electric Utilities", Sandia Report, August 1993, Link:http://prod.sandia.gov/techlib/access-control.cgi/1993/931754.pdf

[40]   Joseph Lannucci and Susan Schoenung, "Energy Storage Concepts for a Restructured Electric Utility Industry", Sandia Report, July 2000.

[41]   Tim De Vries, Jim Mc Dowalln Niklaus Umbricht, Gerhard Linhofer, "Cold Storage- Battery Energy Storage System for Golden Valley Electric Association", ABB Review, 2004.

[42]   Janice Lin, Giovanni Damato, "Energy Storage-a Cheaper and Cleaner Alternative to Natural Gas-Fired Peaker Plants", Prepared for California Energy Storage Alliance (CESA), February 2011.

[43]   Bharat Bhargava, Gary Dishaw, "Application of an Energy Storage Power System Stabilizer on the 10 MW Battery Energy Storage System at Chino Substation", IEEE Transactions on Power Systems, Vol. 13, No. 1, February 1998, pp145-151.

[44]   "DynaPeaQ, SVC Light with Energy Storage", ABB: http://www05.abb.com/global/scot/scot221.nsf/veritydisplay/4a545a2a4b110534c 12578840048c853/$file/a02-0210e_dynapeaq%20svc%20light%20with% 20energy%20storage_lr.pdf

[45]   "Mid-American Energy Technical Requirements for New Interconnections of Generation to the MidAmerican Energy Transmission System", MidAmerican Energy, March 23, 2011.

[46]   Mindi Farber-DeAnda, "Puerto Rico's 20 MW Battery Energy Storage-The World's Largest Lead Acid Battery System is Repowered", California Energy Commission, US DOE, Workshop on Electricity Storage, Sacramento, CA, February 24, 2005.

[47]   M. M. Adibi, D. P. Milanicz, "Protective System Issues During Restoration", IEEE Transactions on Power Systems, Vol. 10, No. 3, August 1995, pp1492-1497.

[48]   IEEE Standard 1547.4, for Design, Operation, and Integration of Distributed Resource Island Systems with Electric Power Systems. April, 2011.

[49] Chaitanya A. Baone, Yan Xu and John D. Kueck, "Local Voltage Support from Distributed Energy Resources to Prevent Air Conditioner Motor Stalling", Innovative Smart Grid Technologies (ISGT), 19-21 Jan. 2010, pp 1-6.

[50] J Prousalidis and E Styvaktakis, "Introducing a Classification Method of Voltage dips in a ship electric energy systems", Proceedings of the Institure of Marine Engineering, Science, and Technology. Journal of marine engineering and technology, Vol.: a11, 2008, pp 53-62.

[51] K. L. Butler and M. Ehsani, "Flexible Ship Electric Power System Design."

[52] Thomasnet.com, Link: http://www.thomasnet.com/nsearch.html?cov=NA&what =Extruded+Plastic+Insulation&heading.

[53] Z. Yang, C. Shen, L. Zhang, M. L. Crow, S. Atcitty, "Integration of a StatCom and Battery Energy Storage", IEEE Transactions on Power Systems, Vol. 16, No. 2, May 2001, pp 254-260.

[54] *IEEE Recommended Practice for Emergency and Standby Power Systems for Industrial and Commercial Applications*, IEEE Std 446-1995 (The Orange Book).

[55] Robbie F. McElveen, Michael K. Toney, "Starting High-Inertia Loads". IEEE Transactions on Industry Applications, Vol. 37, No. 1, January/February 2001, pp 137-144.

[56] G. Sulligoi, "All Electric Ship Power Stations : Analysis of Voltage Controls and Protections."

[57] ESRDC, "Documentation for Notional Baseline System Models Version 0.7 DRAFT April 2012," no. April, 2012.

[58] Eaton Corporation "Success Story : Oasis of the Seas sets sail with Eaton UPS's on board," no. December, 2010.

[59] J. R. Jacobs, Baldwin P. Lam, and Ray P. Stratford, "A Comparison of ANSI-Based and Dynamically Rigorous Short-Circuit Current Calculation Procedures", IEEE Transactions on Industry Applications, Vol. 24, No. 6, November/December 1988, pp 1180-1194.

[60] Ned Mohan, Tore M. Undeland, William P. Robbins, "Power Electronics - Converters, Applications and Design", 3rd Ed, John Wiley & Sons, Inc, 2003.

[61] ABB Soft Starter Handbook: http://www05.abb.com/global/scot/scot209.nsf/
veritydisplay/2985284834bcff7fc1256f3a00274038/$File/1SFC132002M0201.pdf

[62] FredeBlaabjerg, Remus Teodorescu, Marco Liserre, and Adrian V. Timbus, "Overview of Control and Grid Synchronization for Distributed Power Generation Systems", IEEE Transactions on Industrial Electronics, Vol. 53, No. 5, October 2006, pp 1398-1409.

[63] Davood Yazdani, Mohsen Mojiri, Alireza Bakhshai, and Geza Joos, "A Fast and Accurate Synchronization Technique for Extraction of Symmetrical Components", IEEE Transactions on Power Electronics, Vol. 24, No. 3, March 2009, pp 674-684.

[64] M. M. Abdel Hakim, G. J. Berg, "Dynamic Single-Unit Representation of Induction Motor Groups", *IEEE Transactions on Power Apparatus and Systems*, Vol. PAS-95, No. 1, January/February 1976. pp 155-165.

[65] Carl D. Parker, "Lead-acid battery energy-storage systems for electricity supply networks, Journal of Power Sources, Vol. 100, 2001, pp 18-28.

[66] J. F. Cole, "Battery energy-storage systems – an emerging market for lead/acid batteries", Journal of Power Sources, Vol 53, 1995, pp 239-243.

[67] C. E. AEP , Commission, "Certs microgrid laboratory test bed," No. February, 2009.

[68] P. M. Anderson, "Power System Protection", McGraw-Hill, 1998.

[69] Asif Anwar, Yucheng Zhang and Roger A. Dougal, "Soft-Restarting of Industrial Power Network Using Inverter-Controlled Energy Storage System", Proceedings of the IEEE Power and Energy Society General Meeting (PESGM) 2012, July 22-26, San Diego, CA, pp 1-8.

[70] Asif Anwar, Mohd. Hasan Ali, Roger A. Dougal, "Supercapacitor Energy Storage for Low-Voltage Ride Through in a 13.8 kV AC System", IEEE SoutheastCon 2010, March 18-21, 2010, Charlotte-Concord, North Carolina.

[71] A. D. W. Flyback, J. L. Durán-gómez, and P. N. Enjeti, "An Approach to Achieve Ride-Through of an Adjustable Speed Drive With Flyback Converter Modules Powered by Supercapacitors," *IEEE Trans. On Industry Applications,* vol. 38, no. 2, pp. 514–522, 2002.

[72] MIL-Std-1399, "Interface Standard Section 300B: Electric Power, Alternating Current," April, 2008.

[73] Naval Ships' Technical Manual, Chapter 320 – Electric Power Distribution Systems. Revision 2, April 1998. Web: Link: http://www.hnsa.org/doc/nstm/ch320.pdf.

[74] Asif Anwar, Yucheng Zhang and Roger A. Dougal, Fault Current Reduction Using Inverter Controlled Energy storage for Shipboard MVAC Power System", *IEEE Electric Ship Technologies Symposium (ESTS) 2011*, Alexandria, Virginia, April 10-13, pp 315-318.

[75] R. N. Allan and K. K. Kariuki, "Reliability Worth Assessments of Electrical Distribution Networks". Quality and Reliability Engineering International. Vol. 15, pp 79-85.

[76] A. A. Chowdhury, and Don O. Koval, "Application of Customer Interruption Costs in Transmission Network Reliability Planning", IEEE Transactions on Industry Applications, Vol. 37, No. 6, November/December 2001, pp 1590-1596.